McKelvey School of Engineering Theses & Dissertations

McKelvey School of Engineering

Winter 1-15-2021

Neural Coding and Organization Principles in the Drosophila Olfactory System

Haoyang Rong
Washington University in St. Louis

WASHINGTON UNIVERSITY IN ST. LOUIS

Department of Biomedical Engineering

Dissertation Examination Committee:

Barani Raman, Chair
Dennis Barbour
Yehuda Ben-Shahar
Bruce Carlson
Timothy Holy

Neural Coding and Organization Principles in the Drosophila Olfactory System

by

Haoyang Rong

A dissertation presented to
the Graduate School
of Washington University in
partial fulfillment of the
requirements for the degree
of Doctor of Philosophy

January 2021

St. Louis, Missouri

Table of Contents

List of Figures

<u>Acknowledgments</u>

What is supposed to be said, when 8 years of one's life, more specifically, 8 years of one's youth, have turned into merely a few pages?

There's hardly an answer. Nevertheless, I'd like to express my gratitude to many people that I have encountered along the way.

I'd like to thank the members of the Raman lab. Thank Dr. Li, Chao for inspiring me to take the path of data science; Zhang, Lijun for helping with the challenging image processing and collaborating on the Kaggle challenges.

The fly brain surgeries and fly maintenance were performed in the Taghert lab. Thank Dr. Paul Taghert and his lab, for letting me be a "lab member" for years, even though my work does not contribute to the lab.

Thank Dr. Tim Holy and his lab. The first time I was introduced to the OCPI imaging system, Tim demonstrated the usage in very detail by himself, rather than delegating a student. Despite being very busy, he's always ready to offer help. His enthusiasm for engaging in research and kindness always inspire me. I highly appreciate the numerous help from Dr. Cody Greer, who built OCPI2, the lightsheet imaging system I collected my data with. I gained a deep understanding of the system by learning all aspects from him, ranging from aligning optics to the low-level control interfaces. I won't forget how well organized and detailed his email replies to my questions were. It's a very unique experience that my project grew along with his dissertation project, the development of the OCPI2.

Thank Dr. Li, Donghoon (Jerry), who's always kind to offer all sorts of help, especially problems in Julia programming. He never gives up any chance to absorb new knowledge, which

My career as a Ph.D. student can be divided into two eras, the time before one's leave (which coincided with the start of the imaging project), where all the only vivid memories come from, and the time after, during which I kept relearning from the first 3 years, struggling with endless failures, and chewing on the absurdity and void.

I worked hard just to get hit harder; I kept missing just to miss the one I love.

Over the years, I've witnessed the busy halls in the day, and empty corridors at night at the medical school; I've witnessed the seasons change outside the windows of the metro train; I've witnessed buildings rise and fall in this static city; I've witnessed new faces greeting; I've witnessed the then familiar faces turn into silent icons in WeChat. I've witnessed my parent's gray hair grow, on the other side of the screen, tens of thousands of miles away.

I've witnessed her smile under a blooming cherry blossom tree; I've witnessed her silhouette disappearing at the C gate in the airport. I acknowledge time, though I do not necessarily thank it.

Finally, I'd like to thank all my family and friends. It's you that made this long, long journey a little bit more bearable.

Haoyang Rong

Washington University

January 2021

Dedicated to:

Jiaxin Yang,

the girl who taught me what is love,

and love of my life

Abstract of the dissertation

Neural Coding and Organization Principles in the Drosophila Olfactory System

by

Haoyang Rong

Doctor of Philosophy in Biomedical Engineering

Washington University in St. Louis, 2020

Professor Barani Raman, Chair

Sensory systems receive and process external stimuli to allow an organism to perceive and react to the environment. How is sensory information subsequently represented, transformed, and interpreted in the neural system? In this dissertation, I have investigated this fundamental question using the fruit fly (Drosophila melanogaster) olfactory system.

Chemical cues are transduced into neural signals in the insect antenna by the olfactory receptor neurons (ORNs). The ORNs send their axons to the antennal lobe (AL), with each ORN type innervating a specific neuropil (glomerulus), where they synapse onto excitatory and inhibitory projection neurons (ePNs and iPNs). The ePNs project their axons to the 3rd order stages, the calyx (CL) and lateral horn (LH). On the other hand, the iPNs only innervate the LH.

In this dissertation, I first examined how well the peripheral neural activities evoked by an odorant could predict the final behavioral output. As the stimulus intensity increases, a fly's preference for some odorants switch from attraction to aversion. Behavior assay suggested this phenomenon may help the fly evade harmful environment. Our results indicate that at the level of ORNs, increases in stimulus intensity could result in oscillatory extracellular field potentials

that arise entirely due to abrupt changes in cell excitability. Notably, combining the activity of a few ORNs was sufficient to predict intensity-dependent preference changes with odor intensity.

How is the sensory input organized in the downstream neural circuit, the insect antennal lobe? Odor-evoked signals from sensory neurons (ORNs) triggered neural responses that were patterned over space and time in cholinergic ePNs and GABAergic iPNs within the antennal lobe. The dendritic-axonal (I/O) response mapping was complex and diverse, and the axonal organization was region-specific (mushroom body vs. lateral horn). In the lateral horn, feed-forward excitatory and inhibitory axonal projections matched 'odor tuning' in a stereotyped, dorsal-lateral locus, but mismatched in most other locations. In the temporal dimension, ORN, ePN, and iPN odor-evoked responses had similar encoding features, such as information refinement over time and divergent ON and OFF responses. Notably, analogous spatial and temporal coding principles were observed in all flies, and the latter emerged from idiosyncratic neural processing approaches.

In sum, these results provide key insights necessary for understanding how sensory information is organized along spatial and temporal dimensions.

Chapter 1: Introduction

1.1 Overview: the road to "know thyself"

Since the birth of modern science, we human beings have made enormous progress in understanding the physical world we live in, from the atoms to the galaxies. However, we still lack understanding of the little galaxy sitting in our head, the brain, where science originates.

We are still far from answering what exactly the high-level cognitive processes such as attention, learning, memory, and emotion, are. Let alone the "free will" or consciousness. The human brain is estimated to have 86 billion neurons (Azevedo et al., 2009), within the same order of magnitude as the number of stars in the Milky Way. Even the brain of a fruit fly, at the size of a needlepoint, has 100,000 neurons (Simpson, 2009; Zheng et al., 2018). In addition to the sheer number of neurons, the numerous connections make the system even more complex (when oversimplified, the neural system can be viewed as a gigantic directed graph, where nodes being neurons, directed edges being dendrites/axons.). Moreover, the neural systems are highly dynamic and are endowed with the capability of constantly "updating" itself, in response to the changes in the environment or inside the animal itself.

To understand the brain, a vital part is to study the neural coding principles. Namely, how information is represented (encoding), transformed, and interpreted (decoding) in the neural system. This requires knowledge of the input information, the recordings of the neural activities, and ideally the relevant behavioral output. Therefore, the sensory systems, including vision, hearing, touch, smell, taste, etc., are good starting points in our journey to "know thyself", whereas the high level cognitive processes often lack one or more of these attributes. For example, in an animal model of depression, it's impractical to control the exact degree of

depression. On the other hand, a sensory system, being a "black box" at first, can be probed by carefully designed inputs. The input information such as visual cues, sound tones, mechanical stimuli, and so on, can be artificially generated and quantitatively manipulated. The neuronal populations in the early stages are often accessible to electrodes or microscopes. The behavioral output, for instance, how fast a monkey can react to a visual cue, can be measured.

1.2 The olfactory system: a unique signal processing system

It's been reported that humans can recognize a great number of olfactory stimuli (Bushdid et al., 2014; Gottfried et al., 2006). Olfaction plays a role in the regulation of human emotion and social interactions (Hutmacher, 2019; Sarafoleanu et al., 2009). For insects, the olfactory system is even more important for its survival. Many insect species rely on olfactory cues to navigate, seek food, and reproduce (Buehlmann et al., 2015; Hansson and Stensmyr, 2011; Sachse and Krieger, 2011; Wright and Schiestl, 2009).

Though being powerful, the olfactory system is "shallow": the olfactory information only needs to pass two stages before reaching centers responsible for behavior output (Wilson and Mainen, 2006) This simplicity alleviates the difficulty in tracking what happens along the path, from input to output. What also makes the olfactory system unique is that, distinct from visual and auditory stimuli, which can be simply characterized by a couple of continuous quantities, e.g. wavelength/frequency and intensity, the olfactory stimuli do not reside in a well-defined input space. There's no such a small set of quantities that can lay out the olfactory stimuli on a continuous spectrum (Hettinger, 2011). That being said, the dimensionality of the olfactory input

space, if to be defined, can be almost arbitrarily large. Therefore, it's of particular interest to study how this compact system manages to process the intricate input information efficiently.

1.3 The anatomy of the olfactory system: the hardware implementation

The anatomical organization of the olfactory system is hierarchical. In mammals, the sensory neurons in the epithelium of the nasal cavity transduce chemical cues into neural signals and such signals are transmitted to projection neurons, e.g. mitral cells and tuft cells, in the olfactory bulb, where a process called "lateral inhibition" takes place to reformat the signals (Lledo et al., 2005). Interneurons and granule cells are believed to perform feedback inhibition on mitral cells, which enhances odor discrimination. The reformatted signals are projected to multiple target regions, such as the amygdala, responsible for associative learning, and the hippocampus, in charge of memory and learning.

The general organization of the insect olfactory system resembles its mammalian counterpart (Wilson and Mainen, 2006). The insects have two primary olfactory organs: the antennae and the maxillary pulps (Carey and Carlson, 2011). The 1st order neurons, the olfactory receptor neurons (ORNs), housed in hair-like structures called sensillum, connect with projection neurons (PNs) in the antennal lobes (ALs), the insect equivalent of olfactory bulbs. The signals are then relayed to the mushroom body, associated with memory and learning (Akalal et al., 2006; McGuire et al., 2001; Menzel and Muller, 1996; Mizunami et al., 1998), and lateral horn for innate behavioral response (Gupta and Stopfer, 2012; Schultzhaus et al., 2017).

In Drosophila, the model organism used in this study, an ORN's type is defined by the unique olfactory receptor it expresses (Fishilevich and Vosshall, 2005; Hallem et al., 2004; Vosshall et al., 1999). The OR along with a universal co-receptor Or83b (Orco) (Larsson et al., 2004), gives the ORN its unique response characteristics (Dobritsa et al., 2003; Hallem et al., 2004). Typically, each sensillum contains 2 distinct ORNs. On the antenna surface, more precisely, the third antennal segment (funiculus), there are 3 major morphological sensillum classes: basiconic, trichoid, and coeloconic, with the basiconic being the major type (de Bruyne et al., 2001; Venkatesh and Naresh Singh, 1984). In exposure to a stimulus, odor molecules enter the sensillum through the pores on the surface, bind to the ORs on the ORN dendrites, trigger cellular events, and produce odor-evoked action potentials or inhibition (de Bruyne et al., 2001; Hallem and Carlson, 2006a; Stocker, 1994).

ORNs are bipolar neurons, with dendrites extending to the sensilla and axons projecting to the ALs. Notably, in most of the cases, ORNs of the same type, though may be distributed on the antennal surface, project their axons bilaterally to the same glomerulus, a spherical neuropil, in each AL. Likewise, the current dogma is that each AL glomerulus only receives input from one ORN type (Hallem and Carlson, 2004; Stocker, 1994). A smaller portion of OSNs express ionotropic receptors (IR) (Benton et al., 2009; Rytz et al., 2013). OSNs in maxillary palps are more specialized, with each type only responding to a small set of compounds (Dweck et al., 2016). Maxillary palps have just one sensillum type and 120 ORNs (de Bruyne et al., 1999).

Post-synaptic to the ORNs are the 2nd order principal neurons of the AL, also called the projection neurons (PNs). Excitatory projection neurons (ePNs), one of the major PN populations, are uni-glomerular, e.g. each ePN innervating only one glomerulus, such that an ePN only receives input from one type of ORNs. On the other hand, a glomerulus may be

innervated by several (2-6) ePNs (homotypic PNs or sister PNs). These sister ePNs exhibit correlated spontaneous activities. Such synchrony increases even more in response to odor stimulus, because 1. sister PNs sample largely overlapping sets of ORNs in the same glomerulus 2. Mixed electrical/chemical synapses between the sister PNs. Interestingly, sister PNs have the same innervation pattern in the LH, but they differ in the MB (Kazama and Wilson, 2009). This mechanism is thought to implement coincidence detection in the LH (Jeanne and Wilson, 2015).

Another lesser-known group of inhibitory projection neurons (iPNs), which releases GABA, form a parallel pathway in addition to the ePNs. The ePNs convey signals to MB and LH via the medial antennal lobe tract (mALT), whereas iPNs only project to the LH via the mediolateral antennal lobe tract (mlALT), bypassing the MB(Shimizu and Stopfer, 2017). iPNs can be both uni-glomerular or multi-glomerular, even pan-glomerular(Lai et al., 2008).

Similar to PNs, another important group of players in the AL, the local interneurons (LNs), have two major functional categories, the inhibitory LNs (iLNs) and excitatory LNs (eLNs), crucial to the reformatting of signals. The recruitment of iLNs is not odor specific. Even the activation of a single glomerulus can trigger global lateral inhibition from GABAergic LNs. But the degree of inhibition that each glomerulus receives can vary owing to the glomeruli's varying sensitivities to GABA (Hong and Wilson, 2015). However, eLNs can both depolarize and hyperpolarize PNs, primarily through electrical synapses. Meanwhile, eLNs and iLNs are interconnected via mixed synapses (Yaksi and Wilson, 2010a).

The MB has around 2000 intrinsic neurons, the Kenyon cells (KCs, 3rd order), in each hemisphere. It serves as an "expansion layer" by significantly increasing the dimension from ~50 to ~2000. The representation of odor stimulus in the MB is sparse (Honegger et al., 2011).

Each KC extends several "claws" to connect with boutons of distinct PNs, with one "claw" only sampling from one PN. However, a PN bouton can synapse with "claws" from several KCs, forming a microneuropil (Caron et al., 2013).

Apart from the basic characterizations, the general consensus on the MB is probably the ubiquitous existence of disagreements. Contradictory results have been reported regarding the organization and coding principles of the MB. It remained controversial whether individuality or stereotypy dominates the circuit.

An early functional imaging study suggests the KCs' odor-evoked activities are stereotyped in both the soma layer and the calyx (Wang et al., 2004). Each PN type's innervation patterns in the calyx and LH are conserved among individuals. What's more, the KC innervations in the calyx are also stereotyped (Lin et al., 2007; Zheng et al., 2018). On the contrary, some other studies suggest the KC-PN connections are random (Caron et al., 2013; Murthy et al., 2008). At the single cell level, a KC's input glomeruli don't follow any rules in terms of odor tuning, anatomical features, etc. At the population level, no KC class exhibits preference over any specific glomeruli combination.

The KCs project axons to one of the three lobes of the MB, where they synapse onto the mushroom body output neurons (MBON, 4th order). The MBON population is small. Despite the randomness in the KC layer, MBONs' responses are stereotyped, possibly because each MBON integrates signals from a large subset of KCs (Mittal et al., 2020). However, this seems to defeat the purpose of sparse coding in the KC layer. Another study reported MBONs' tunings are individual dependent, and this variability is shown to be related to learning. The mutant lacking a learning-related gene showed a decrease in the MBON tuning variability. (Hige et al., 2015)

In the lateral horn, a confocal imaging study suggested that the projection of pheromone-specific and general purpose fruit odor responsive PNs are spatially segregated (Jefferis et al., 2007). The LHNs are diverse in morphology, though there's no apparent mapping between specific groups of glomeruli and LHNs of a specific morphology type. Even LHNs within the same morphological category can receive input from different glomeruli combinations (Jeanne et al., 2018). Some glomeruli combinations are over-represented, with members having diverse odor specificity.

1.4 Neural coding: the "data structures and algorithms"

The early discoveries regarding neural coding date back to the late 1950s. Works on cat primary visual cortex revealed a group of neurons responded most strongly to slits of light at specific orientations (optimal stimulus), the response strength varied according to the similarity between the present stimulus and the optimal stimulus, thereby encoding the orientation of the visual stimulus (Hubel and Wiesel, 1959; Marin et al., 2002). Since then, a wide range of coding schemes have been proposed.

A single action potential (a "spike"), which takes place at the scale of milliseconds, is usually regarded as the basic information unit in the neural system, analogous to a "bit" in a computer system.

1.4.1 Rate coding

Rate coding is one of the most basic coding schemes. The rate of the spiking activities is defined as the average spike count during the course of a trial or stimulus. The value of the neuron's

firing rate encodes the information concerning the stimulus. Hence, the aforementioned orientation-specific neuron's tuning is a classic example of rate codes.

1.4.2 Labeled line coding

Another connection-based coding scheme, e.g. the "labeled line" or place coding, is also fairly intuitive. It states the activation of one information channel exclusively triggers the corresponding response in the downstream channel it directly connects to. Just like flipping the light switch (sending information through a dedicated channel) will turn on the light (a downstream responder).

1.4.3 Temporal coding

The structures in a spike train to be exploited for coding is rich. Among them, the temporal information regarding the spikes sometimes plays an important role (temporal coding). In contrast to rate coding, in which only the mean firing rate during a unit time window matters, the temporal coding scheme utilizes fine-grained temporal features such as first-spike latency, oscillation phases, and spike intervals. For instance, neural oscillations, characterized as periodic neural activities, is a prevalent form of temporal coding among phyla of the kingdom Animalia(Kay, 2015). Various types of neural oscillations are proposed to be closely associated with multiple neural functions(Kay et al., 2009; Kay and Stopfer, 2006), such as representing the sensorimotor act of sniffing/breathing(Bhalla and Bower, 1997; Kay, 2005), and indicating movement preparation(Zhang et al., 2008). Albeit oscillations are found to play an important role in some insect olfactory systems(Laurent, 2002; Stopfer et al., 1997) by enhancing odor discriminability, they are less prominent in flies(Tanaka et al., 2009; Wilson, 2013).

1.4.4 Population coding

Neurons are noisy. Randomness is a fundamental aspect of any neural system. Even presented with the exact same stimuli, a given neuron will almost never produce two identical spike trains. Considering a neuron's response can be so variable, estimating the information solely based on one neuron is unreliable. This problem can be mitigated by combining signals from a population of neurons. Imagine a neuron is repeatedly presented with a stimulus, it will ultimately yield a distribution of firing rates given this stimulus (conditional probability. Note the difference from a tuning curve.). When the stimulus is altered, the neuron will have a corresponding response distribution. Likewise, every neuron in the population has its own firing rate distributions conditioned on varying stimuli. Therefore, the decoder, when given the responses from a group of such neurons, can more robustly estimate the stimulus through the maximum likelihood estimation approach, e.g. finding the parameter/stimulus that maximizes the probability of observing the current responses generated by this neuron group. Such a coding scheme is especially suitable for stimuli that can be described by continuous quantities, such as bar orientations, but less straightforward to be applied to the olfactory system, as the olfactory input space is so fragmented.

1.4.5 Spatiotemporal coding

This dissertation adopted a spatiotemporal scheme demonstrated to be effective in the olfactory system, that combines both the population and temporal aspect of the population's response. The neural ensemble's response at a time instance (as a short time window) is represented by a high-dimensional vector, with each dimension being a functional unit's activity (firing rate or normalized Calcium signal change). Loosely speaking, the overall response strength determines the length of the vector. The stronger the responses are, the farther away the point is from the

origin. The relative strength across the functional units (the ensemble pattern) determines the direction of the vector. The evolution of ensemble dynamics as time elapses thus can be concisely described by the trajectory of the response vector. For visualization, the trajectory can be mapped to a 2 or 3D space using dimensionality reduction techniques (Saha et al., 2013; Saha et al., 2015; Stopfer et al., 2003).

In the locust, a PN's response to a lengthy stimulus can typically be divided into three phases. The on-transient phase, where the PN's firing rate rises rapidly from the baseline level upon the onset of the stimulus. Then it enters the 2nd phase, the steady state, where the firing rate stabilizes. When the stimulus terminates, the firing rises again (off-transient phase) before returning to the baseline.

From the view of spatiotemporal codes, the ensemble PN response can be depicted as follows.

Before the stimulus, the ensemble trajectory randomly "fluctuate?" around the origin, since the spontaneous activities are low and largely random. As soon as the stimulus onsets, the high-dimensional neural response trajectory deviates from the origin along a certain direction. The trajectory moves closer to the origin, and loops around in a small region (a "fixed point") as if the system's state had been "attracted" to a stable point in the state space. Once the stimulus terminates, the trajectory again picks up speed and enters another region before finally returns to the origin (Saha et al., 2013).

Consequently, the trajectory can be viewed as moving on a manifold (loosely speaking, a lower-dimensional structure embedded in a high dimensional space). Varying concentrations of the same chemical produce trajectories on the same manifold. But the trajectories of high concentration stimuli form larger "loops" on the manifold (the ensemble patterns remain similar,

10

but scaled differently). It also takes longer for the trajectories of high concentration stimuli to return to the origin. Thus, the stimulus intensity can be resolved. When given different odors, the trajectories of each odor lie in a unique manifold (the ensemble patterns are different). Thus the stimulus identity can be resolved. (Stopfer et al., 2003)

1.4.6 Neural coding in Drosophila

In Drosophila, comprehensive descriptions of the ensemble spatiotemporal dynamics in the fly olfactory system have been very scarce, let alone the simultaneous monitoring of several populations/stages.

The "labeled line" hypothesis has gained popularity, possibly due to the relative ease of testing causal relationships in flies by knocking out a specific neuronal population and observe the physiological or behavioral consequences. However, the coding capacity of the labeled line is limited, which only scales linearly with the number of neurons. Though possibly deployed in the fly brain, the encoding of diverse odorants requires a combinatorial coding strategy, whose coding capacity can scale exponentially with the neuron number.

1.5 Idiosyncrasy: what makes me ME?

It's said that "no two leaves are alike". How about the neural systems and the behaviors driven by the neural systems?

In behavioral tests, the variability among individual behaviors is usually treated as noise that hinders the discovery of the underlying "true behavior", thus the common strategy of taking the average value across individuals. Likewise, the inter-individual variation in neural responses is often regarded as noise. However, individuals in the population are often diverse in one or more

aspects like genotypes, development, and experience. Different genotypes commonly lead to different phenotypes (Alberch, 1991; Pigliucci, 2010). Even if two individuals are genetically identical, numerous epigenetic mechanisms, such as DNA methylation and histone modification, will still have varying impacts on the development of the individuals (Cedar and Bergman, 2009). Therefore, the variability in both neural systems and behavior should be expected as a result. But rather than meaningless noises, such variabilities may actually carry key information that can give us more insights.

Consider a hypothetical scene. There're 100 guests at a banquet being asked whether he/she likes a chief's-special spicy dish. Half of the people answer they do, while the others don't. Now suppose these guests are placed in a T-maze assay one by one. The results will appear highly random/noisy. As the usual way of interpreting T-maze results, we may conclude the spicy flavor has no influence on human being's gustatory preference. However, as human beings ourselves, we know each guest probably has a good reason for his/her unique preference. For instance, maybe people who grow up in a family that cooks spicy food frequently are more likely to appreciate the dish. Subsequently, whether a person's childhood environment affects his food preference becomes a meaningful hypothesis to test, and it will help to unveil the mechanisms behind the food preference. This example illustrates how neglecting idiosyncrasy can hinder the true understanding and even lead to a false conclusion.

Thankfully, some works have already started to reveal the existence and mechanisms of idiosyncrasy in multiple neural systems, from animals at distinct branches of the evolutionary tree. Here I briefly discuss examples from 3 species: C.elegans (Nematoda), Drosophila (Arthropoda), and mice (Vertebrata).

In C. elegans, some individuals' spontaneous behavior parameters, such as the fraction of roaming and locomotion speed consistently deviate from the population mean, in spite of the developmental stages, even though the test subjects are isogenic worms raised individually under the same environmental conditions. And neuromodulation is found to regulate the level of individuality (Stern et al., 2017).

Highly inbred Drosophila individuals showed different types of stimulus-tracking behaviors, in a visual behavior paradigm (Buridan's paradigm) (Colomb et al., 2012; Gotz, 1980). These tracking styles were demonstrated to be inherent to individuals, notwithstanding the stage of development. This individuality was further traced to the variation in neuron wirings, thanks to the difference in molecular signaling events during the development (Linneweber et al., 2020).

In the fly antennal lobe, a comprehensive study including >1500 LNs revealed "an unexpected degree of" inter-individual variability in the LN innervation patterns. The inter-individual variability is especially prominent in a class of "patchy LNs", with no pair of patchy LNs, among the 161 patchy LNs being investigated, innervating the same set of glomeruli (Chou et al., 2010).

Steroid-responsive vomeronasal sensory neurons (VSNs) in mice exhibit idiosyncrasy in terms of the number of each identified neuron type among individuals. What's more, the variabilities in VSN numbers are cell type dependent (Xu et al., 2016).

1.6 Recording Techniques: tools to crack the neural circuits

Undoubtedly, the progression of scientific research is tightly coupled with the development of new experimental techniques. Despite the advantages, the extremely small brain size of the flies impeded the attempts to crack the neural codes. The classical approach of inserting a sharp

electrode into the neuropil does not work for fly neurons, since the neurites are very small. The constantly moving brain also prevented stable recordings (Wilson, 2011). As a result, the neural activities of the fly olfactory circuits beyond the periphery level remained inaccessible to researchers until the whole-cell patch-clamp technique was adopted for neural recordings (Wilson et al., 2004). In contrast, sensillum recordings were successfully conducted earlier, owing to the easier access to the ORNs (Clyne et al., 1997).

Electrophysiology is the most direct manner of measuring neural activities. Capable of detecting subthreshold events, it offers excellent sensitivity and temporal resolution. But it comes with a downside, too: the number of neurons it can accurately record from at a time is limited. One typical approach to tackle the problem is to assemble a "pseudo-subject", in which neural recordings from multiple animals are combined into one data set. The variation between individuals, impossible to quantify in this case, is intrinsically embedded in the combined dataset, which confounds the statistical relationship between the variables (Averbeck et al., 2006). Hence, a method to monitor a broader population of neurons is needed, and the imaging techniques come to the rescue. Calcium imaging, the monitoring of the fluctuation in calcium concentration in the biological structures through a light-emitting indicator that changes its fluorescence level according to the calcium concentration.

Calcium is heavily involved in cell signaling and neural activities. The generation of an action potential often accompanies the influx of Ca2+ through voltage-gated calcium channels(Katz and Miledi, 1968; Rusakov, 2006). Is also important for triggering the release of neurotransmitters (Neher and Sakaba, 2008). Therefore, calcium imaging is suitable for the monitoring of neural activities. There are two major types of calcium indicators: Synthetic indicators and fluorescent protein based indicators. Considering the fluorescent proteins can be genetically encoded, this

approach is especially advantageous when combined with the abundant genetic tools of Drosophila.

First attempts to perform calcium imaging on the fly brains also took place in the late 1990s' (Karunanithi et al., 1997). However, genetically encoded calcium indicators in early times were not sensitive enough to detect sparse spikes (Jayaraman and Laurent, 2007; Mao et al., 2008), making them inadequate for studying the temporal dynamics. Through protein engineering, new generations of GCamp proteins have been emerging. Prior to the launch of the imaging project in this dissertation, a new family of GCamp proteins, the GCamp6, capable of detecting a single spike (Note it's still impractical to resolve single spikes from fluorescence signals when the firing rate is high.), had become available (Chen et al., 2013). The GCamp6f was chosen for this study because, despite weaker signal strength, it has the fastest kinetics better suited for monitoring fast neural dynamics.

Functional calcium imaging studies have been mostly conducted with confocal microscopy and two-photon microscopy. Both are very limited in acquisition speed, owing to the point-scanning nature of their operation. The spinning-disc technique may offer higher speed since it can project multiple laser beams on the sample simultaneously, but the improvement is not so significant. On the other hand, the lightsheet imaging, an emerging imaging modality mostly used for developmental studies, has started to see its humongous potential in functional imaging as well (Ahrens et al., 2013; Chen et al., 2018; Greer and Holy, 2019; Xu et al., 2016).

1.7 Dissertation Outline:

This dissertation focuses on uncovering the neural coding and functional organization of the fly olfactory system. Chapter 2 describes the study relating peripheral neural response to behavior outcome, where I combine electrophysiology, neural manipulation, numerical modeling, and behavior assays. A novel behavior paradigm is presented. Next, I look into the olfactory circuits in the brain comprehensively using data collected from a new generation lightsheet imaging system. In Chapter 3, I discuss the functional organization/interaction across the circuits. This study, to the author's knowledge, provides not only a much more comprehensive 4D (volumetric + temporal) characterization of multiple Drosophila olfactory neuronal populations/regions, but also the first simultaneous recordings on different PN compartments in brain regions that are anatomically far apart. A novel technique mapping the circuits' functional attributes to the anatomical space is presented. Next, I investigate the temporal evolution of the ensemble neural coding during and after the stimulation. The idiosyncrasy in both the spatial and temporal aspects studied above are also discussed.

1.8 References

Ahrens, M.B., Orger, M.B., Robson, D.N., Li, J.M., and Keller, P.J. (2013). Whole-brain functional imaging at cellular resolution using light-sheet microscopy. Nat Methods 10, 413-+.

Akalal, D.B., Wilson, C.F., Zong, L., Tanaka, N.K., Ito, K., and Davis, R.L. (2006). Roles for Drosophila mushroom body neurons in olfactory learning and memory. Learn Mem 13, 659-668.

Alberch, P. (1991). From genes to phenotype: dynamical systems and evolvability. Genetica 84, 5-11.

Averbeck, B.B., Latham, P.E., and Pouget, A. (2006). Neural correlations, population coding and computation. Nature Reviews Neuroscience 7, 358-366.

Azevedo, F.A.C., Carvalho, L.R.B., Grinberg, L.T., Farfel, J.M., Ferretti, R.E.L., Leite, R.E.P., Jacob, W., Lent, R., and Herculano-Houzel, S. (2009). Equal Numbers of Neuronal and Nonneuronal Cells Make the Human Brain an Isometrically Scaled-Up Primate Brain. J Comp Neurol 513, 532-541.

Benton, R., Vannice, K.S., Gomez-Diaz, C., and Vosshall, L.B. (2009). Variant Ionotropic Glutamate Receptors as Chemosensory Receptors in Drosophila. Cell 136, 149-162.

Bhalla, U.S., and Bower, J.M. (1997). Multiday recordings from olfactory bulb neurons in awake freely moving rats: Spatially and temporally organized variability in odorant response properties. J Comput Neurosci 4, 221-256.

Buehlmann, C., Graham, P., Hansson, B.S., and Knaden, M. (2015). Desert ants use olfactory scenes for navigation. Anim Behav 106, 99-105.

Bushdid, C., Magnasco, M.O., Vosshall, L.B., and Keller, A. (2014). Humans Can Discriminate More than 1 Trillion Olfactory Stimuli. Science 343, 1370-1372.

Carey, A.F., and Carlson, J.R. (2011). Insect olfaction from model systems to disease control. Proc Natl Acad Sci U S A 108, 12987-12995.

Caron, S.J., Ruta, V., Abbott, L.F., and Axel, R. (2013). Random convergence of olfactory inputs in the Drosophila mushroom body. Nature 497, 113-117.

Cedar, H., and Bergman, Y. (2009). Linking DNA methylation and histone modification: patterns and paradigms. Nat Rev Genet 10, 295-304.

Chen, T.W., Wardill, T.J., Sun, Y., Pulver, S.R., Renninger, S.L., Baohan, A., Schreiter, E.R., Kerr, R.A., Orger, M.B., Jayaraman, V.*, et al.* (2013). Ultrasensitive fluorescent proteins for imaging neuronal activity. Nature 499, 295-300.

Chen, X., Mu, Y., Hu, Y., Kuan, A.T., Nikitchenko, M., Randlett, O., Chen, A.B., Gavornik, J.P., Sompolinsky, H., Engert, F., and Ahrens, M.B. (2018). Brain-wide Organization of Neuronal Activity and Convergent Sensorimotor Transformations in Larval Zebrafish. Neuron 100, 876-890 e875.

Clyne, P., Grant, A., O'Connell, R., and Carlson, J.R. (1997). Odorant response of individual sensilla on the Drosophila antenna. Invert Neurosci 3, 127-135.

Colomb, J., Reiter, L., Blaszkiewicz, J., Wessnitzer, J., and Brembs, B. (2012). Open Source Tracking and Analysis of Adult Drosophila Locomotion in Buridan's Paradigm with and without Visual Targets. Plos One 7.

de Bruyne, M., Clyne, P.J., and Carlson, J.R. (1999). Odor Coding in a Model Olfactory Organ: TheDrosophila Maxillary Palp. The Journal of Neuroscience 19, 4520-4532.

de Bruyne, M., Foster, K., and Carlson, J.R. (2001). Odor coding in the Drosophila antenna. Neuron 30, 537-552.

Dobritsa, A.A., van der Goes van Naters, W., Warr, C.G., Steinbrecht, R.A., and Carlson, J.R. (2003). Integrating the molecular and cellular basis of odor coding in the Drosophila antenna. Neuron 37, 827-841.

Dweck, H.K., Ebrahim, S.A., Khallaf, M.A., Koenig, C., Farhan, A., Stieber, R., Weissflog, J., Svatos, A., Grosse-Wilde, E., Knaden, M., and Hansson, B.S. (2016). Olfactory channels associated with the Drosophila maxillary palp mediate short- and long-range attraction. Elife 5.

Fishilevich, E., and Vosshall, L.B. (2005). Genetic and Functional Subdivision of the Drosophila Antennal Lobe. Current Biology 15, 1548-1553.

Gottfried, J., Hummel, T., and Welge-Lüssen, A. (2006). Taste and smell: An update. Chap Smell: Central nervous processing, Vol 63, pp 44–69) Hummel, T and Welge-Lüssen, A doi 10, 000093750.

Gotz, K.G. (1980). Visual guidance in Drosophila. Basic Life Sci 16, 391-407.

Greer, C.J., and Holy, T.E. (2019). Fast objective coupled planar illumination microscopy. Nat Commun 10.

Gupta, N., and Stopfer, M. (2012). Functional Analysis of a Higher Olfactory Center, the Lateral Horn. J Neurosci 32, 8138-8148.

Hallem, E.A., and Carlson, J.R. (2004). The odor coding system of Drosophila. Trends Genet 20, 453-459.

Hallem, E.A., and Carlson, J.R. (2006). Coding of odors by a receptor repertoire. Cell 125, 143-160.

Hallem, E.A., Ho, M.G., and Carlson, J.R. (2004). The molecular basis of odor coding in the drosophila antenna. Cell 117, 965-979.

Hansson, B.S., and Stensmyr, M.C. (2011). Evolution of insect olfaction. Neuron 72, 698-711.

Hettinger, T.P. (2011). Olfaction is a chemical sense, not a spectral sense. P Natl Acad Sci USA 108, E349-E350.

Hige, T., Aso, Y., Rubin, G.M., and Turner, G.C. (2015). Plasticity-driven individualization of olfactory coding in mushroom body output neurons. Nature 526, 258-262.

Honegger, K.S., Campbell, R.A., and Turner, G.C. (2011). Cellular-resolution population imaging reveals robust sparse coding in the Drosophila mushroom body. J Neurosci 31, 11772-11785.

Hong, E.J., and Wilson, R.I. (2015). Simultaneous encoding of odors by channels with diverse sensitivity to inhibition. Neuron 85, 573-589.

Hubel, D.H., and Wiesel, T.N. (1959). Receptive fields of single neurones in the cat's striate cortex. J Physiol 148, 574-591.

Hutmacher, F. (2019). Why Is There So Much More Research on Vision Than on Any Other Sensory Modality? Front Psychol 10, 2246-2246.

Jayaraman, V., and Laurent, G. (2007). Evaluating a genetically encoded optical sensor of neural activity using electrophysiology in intact adult fruit flies. Frontiers in Neural Circuits 1.

Jeanne, J.M., Fisek, M., and Wilson, R.I. (2018). The Organization of Projections from Olfactory Glomeruli onto Higher-Order Neurons. Neuron 98, 1198-1213 e1196.

Jeanne, J.M., and Wilson, R.I. (2015). Convergence, Divergence, and Reconvergence in a Feedforward Network Improves Neural Speed and Accuracy. Neuron 88.

Jefferis, G.S., Potter, C.J., Chan, A.M., Marin, E.C., Rohlfing, T., Maurer, C.R., Jr., and Luo, L. (2007). Comprehensive maps of Drosophila higher olfactory centers: spatially segregated fruit and pheromone representation. Cell 128, 1187-1203.

Karunanithi, S., Georgiou, J., Charlton, M.P., and Atwood, H.L. (1997). Imaging of calcium in Drosophila larval motor nerve terminals. J Neurophysiol 78, 3465-3467.

Katz, B., and Miledi, R. (1968). The role of calcium in neuromuscular facilitation. J Physiol 195, 481-492.

Kay, L.M. (2005). Theta oscillations and sensorimotor performance. P Natl Acad Sci USA 102, 3863-3868.

Kay, L.M. (2015). Olfactory system oscillations across phyla. Curr Opin Neurobiol 31, 141-147.

Kay, L.M., Beshel, J., Brea, J., Martin, C., Rojas-Libano, D., and Kopell, N. (2009). Olfactory oscillations: the what, how and what for. Trends in Neurosciences 32, 207-214.

Kay, L.M., and Stopfer, M. (2006). Information processing in the olfactory systems of insects and vertebrates. Semin Cell Dev Biol 17, 433-442.

Kazama, H., and Wilson, R.I. (2009). Origins of correlated activity in an olfactory circuit. Nat Neurosci 12, 1136-1144.

Lai, S.L., Awasaki, T., Ito, K., and Lee, T. (2008). Clonal analysis of Drosophila antennal lobe neurons: diverse neuronal architectures in the lateral neuroblast lineage. Development 135, 2883-2893.

Larsson, M.C., Domingos, A.I., Jones, W.D., Chiappe, M.E., Amrein, H., and Vosshall, L.B. (2004). Or83b Encodes a Broadly Expressed Odorant Receptor Essential for Drosophila Olfaction. Neuron 43, 703-714.

Laurent, G. (2002). Olfactory network dynamics and the coding of multidimensional signals. Nat Rev Neurosci 3, 884-895.

Lin, H.H., Lai, J.S., Chin, A.L., Chen, Y.C., and Chiang, A.S. (2007). A map of olfactory representation in the Drosophila mushroom body. Cell 128, 1205-1217.

Linneweber, G.A., Andriatsilavo, M., Dutta, S.B., Bengochea, M., Hellbruegge, L., Liu, G., Ejsmont, R.K., Straw, A.D., Wernet, M., Hiesinger, P.R., and Hassan, B.A. (2020). A neurodevelopmental origin of behavioral individuality in the Drosophila visual system. Science 367, 1112-1119.

Lledo, P.M., Gheusi, G., and Vincent, J.D. (2005). Information processing in the mammalian olfactory system. Physiol Rev 85, 281-317.

Mao, T., O'Connor, D.H., Scheuss, V., Nakai, J., and Svoboda, K. (2008). Characterization and subcellular targeting of GCaMP-type genetically-encoded calcium indicators. PLoS One 3, e1796.

Marin, E.C., Jefferis, G.S., Komiyama, T., Zhu, H., and Luo, L. (2002). Representation of the glomerular olfactory map in the Drosophila brain. Cell 109, 243-255.

McGuire, S.E., Le, P.T., and Davis, R.L. (2001). The role of Drosophila mushroom body signaling in olfactory memory. Science 293, 1330-1333.

Menzel, R., and Muller, U. (1996). Learning and memory in honeybees: from behavior to neural substrates. Annu Rev Neurosci 19, 379-404.

Mittal, A.M., Gupta, D., Singh, A., Lin, A.C., and Gupta, N. (2020). Multiple network properties overcome random connectivity to enable stereotypic sensory responses. Nat Commun 11, 1023.

Mizunami, M., Weibrecht, J.M., and Strausfeld, N.J. (1998). Mushroom bodies of the cockroach: Their participation in place memory. J Comp Neurol 402, 520-537.

Murthy, M., Fiete, I., and Laurent, G. (2008). Testing odor response stereotypy in the Drosophila mushroom body. Neuron 59, 1009-1023.

Neher, E., and Sakaba, T. (2008). Multiple roles of calcium ions in the regulation of neurotransmitter release. Neuron 59, 861-872.

Pigliucci, M. (2010). Genotype-phenotype mapping and the end of the 'genes as blueprint' metaphor. Philos T R Soc B 365, 557-566.

Rusakov, D.A. (2006). Ca2+-dependent mechanisms of presynaptic control at central synapses. Neuroscientist 12, 317-326.

Rytz, R., Croset, V., and Benton, R. (2013). Ionotropic receptors (IRs): chemosensory ionotropic glutamate receptors in Drosophila and beyond. Insect Biochem Mol Biol 43, 888-897.

Sachse, S., and Krieger, J. (2011). Olfaction in insects. e-Neuroforum 2, 49.

Saha, D., Leong, K., Li, C., Peterson, S., Siegel, G., and Raman, B. (2013). A spatiotemporal coding mechanism for background-invariant odor recognition. Nat Neurosci 16, 1830-1839.

Saha, D., Li, C., Peterson, S., Padovano, W., Katta, N., and Raman, B. (2015). Behavioural correlates of combinatorial versus temporal features of odour codes. Nat Commun 6, 6953.

Sarafoleanu, C., Mella, C., Georgescu, M., and Perederco, C. (2009). The importance of the olfactory sense in the human behavior and evolution. J Med Life 2, 196-198.

Schultzhaus, J.N., Saleem, S., Iftikhar, H., and Carney, G.E. (2017). The role of the Drosophila lateral horn in olfactory information processing and behavioral response. J Insect Physiol 98, 29-37.

Shimizu, K., and Stopfer, M. (2017). A Population of Projection Neurons that Inhibits the Lateral Horn but Excites the Antennal Lobe through Chemical Synapses in Drosophila. Frontiers in Neural Circuits 11.

Simpson, J.H. (2009). Mapping and Manipulating Neural Circuits in the Fly Brain. Adv Genet 65, 79-143.

Stern, S., Kirst, C., and Bargmann, C.I. (2017). Neuromodulatory Control of Long-Term Behavioral Patterns and Individuality across Development. Cell 171, 1649-1662 e1610.

Stocker, R.F. (1994). The organization of the chemosensory system in Drosophila melanogaster: a rewiew. Cell and Tissue Research 275, 3-26.

Stopfer, M., Bhagavan, S., Smith, B.H., and Laurent, G. (1997). Impaired odour discrimination on desynchronization of odour-encoding neural assemblies. Nature 390, 70-74.

Stopfer, M., Jayaraman, V., and Laurent, G. (2003). Intensity versus identity coding in an olfactory system. Neuron 39, 991-1004.

Tanaka, N.K., Ito, K., and Stopfer, M. (2009). Odor-evoked neural oscillations in Drosophila are mediated by widely branching interneurons. J Neurosci 29, 8595-8603.

Venkatesh, S., and Naresh Singh, R. (1984). Sensilla on the third antennal segment of Drosophila melanogaster meigen (Diptera : Drosophilidae). International Journal of Insect Morphology and Embryology 13, 51-63.

Vosshall, L.B., Amrein, H., Morozov, P.S., Rzhetsky, A., and Axel, R. (1999). A spatial map of olfactory receptor expression in the Drosophila antenna. Cell 96, 725-736.

Wang, Y., Guo, H.F., Pologruto, T.A., Hannan, F., Hakker, I., Svoboda, K., and Zhong, Y. (2004). Stereotyped odor-evoked activity in the mushroom body of Drosophila revealed by green fluorescent protein-based Ca2+ imaging. J Neurosci 24, 6507-6514.

Wilson, R.I. (2011). Understanding the functional consequences of synaptic specialization: insight from the Drosophila antennal lobe. Curr Opin Neurobiol 21, 254-260.

Wilson, R.I. (2013). Early olfactory processing in Drosophila: mechanisms and principles. Annu Rev Neurosci 36, 217-241.

Wilson, R.I., and Mainen, Z.F. (2006). Early events in olfactory processing. Annu Rev Neurosci 29, 163-201.

Wilson, R.I., Turner, G.C., and Laurent, G. (2004). Transformation of olfactory representations in the Drosophila antennal lobe. Science 303, 366-370.

Wright, G.A., and Schiestl, F.P. (2009). The evolution of floral scent: the influence of olfactory learning by insect pollinators on the honest signalling of floral rewards. Functional Ecology 23, 841-851.

Xu, P.S., Lee, D., and Holy, T.E. (2016). Experience-Dependent Plasticity Drives Individual Differences in Pheromone-Sensing Neurons. Neuron 91, 878-892.

Yaksi, E., and Wilson, R.I. (2010). Electrical Coupling between Olfactory Glomeruli. Neuron 67, 1034-1047.

Zhang, Y., Chen, Y., Bressler, S.L., and Ding, M. (2008). Response preparation and inhibition: the role of the cortical sensorimotor beta rhythm. Neuroscience 156, 238-246.

Zheng, Z.H., Lauritzen, J.S., Perlman, E., Robinson, C.G., Nichols, M., Milkie, D., Torrens, O., Price, J., Fisher, C.B., Sharifi, N., *et al.* (2018). A Complete Electron Microscopy Volume of the Brain of Adult Drosophila melanogaster. Cell 174, 730-+.

Chapter 2: Relating peripheral odor-evoked responses to behavior output

2.1 Summary

The olfactory system is uniquely positioned to warn an organism of environmental threats. Whether and how it encodes such information is not understood. Here, we examined this issue in the fruit fly Drosophila melanogaster. We found that intensity-dependent repulsion to chemicals safeguarded flies from harmful, high-intensity vapor exposures. To understand how sensory input changed as the odor valence switched from innocuous to threatening, we recorded from olfactory receptor neurons (ORNs) in the fly antenna. Primarily, we observed two response non-linearities: recruitment of non-active ORNs at higher intensities, and abrupt transitions in neural excitability from regular spiking to high-firing oscillatory regime. Although non-linearities observed in any single ORN was not a good indicator, a simple linear combination of firing events from multiple neurons provided robust recognition of threating/repulsive olfactory stimuli. In sum, our results reveal how information necessary to avoid environmental threats may also be encoded in the insect antenna.

2.2 Introduction

Animals exhibit various degrees of behavioral preference to olfactory cues. They are attracted by food odors and pheromone, as a way to guarantee their survival and reproduction(Aron, 1979; Bronson, 1979; Reinhard et al., 2004; Wyatt, 2003). On the other hand, odorants produced by toxic substances that signal potential environmental danger lead to aversion(Stensmyr et al.; Zhang et al., 2005). While, odorants tend to maintain their overall odor valence over a wide

range of concentrations, most drastically alter the polarity of odor valence as the concentration increases, i.e. the behavior preference switches from attraction to aversion(Stensmyr et al., 2003). What determines whether an odorant's valence remains constant or changes with intensity?

The early olfactory circuits of Drosophila have been well studied both from an anatomical(Couto et al., 2005a) and functional perspective(Hallem and Carlson, 2006b). However, the rules that govern how sensory stimuli get translated to behavioral outcomes remains poorly understood. For example, changing the intensity of a stimulus is arguably the smallest manipulation to the sensory input possible as only the number of molecules is varied not its identity or other chemical features. Yet, existing behavioral data reveals that for many odorants the overall preference can switch as stimulus intensity is increased beyond a threshold value. This mismatch between the degree of variation in the sensory input and behavioral output raises the following important fundamental question: when and why do the same stimuli repel flies when delivered at higher intensities? And, how is this information encoded?

The repulsion to high intensity chemical vapors has been observed in many species(Poucher, 1974; Stensmyr et al., 2003; Yoshida et al., 2012), although, its significance is yet to be understood. Such a response is particularly confounding considering that many of these stimuli may otherwise not evoke any innate response, or even be attractive to them at lower intensities. How then are such stimuli represented in the olfactory system and what aspects of neural responses change abruptly with intensity? Electrophysiological and imaging studies have shown that increasing odor intensity activates additional olfactory receptor neurons that are not responding at a lower concentration(Duchamp-Viret et al., 2000; Knaden et al., 2012a; Rubin and Katz, 1999; Semmelhack and Wang, 2009). Previous works have proposed that this

recruitment of additional activity might be sufficient to explain both invariance in neural encoding(Asahina et al., 2009) and changes in behavioral response (i.e. 'the recruitment hypothesis')(Suh et al., 2004). If this recruitment hypothesis is indeed true, then behavioral variance with intensity may simply arise as a result of recruiting exclusive sensory channels or 'labelled lines' that mediate aversion(Knaden et al., 2012a; Semmelhack and Wang, 2009). Whether such recruitment of additional activity at higher intensities happens for all or a subset of odorants is not clear. Furthermore, it is unclear whether the spiking activity in these additionally activated receptor neurons alone determines the odor intensity at which the behavioral preference to this stimulus switches from attraction to repulsion.

Here, we explored this issue in the Drosophila olfactory system. We found that flies were repelled by odorants at intensities beyond which the vapors were harmful to them. Exposure of flies to such high-intensity vapors anesthetized them. To understand how the information regarding odorants was encoded as their intensities were altered from innocuous to threatening, we recorded from olfactory receptor neurons on the antenna. Our results indicate that in addition to recruitment of receptor neurons at higher concentrations, abrupt transitions in neural excitability also occur as stimulus intensity is increased. Furthermore, our data reveals that while activity recruitment or excitability changes in receptor neurons may correlate with behavioral preference changes for some select odorants, they do not provide a general rule for translating sensory input to behavior. Notably, our results indicate that total spiking activity in a select few receptor neurons may serve as a robust indicator of changes in behavioral preference with intensity and thereby may act as a neural basis for an early warning signal.

2.3 Methods

2.3.1 Fly Stocks

Flies (Canton-S) were raised on cornmeal medium at 25 ± 1°C under 12:12 light-dark cycle. For

experiments with transgenic flies (Figure 2. 4), ORNs were selectively ablated by crossing UAS-

DTI flies with Or59b-Gal4 or Or85a-Gal4 lines.

2.3.2 Odor Stimuli

7 odorants were used in both electrophysiology and behavior experiments: 2,3-butanedione

(97%, Sigma-Aldrich Co. LLC.), ethyl acetate (99.8%, Sigma-Aldrich Co. LLC.), ethyl butyrate

(99%, Sigma-Aldrich Co. LLC.), ethyl-3-hydroxybutyrate (≥97%, SAFC, Sigma-Aldrich Co.

LLC.), hexanol (≥98%, SAFC, Sigma-Aldrich Co. LLC.), methyl acetate (≥99%, SAFC, Sigma-

Aldrich Co. LLC.), and methyl hexanoate (≥99%, SAFC, Sigma-Aldrich Co. LLC.). Except pure

odors, all dilutions were made by dissolving pure odor solutions in paraffin oil (J.T.Baker).

2.3.3 Single-Sensillum Recordings

Female flies aged from 5-8 days after eclosion were used. To perform extracellular recordings

from receptor neurons we followed a previously published procedure(Dobritsa et al., 2003). The

fly antenna was extended and fixed using a glass capillary on a coverslip. To acquire action

potentials, a glass electrode filled with saline (impedance ~40MΩ) was inserted into the middle

portion of a sensillum. Another reference glass electrode was inserted into the contralateral eye.

The signals were amplified (gain =10; Axon 900A, Molecular Devices) and filtered with a high-

pass filter set to DC and a low-pass filter set at 10kHz. A custom Labview software was used to acquire samples at 15 kHz. No more than two sensilla from the same fly were recorded.

For each of the 7 odors described above, we tested 5 concentrations: undiluted, 10-2, 10-4, 10-6, and 10-8dilutions.

For each trial, 50µL odor dilution was added to a filter paper strip and placed in a Pasteur pipette(Dobritsa et al., 2003). A humidified, carrier air stream at a flowrate of 2000 sccm was directed at the fly antenna throughout the experiment. To present an odor stimulus, a 200 sccm air puff was passed through the filter paper strip containing the odor solution and into the carrier airstream.

Each trial lasted 60s with an intertrial interval > 30s, and the stimulus was delivered from the 10th second to the 11th second of the trial. Odors were presented in pseudo-random blocks based on odor identity. Different concentrations of a single odorant were also presented in a random order, except for the undiluted stimuli which was always presented as the last stimulus in each block.

2.3.4 T-maze Behavior Assay

We used 5 – 8 day old male and female flies. To be consistent with electrophysiology experiments, flies used in our behavioral experiments were also unstarved.

We tested the same 7 odors used in our electrophysiology experiments. Each odorant was presented at the following concentrations: 10-1, 10-2, 10-4, 10-6, and 10-8 v/v.

One piece of folded filter paper was placed at the end of each of the two plastic test tubes (17mm×100mm, 14mL Round-Bottom Polypropylene Tubes, Falcon). After adding 50µL odor

dilution and paraffin oil to the filter papers in each of the two test tubes, they were sealed with

Paraflim (Bemis Company, Inc.). To allow sufficient evaporation of odorants, test tubes were left

undisturbed for ~10mins before further use. For each trial, 150~200 flies were placed into the T-

maze fly chamber. Assays were conducted in a dark room to prevent interference from any visual

cues. Before testing, flies were given 1 min acclimatization time. Then, the fly chamber was

lowered to allow the flies to access the two test tube arms. The flies were given 1 min to make

their decision. The preference index was calculated using the following formula:

$$x = \frac{number \text{ of flies in test tube} - \text{number of flies in control tube}}{\text{total number of flies}}$$

2.3.5 Geotaxis Behavior Assay

Unstarved flies aged between 5-9 days were used. 8-12 flies were placed in test tubes

(17mm×100mm, 14mL Round-Bottom Polypropylene Tubes, Falcon). To prevent flies from

escaping the test tube, a piece of metal mesh was attached to cover the open end of the test tube.

The tube was inverted and kept perpendicular to the table, so the flies could climb toward the top

of the tube. Another test tube was cut off about 1.7 cm from the opening, and one end sealed

using a round glass cover-slip (12-546-2, Fisherbrand) to form a manifold for a filter paper

containing the odor solution. Right before the experiment, 50μL of odor dilution or paraffin oil

was added to the filter paper and placed in this manifold. The test tube with flies was inverted on

top of the odor manifold. The connection between the tubes was sealed with dental wax

(Surgident, Heraeus Kulzer Inc.). The assembly was then placed in front of a red LED panel. Fly

movements on the test tube walls were recorded using a camera (C920, Logitech) at 30 frames/s.

Movies were analyzed using OpenCV 3.0.0 in Python 2.7.10. Region of interest (ROI) was manually picked to track the fly movement. The starting time for each trial was manually set to be the frame at which the assembly was stably placed in front of the background light panel and the camera self-adjusted to a stable setting. Only signals from the blue channel were used, so the frames became gray-scale with each pixel value ranging from 0 to 255. Every frame was thresholded to separate shadows created by flies from those of the test tube itself. Number of pixels with a value below a threshold value (set to 100) was regarded as the total shaded area. To obtain the fly occupancy area (FOA) in each frame, the tube shaded area was subtracted from the total shade area. To compute the tube shaded area, we averaged across all 20000 frames from each movie to obtain the average frame. In the average frame, the shade created by the tube itself was much easier to be differentiated from the ones created by flies. Plot shown in Figure 2.1c was generated by passing area occupied by flies across frames through a 30-point moving average filter and normalized to the maximum of that curve.

2.3.6 Pharmacology

Tetrodotoxin (Sigma-Aldrich Co. LLC.) was dissolved in Ringer solution to a concentration of 50μM/L. The extracellular recording electrode was filled with the diluted TTX solution and inserted into the sensillum. About 10~15 min was given to allow the perfusion of TTX and abolish sodium spikes. The recording was not performed until spontaneous spikes were no longer observable, which was visually checked on an oscilloscope.

2.3.7 Current injection

Positive current 0.8nA was injected into the sensillum through saline filled glass electrode. ORN

activities were recorded for current injection, a low concentration of ethyl acetate, and a

combined stimulus of current (0.8nA) and odorant (ethyl acetate) presented simultaneously to the

antenna. The current injection and odor delivery were 1s in duration.

2.3.8 Determination of response onset

We observed that since the odor puff had to travel a distance before reaching the antenna,

ORN response onsets occurred after varying delays following stimulus onset across experiments.

Therefore, to precisely determine the ORN response onset, we used a metric based on changes in

field potential recorded from the sensillum. More precisely, we computed the first derivative of

the band-pass filtered baseline (2nd order Butterworth band-pass filter, 0.1~5 Hz). The first time

point after stimulus onset when the field potential's derivative exceeds a chosen threshold was

treated as the time of ORN response onset.

For most traces, their response onset was directly decided by its baseline drop. For traces

without a detectable baseline drop at low odor intensities, their response onset was determined

by the average response onsets of the same odor at higher concentrations (pure, 10-2).

Firing event detection

Firing events were detected by a custom routine which in principle detected voltage peaks above

a preset threshold (usually 4.5 times the pre-stimulus baseline s.d.).

When ORN responses enter high-activity levels (typically > 200 Hz), low-amplitude oscillatiory waveforms (LAOs) were observed. Therefore LAOs were extremely difficult to detect using the thresholding method. To address this issue, we developed a template-matching algorithm. In this algorithm, signal segments were binned in a short moving window that was compared with an oscillation waveform template. If the signal segment in a particular moving window was similar enough to the template, then the signal segment was counted as an LAO.

To create a template for oscillation waveform, a trace segment with typical, consistent oscillations was manually selected. In this segment, each oscillatory event could be robustly detected due to their large amplitudes. These oscillatory events were peak aligned and binned so that each bin solely contained the complete waveform of only one oscillatory event. Binned waveforms were each normalized by subtracting the mean and dividing by the standard deviation of signals of each time bin. The normalized waveforms were then averaged over 1875 such normalized oscillatory events to generate a oscillation waveform template.

To clean up the original trace for template matching, detectable supra-threshold firing events, including spikes and oscillations, were first removed. The remaining trace was concatenated and binned into 50 ms non-overlapping time segments. Power was computed for each 50 ms time segment. Consecutive segments with power larger than a preselected threshold were considered to contain LAOs. These LAOs-containing bins were again concatenated and pattern matched with the oscillation waveform template. Signals in the moving window were normalized as described above. The angular distance between the windowed signal (Vs) and template (Vt) was calculated to quantify their similarity. Because the window moved by one data point every step, we could obtain a trace of angular distance with high temporal resolution. The local peaks in the angular distance trace with a value > 0.7 were considered to indicate LAOs.

$$angular\ distance = \cos^{-1}\frac{V_t \cdot V_s}{|V_t||V_s|}$$

$$Power = \frac{1}{n}\sum_{i=1}^{n} x_i^2$$

where x_i is the extracellular voltage recorded at time point i, and n is the total number of time points within a time bin.

2.3.9 Classification analysis

We used a linear, optimal margin classifier- support vector machine (SVM) to predict the behavioral outcome (repulsion or non-repulsion based on T-maze results) given the spike counts from a combination of receptor neurons (present in ab2 or ab3 or both). The length of the window used to compute odor-evoked spike counts was systematically varied to quantify performance for different integration length (50 ms to 20 s). A soft margin version of SVM was used to make it more resistant to outliers. A leave-one-out cross-validation scheme (neural and behavioral data for one odorant at one intensity was left out; 34 odor-intensity combinations for training and 1 odorant-intensity for testing) to quantify our results.

Note since flies passed out before they could make a decision when exposed to pure odorants, they were regarded repulsive for the purposes of this analysis.

When only considering spike counts from the two neurons housed in a single sensillum type (i.e. ab2 alone or ab3 alone), we made predictions based on thresholding the input (i.e. if the input is above the threshold, the odor to be repulsive). The threshold value that resulted in the

lowest training error was used. If multiple thresholds generated similar training errors, then the threshold that divides the data more evenly was picked.

We further tested our hypothesis using a published dataset(Hallem and Carlson, 2006b), which contained mean firing rate of 24 types of ORNs to ten odors at four concentrations (10^{-2}, 10^{-4}, 10^{-6}, and 10^{-8}). We found four odors which are also in our research: ethyl acetate, hexanol, ethyl butyrate and 2,3-butanedione. The calculation of success rate was formulated as an "n choose k" problem, where n denotes the total number of ORN types available, and k denotes the number of pooled ORNs. Within each combination, we summed the firing rates of all k pooled ORNs and threshold the sums. If there existed a threshold that could correctly predict the odor valence, we counted it as a "success". If the total number of combinations and "successes" in a given "n choose k" problem was A and S, respectively. we calculated success rate as S/A.

2.3.10 Modeling of Spikes and Oscillation

We simulated regular spikes and oscillation using a reduced two dimensional Hodgkin-Huxley model (HH model) derived from the standard HH model.

The standard HH model describes the membrane potential of a neuron with a set of four ordinary differential equations (ODEs):

$$C\frac{dV}{dt} = I - g_K n^4 (V - E_K) - g_{Na} m^3 h (V - E_{Na}) - g_L (V - E_L)$$

$$\frac{dx}{dt} = \alpha_x (1 - x) - \beta_x x,$$

, where x can be replaced by n, m, and h. V stands for membrane potential. m, n, and h are gating variables with values in the [0,1] range. C is the membrane capacitance. g_K, g_{Na}, and g_L are the

maximum conductance of potassium, sodium and leak channels, respectively. E_x represents reversal potentials of corresponding channels (E_{Na} = 55 mV, E_k = -77 mV and E_L = -61 mV).

Dimensionality reduced HH model: h can be replaced by a linear function of n, since n+h is almost a constant. m can be approximated by a simple polynomial equation. Thus, the standard HH model can be effectively approximated by a two-dimensional version of the model:

$$C\frac{dV}{dt} = I - g_K n^4 (V - E_K) - g_{Na} m_\infty^3 (0.89 - 1.1n)(V - E_{Na}) - g_L(V - E_L)$$

$$\frac{dn}{dt} = \alpha_n(1 - n) - \beta_n n$$

$$m_\infty = \propto_m \tau_m$$

We set constant value for I to make it a constant stimulus. The membrane potential changes caused by a certain amplitude of input can be obtained by solving the ODEs. To simulate regular spiking activities and oscillations, we set I to equal 10 µA and 175 µA, and obtained firing rates of ~90 Hz and ~340 Hz respectively.

2.3.11 Statistical Tests

No statistical method was used to predetermine the sample size.

Paired-sample t-test was performed to compare firing rates of the same sensillum when exposed to odor at different concentrations. The comparison was only performed between neighboring concentrations. Significance levels (0.05) were Bonferroni-corrected for multiple comparisons.

We performed one-sample t-test on behavioral data to identify concentrations with a mean behavior preference index significantly different from 0 (significance level = 0.05). We tested the normality of data using the Jarque-Bera test.

2.4 Results

2.4.1 Behavioral switch to repulsion at high odor intensities

To identify general trends in dose-dependent behavioral preference changes, we used a stimulus set comprising of seven different odorants. Each stimulus was delivered over a wide concentration range (over seven log-units of magnitude) in order to include innocuous and threatening olfactory valences. It is worth noting that the stimulus set included many fruit-related odorants(Laissue and Vosshall, 2008) such as ethyl acetate, methyl acetate, ethyl butyrate, methyl hexanoate and ethyl-3-hydroxy butyrate. In addition, we included odorants such as 2,3-butanedione and 1-hexanol that are known to inhibit innate avoidance response due to CO_2(Turner and Ray, 2009). We examined the behavioral preference of unstarved flies to each odorant on the panel using a standard T-Maze assay. We found that all seven odorants examined were non-repulsive at lower intensities, but the behavioral preference switched to strong aversion at higher intensities. The threshold concentration at which the preference switched varied a little between two subsets of odorants: 10-2 v/v or 10-1 v/v (Figure 2. 1a). Nevertheless, our behavioral data suggests that the switch in overall behavioral preference with intensity may be a common feature in this sensory modality.

Next, we sought to understand the need for repulsion at higher odor intensities. We found that most flies exposed to odorants beyond the repulsion intensities were anesthetized before they could make a decision to enter a T-maze arm. To quantitatively illustrate this, we used another behavioral assay where flies performing geotaxis were exposed to high-intensity vapors of ethyl acetate. We found such high-intensity vapor exposures were unsuitable to flies, and those performing geotaxis were anesthetized and fell from the walls of the climbing tubes. Whereas, control exposures to paraffin oil had no such effect on flies and they managed to hang onto the walls for the entire duration of the experiment.

We tracked the area of the climbing tube that was occupied by the flies as a function of time. As can be expected, this metric remained stable for flies exposed to the paraffin oil, but reduced to zero for high-intensity ethyl acetate exposures (Figure 2. 1b, c)). This effect of high-intensity ethyl acetate vapors on flies was not observed during low intensity exposures (10^{-4} v/v and 10^{-2} v/v) of the same odorant. It might be worth to note that 10^{-2} v/v was the threshold intensity when the overall behavioral preference switched to repulsion for this odorant. Taken together, these results indicate that repulsive response of flies to high-intensity chemical vapors is a protective mechanism that allows them to avoid exposures to harmful chemicals.
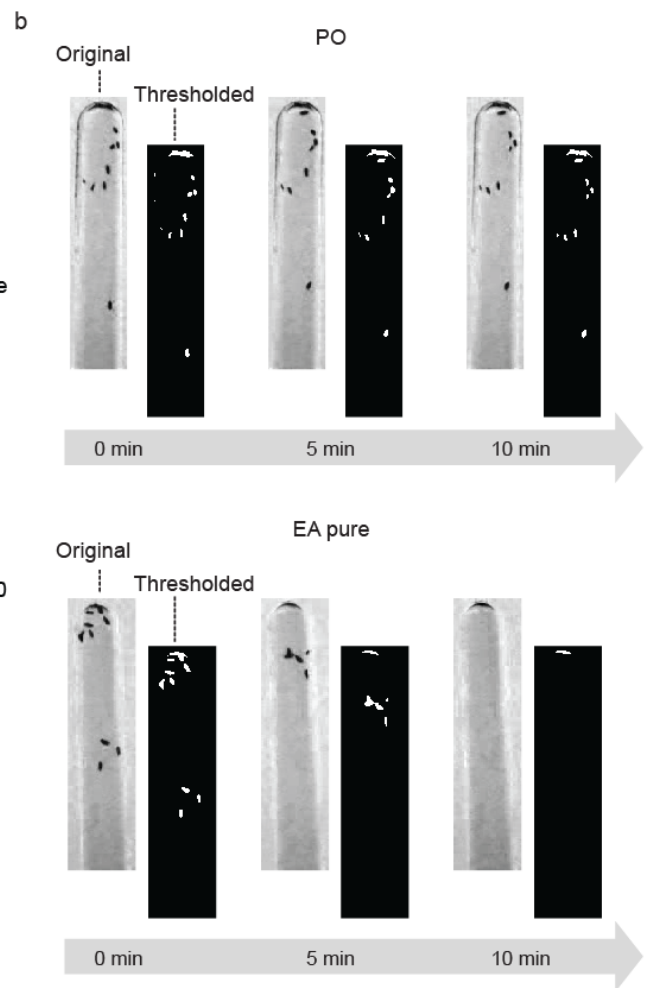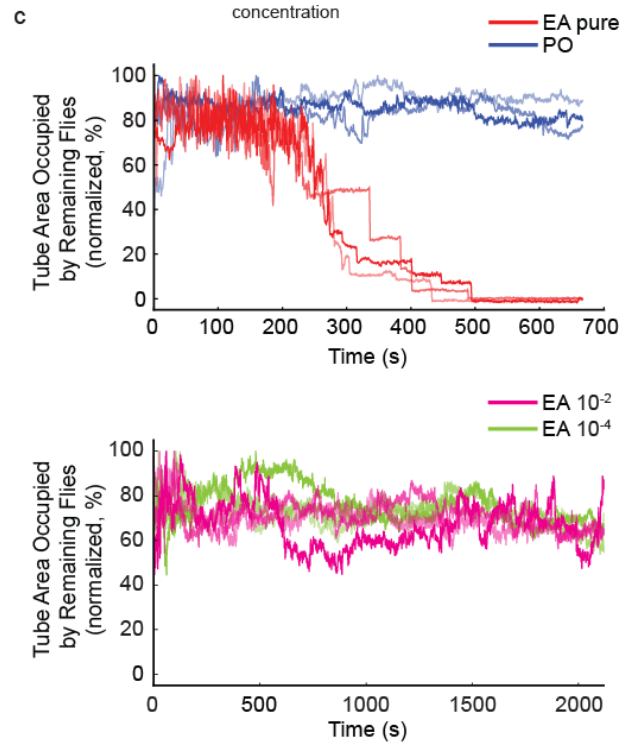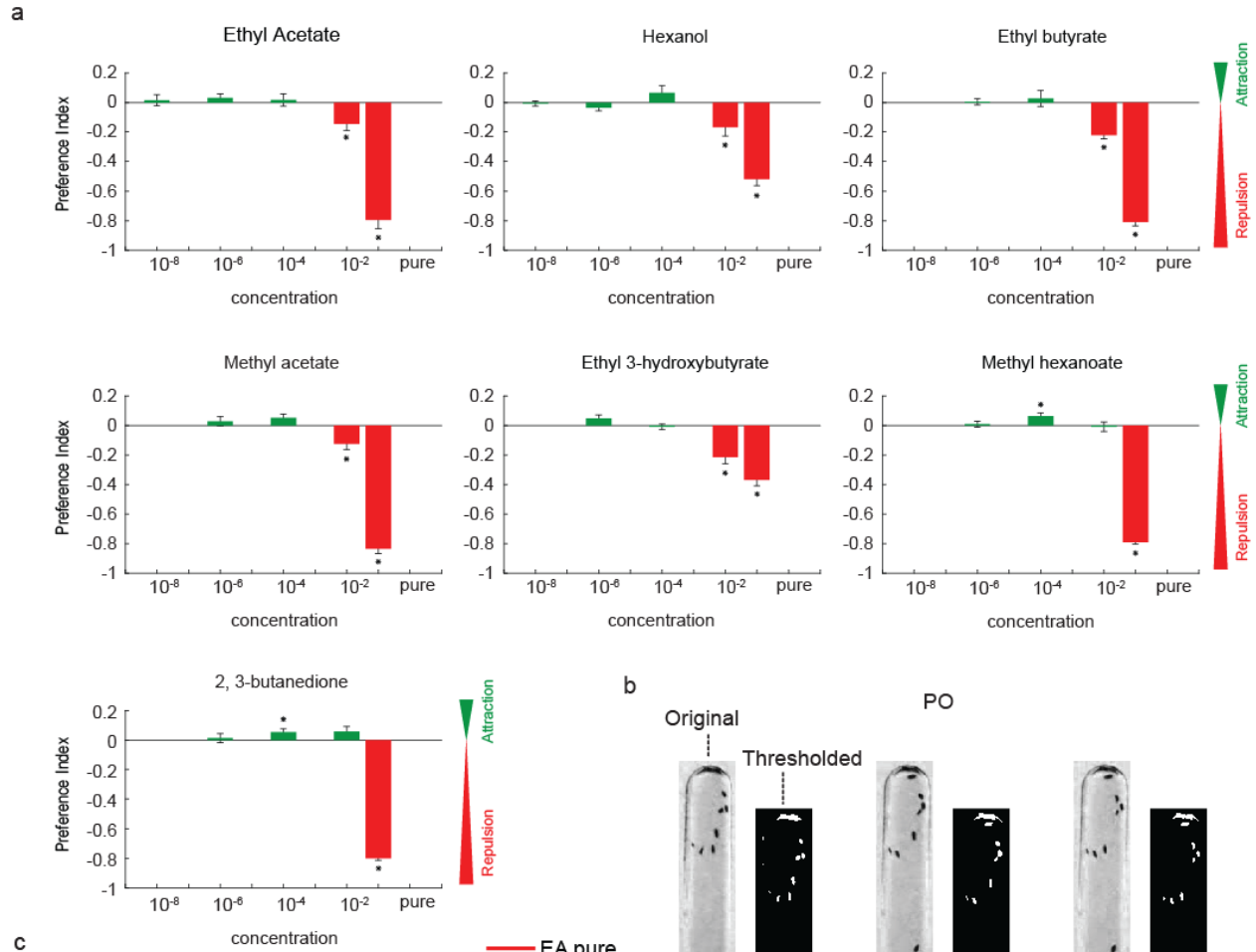
Figure 2.1: Dose-dependent behavioral responses to odorants

a, Behavior preferences of fruit flies to different odor-intensity combinations were assayed using a T-maze assay and shown. Positive and negative preference index values represents attraction and repulsion respectively. Mean ± s.e.m is shown for all concentrations (N = 10 for all concentrations but 10^{-1} concentrations for which N=5). Asterisks indicate significant increase or decrease in behavioral preference values at $p<0.05$.

b, Representative results from a geotaxis assay are shown. Note that while the flies clung onto the test tube walls they were also exposed to either paraffin oil vapors (control; top panel) or ethyl acetate vapors (bottom panel). Both original and the thresholded image highlighting the position of flies (in white) on the test tube walls are shown for three different time points. Note that the number of flies stuck to the walls reduced over time when they were exposed to high-intensity ethyl acetate vapors.

c, The area of test tube wall occupied by flies (y-axis) was tracked as a function of time and plotted for four different conditions: paraffin oil (PO; blue traces in the top panel; n =3), undiluted ethyl acetate vapors (EA; red traces in the top panel; n=3), ethyl acetate at 10^{-2} (magenta traces in the bottom panel; n=3), and 10^{-4} ethyl acetate vapors (green traces in the bottom panel; n=3). Each curve was normalized by its maximum to facilitate comparison across experiments. Note that the area occupied by flies on the tube walls dropped to zero only for all pure ethyl acetate cases.

2.4.2 Olfactory receptor neurons' response non-linearities

Given the drastic change in the behavioral response for all odorants tested, we examined how the sensory input from ORNs change with odor intensity. First, we performed extracellular recordings from fruit fly ORNs in the ab3 sensillum when the antenna was puffed with ethyl acetate vapors at different concentrations (schematically shown in Figure 2. 2a). We found that both neurons in the ab3 sensillum were not activated at low intensities of ethyl acetate exposure but became activated at a threshold concentration of 10-2 v/v (Figure 2. 2b). Since the ab3 neurons were recruited at a certain threshold intensity of the odorant, we examined if this recruitment correlated with the behavioral preference switch. As can be noted, the increase in neural activity in this sensory channel reflects when flies were repelled by ethyl acetate in the T-Maze assay (Figure 2. 2c). Therefore, these neural and behavioral data taken together suggest that recruitment of spiking activities in additional receptor neurons may correlate with intensity-dependent behavioral response switch for ethyl acetate.

Next, we examined how neural activities in other receptor neurons that were strongly activated by ethyl acetate (Or59b expressing ORN housed in the ab2 sensillum) were altered as a function of stimulus intensity (Figure 2. 2a). Consistent with existing data(Hallem and Carlson, 2006b), we found that at lower intensities the spiking activity increased beyond the baseline levels particularly for the ab2A neuron expressing Or59b receptor (Figure 2. 2d). However, as the odor intensity was increased beyond a threshold concentration (10-2 for ethyl acetate) the spiking activity transitioned from clearly distinguishable spikes to a response regime where individual action potentials were no longer resolvable (Figure 2. 2d). Rather, it appeared that spikes collided with each other and generated oscillatory field potential activity with increased power in the high-gamma band (~ 200 Hz; Figure 2. 2f). This oscillatory extracellular activity

38

was detected in all our ab2 sensilla extracellular recordings following exposures to high concentrations of this odorant (n=12). Notably, both the frequency content of the field potential activity and its amplitude varied as a function of ethyl acetate intensity (Figure 2. 2d).

Since we were unable to resolve individual spikes at high intensities, to characterize the dose-response curve, we counted the total number of firing events during any single ethyl acetate exposure and plotted it as a function of odor intensity (Figure 2. 2e; see Methods). The mean dose-response curve was sigmoidal with the number of firing events making an abrupt increase right when the extracellular activity transitioned from spiking to oscillatory field potentials. Interestingly, a qualitatively similar dose-response curve could also be generated by examining the total change in oscillator power in the high-gamma range (Figure 2. 2f,g). More importantly, the switch in behavioral preference for ethyl acetate occurred right at the threshold intensity when the neural activity in the ab2 neurons switched.

These results, taken together suggest that both recruitment of additional receptor neurons' activities and an abrupt switch in receptor neuron firing pattern (from low to high) may both correspond to the switch in the overall behavioral preference for ethyl acetate at higher intensities.
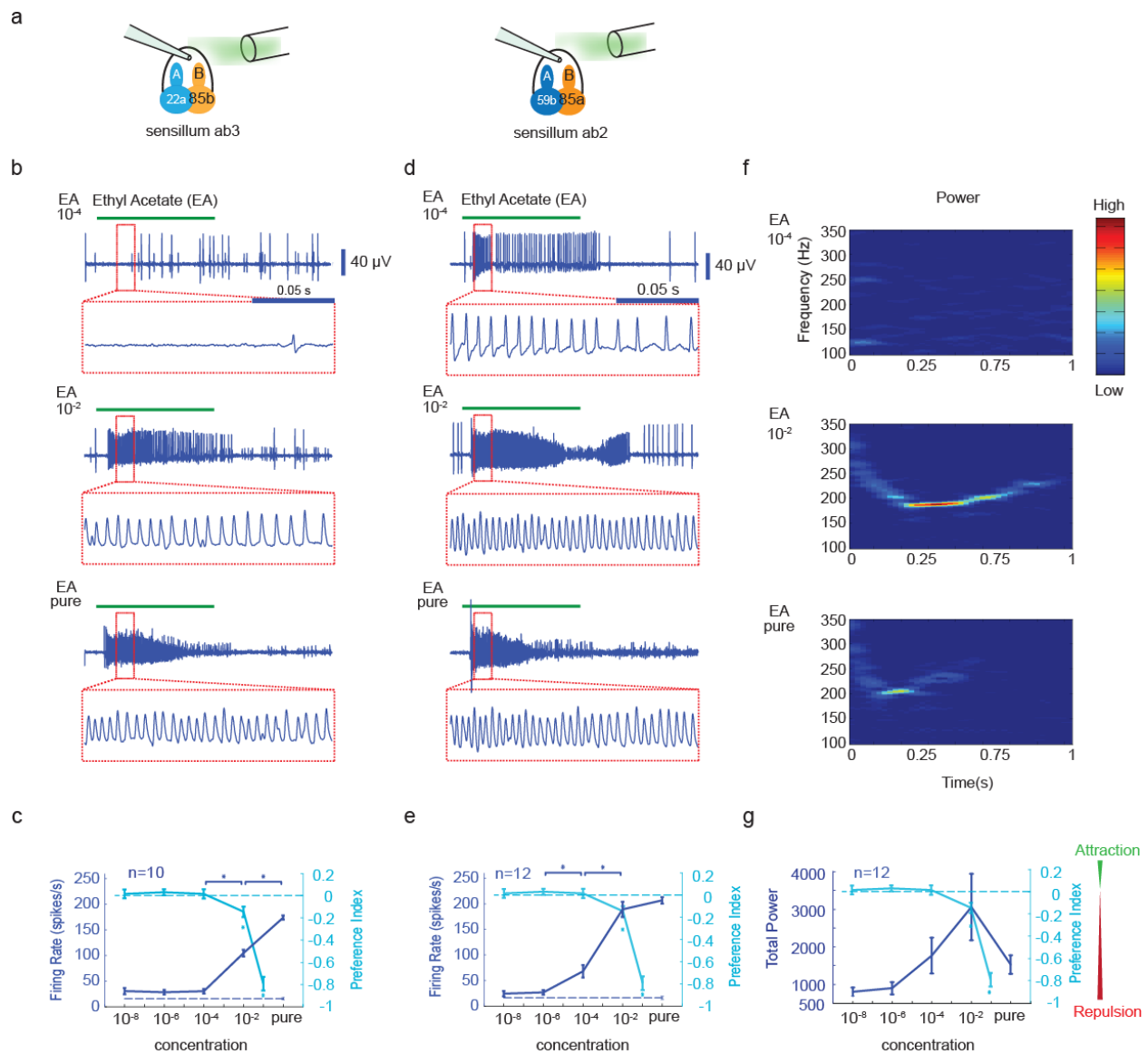
Figure 2.2: Recruitment vs. abrupt transitions in receptor neuron spiking

a. A schematic of ab2 and ab3 sensillum recordings is shown.

b. Representative extracellular recording traces acquired from a ab3 sensillum are shown.
    Raw traces were high-pass filtered at 55 Hz to remove the DC-component. Responses
    elicited by ethyl acetate vapors delivered at 10^{-4}, 10^{-2} and undiluted intensities are shown.
    The green bar above the voltage traces indicate the 1 s time window when the stimulus
    was presented. A small 150 ms segment (red boxes) of the recording was magnified and
    shown underneath each raw trace for clarity.

40

c. The total spiking activity of neurons housed in the ab3 sensillum is plotted as a function of stimulus concentrations (blue, mean±s.e.m.). The dotted line (at the bottom of plot) indicates the spiking activities elicited by paraffin oil exposures. Asterisks indicate significant increase of firing rate compared with the neighboring lower concentration (p<0.05, paired t-tests, n=10 trials). For comparison, the behavioral preference index (cyan, mean±s.e.m.) observed in the T-maze assay for various intensities of ethyl acetate exposures is also shown. Note that the behavioral preference switched to repulsion at 10^{-2} ethyl acetate exposures.

d. Same as 2b, but showing responses of ab2 neurons to ethyl acetate at various intensities. Note that ethyl acetate exposures clearly elicit a detectable response at 10^{-4} dilution. However, note that at higher ethyl acetate intensities only oscillatory field potentials of varying amplitudes are observed.

e. Similar comparison as in panel c, but comparision between firing rates of neurons in ab2 sensilla (blue, mean±s.e.m.) with the behavioral preference (cyan, mean±s.e.m.) is shown for ethyl acetate presented at various concentrations.

f. A moving window power spectra of a representative extracellular trace recorded from ab2 sensillum is shown. Power in the high gamma band frequencies (>150Hz) can be observed during 10^{-2} and undiluted ethyl acetate exposures.

g. Similar comparison as in panel c, but comparison between the total power of signals from ab2 sensilla (blue, mean±s.e.m.) and the behavioral preference (cyan, mean±s.e.m.) is shown for ethyl acetate presented at various concentrations.

2.4.3 Field potential oscillations in olfactory sensillum

How are the receptor neuron oscillations generated? To understand this issue, we added Na+ channel antagonist tetrodotoxin (TTX) to recording glass pipettes(Nagel and Wilson, 2011). This pharmacological manipulation resulted in elimination of all ORN spiking activity and also abolished field potential oscillations observed at high intensities (Figure 2. 3a). However, note

that the DC-component of the sensilla local field potential caused by transduction currents remained unaffected. These results confirm that the field potential oscillations are not an artifact of our extracellular recording approach as they can be abolished using Na+ channel blocker. Furthermore, note that the DC component of the signal is monotonic with odor intensity (Figure 2. 3a). In sum these results suggest that the oscillatory potentials must originate downstream of the transduction machinery possibly due to collision of spikes.

To test the spike collision hypothesis, we examined whether this transition from low firing spiking regime to a high-firing one could be controlled by pairing odor stimulation with electrical stimulation. As noted previously, ethyl acetate at 10-4 dilution elicited clearly resolvable spikes. Similarly, a weak current injection (0.8 nA) alone generated modest increase in spiking activity in the receptor neurons housed in ab2 sensillum. However, when the odor stimulation was combined with the current injection, we found that the extracellular activity transitioned to the oscillatory field potential very similar to those observed at high odor intensities (Figure 2. 3b). These results taken together with the pharmacological manipulation findings confirm that the non-linear switch to a high firing oscillatory field potential regime in ab2 receptor neurons is due to modulation of excitability in these neurons.

Could the recently identified non-synaptic interactions between receptor neurons(Su et al., 2012) influence encoding of stimulus intensity? To examine this issue, we generated transgenic flies with only one functional receptor neuron in the ab2 sensilla. We examined the responses of these transgenic flies to ethyl acetate and compared the same with those obtained from wild-type flies (Figure 2. 4a). Note that transgenic flies with genetically ablated Or85a or Or59b expressing receptor neuron still reveal similar transitions in spiking activity with increase in stimulus intensity (Figure 2. 4a, b). Hence, we conclude that interactions between these receptor neurons

are not necessary to mediate the observed modulation in their excitability.
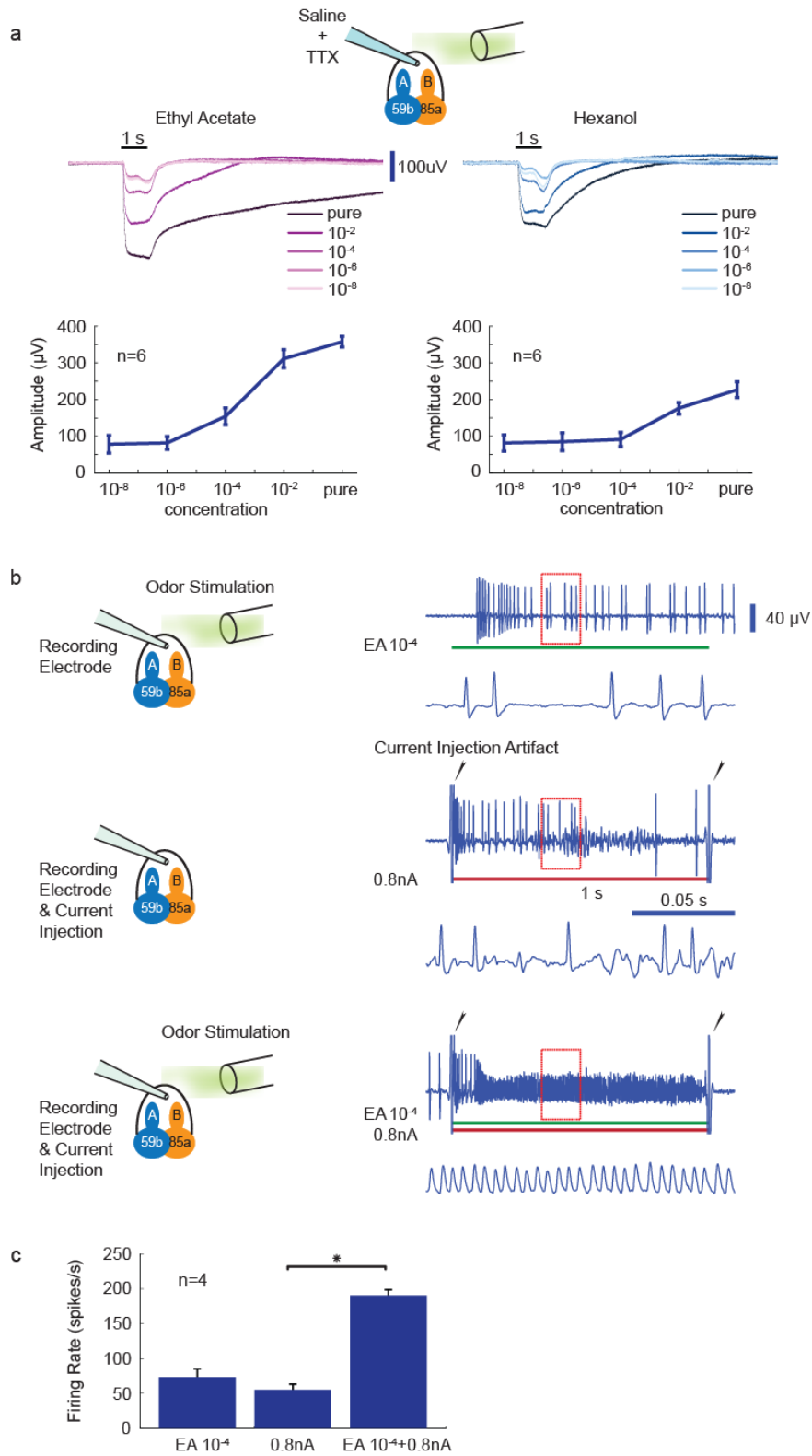
Figure 2.3: Mechanism underlying field potential oscillations in olfactory sensillum

a, Extracellular recordings obtained from an ab2 sensillum with a glass pipette filled with saline and tetrodotoxin (TTX) is shown (see methods). TTX blocked all sodium spikes but the transduction potential due to activation of olfactory receptors by ethyl acetate (left) of hexanol (right) was still observed. The amplitudes of the transduction potential (i.e. magnitude of the DC component) increased monotonically with the concentration for both odorants. Note that neither spikes nor oscillatory field potentials can be observed. Bottom panel: average amplitude of the DC component from 6 trials plotted as a function of stimulus intensities is shown for both ethyl acetate and hexanol.

b, Extracellular recordings obtained from an ab2 sensillum are shown for three different cases: (top row) exposure to 10^{-4} ethyl acetate (second row), direct current injection (0.8 nA) into the sensillum, and (third row) a simultaneous presentation of both ethyl acetate at 10^{-4} and current injection (0.8 nA). The color bars at the bottom of the trace indicate when the odor puff and/or current injections were delivered. Black arrows indicate stimulation artifacts at the onset and offset of current injection. Note that neither odor stimulation (EA at 10^{-4}), nor current injection alone could generate oscillatory extracellular field potentials. However, when they were presented together, oscillations could be observed.

c. Bar plot quantifying the ab2 firing rates observed during the three conditions presented in **panel b**.
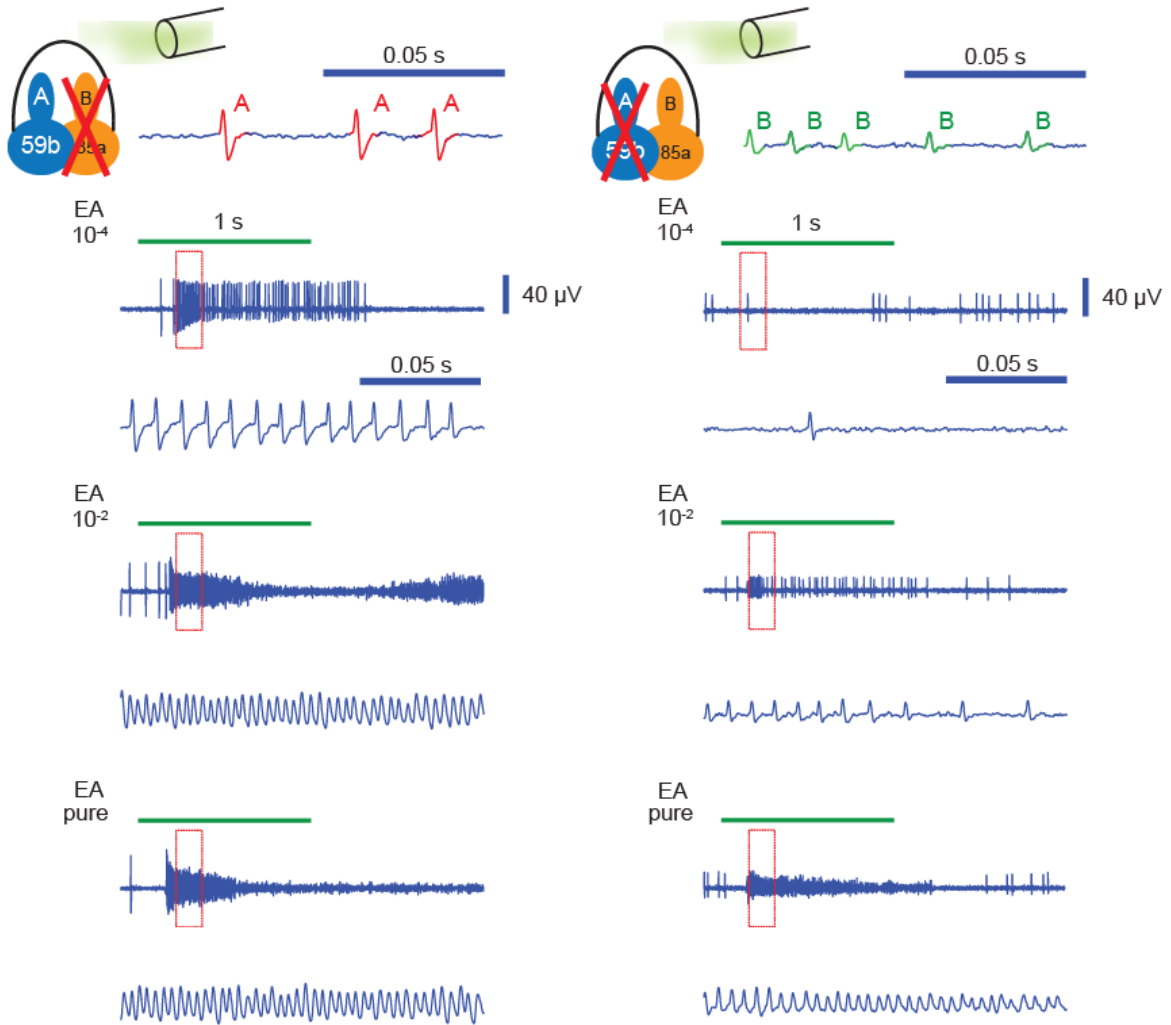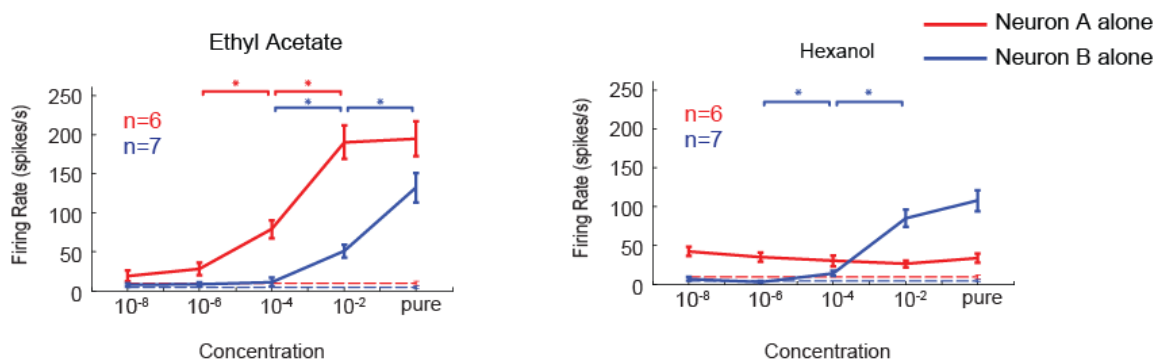
Figure 2.4: Individual receptor neurons can generate oscillatory field potentials

a, Sensillum recording obtained from transgenic flies with either the B neuron (Or85a) or A neuron (Or59b) in the ab2 sensillum ablated are shown. Top: Schematics showing ORN ablation and actual extracellular trace obtained from such genetically modified sensillum are shown. Note only spikes of single amplitude are observed after ablation of one receptor neuron. Bottom panels: Representative extracellular recording traces showing responses elicited by ethyl acetate at different intensities are shown. Note that oscillatory field potentials could still be observed at high ethyl acetate intensities when only A neuron or B neuron remained.

b, EA and Hex Dose-response curves for ab2A and ab2B neurons are shown. Asterisks indicate significant increase of firing rate compared with the neighboring lower concentration (p<0.05, paired t-tests).

2.4.4 Oscillatory dynamics in a Hodgkin-Huxley type neuron

To understand how the same neuron can create firing events of varying shapes, we performed a phase plane analysis of neural excitability for a Hodgkin-Huxley type neuron model (HH model). To perform this 2-d analysis, we reduced the HH model from a system of four ordinary differential equations to two by making two assumptions (see Methods). First, we assumed that the sodium channel activation gating variable 'm' reaches its asymptotic value instantaneously to eliminate one variable. Second, by expressing the sodium channel inactivation gating variable 'h' as a linear function of the potassium channel activation gating variable 'n' we eliminated the second variable.

We found that this reduced HH model could generate spiking activities of different shapes depending on the amplitude of the input current. For depolarizing input up to a certain threshold value, we were able to observe clearly resolvable tri-phasic individual action potential waveforms (Figure 2. 5). Beyond the threshold value, we found the action potential waveform shapes became considerably narrower with smaller peak to trough amplitudes. The spikes produced appeared qualitatively similar to the oscillatory extracellular potentials observed in ORNs during high-intensity odor exposures.

We found that this change in action potential shape was mainly due to the alterations in the dynamics of the fast variable (corresponds to the membrane potential of the neurons, 'V' in the HH model). Note that the shape of the fast variable null cline (the curve along which the membrane potential is held constant) changed depending on the magnitude of the depolarizing current input. This resulted in the shape of the period events changed drastically (i.e. limit cycle in dynamical systems jargon, or, action potentials fired by the neuron model, its biological interpretation). Therefore, these results further support our interpretation that the changes in the spiking activity observed in our receptor neuron recordings could arise due to the changes in ORN excitability.
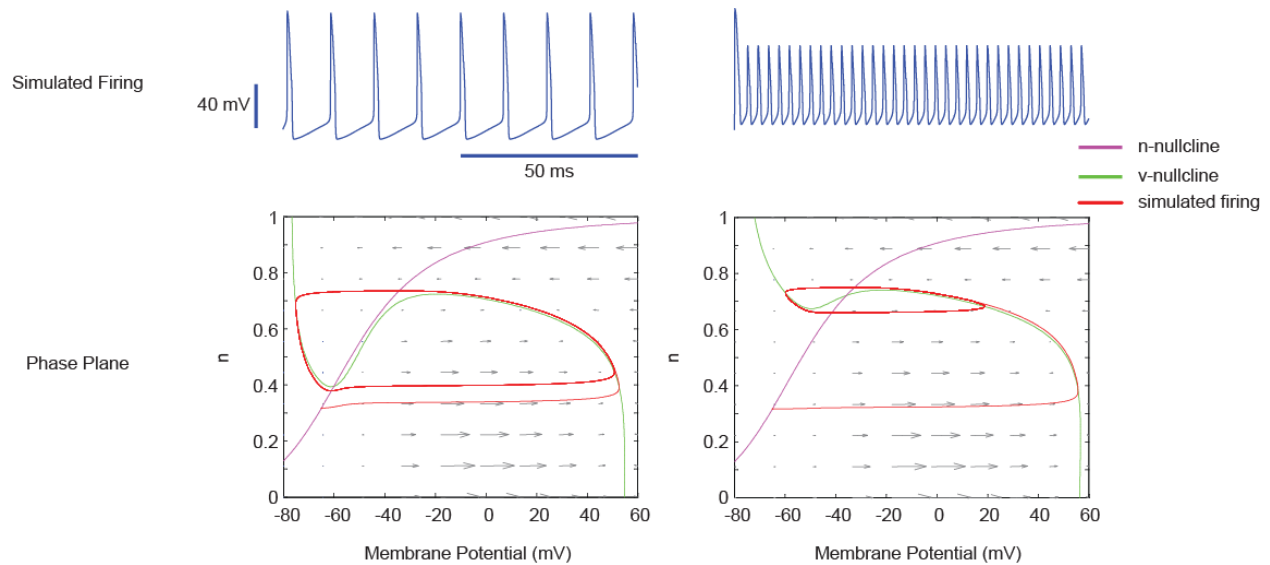
Figure 2.5: Modulation of limit cycle size and shapes in a Hodgkin-Huxley model

Simulated spikes of different amplitudes are shown from a 2-dimensional reduction of Hodgkin-Huxley model are shown (see Methods). All parameters in the model were kept constant for both cases but the amplitude of injected current was substantially increased from 10 µA (left panel) to 175 µA (right panel). Phase-plane analysis: The fast variable (membrane potential; x-axis) is plotted against slow variable (potassium gating variable) for the two different spiking conditions shown above. The fast and slow variable null clines (curves along which the derivatives are zeros) are shown in green and purple, respectively. Gray arrows indicate the direction the system would evolve in the locality of a specific region. The red trace illustrates the simulated firing evolved in the phase plane. Notice that the shape of cubic v-nullcline changes substantially for high current injections thereby making the limit cycle almost bi-phasic.

2.4.5 Rules for predicting behavioral preference changes

Finally, we examined how well spiking activities in receptor neurons (Figure 2. 6.1) correlated with the behavioral preference switch for all odorants in the panel. Our results indicate that spiking activities in ab2 or ab3 receptor neurons when considered individually correlated with the behavioral preference switch in only a select few odorants (Figure 2. 6a). This result was confirmed by plotting the ab2 and ab3 neural spiking response versus behavioral preference for a given odorant at a particular intensity (Figure 2. 6a). A single threshold that separates non-repulsive stimuli from repellent odor-intensity combinations could not be found. However, when we linearly combined the contribution of both these sensory channels, we found that the total activity in these two sensory channels could robustly identify which odorants at what concentrations evoked an attractive or a repulsive response (Figure 2. 6b).

The analyses presented so far examined the segregation of behavioral preferences based on spike counts from two sensory channels but within a specific time window (500 ms from odor onset). How robust are these results when this assumption regarding the spike integration window is removed? To examine this, we compared the prediction performance of an optimal classifier (linear SVM) when the classifier was trained using information obtained from either a single channel (ab2 or ab3; 1-d problem), or from both channels (ab2 and ab3; 2-D problem). We characterized the prediction error for these three cases as a function of spike integration window length (Figure 2. 6c).

We found that the total spiking activities in the ab3 sensory hair alone could provide low prediction error when the integration window was set to a specific value (250 ms). However, beyond this value, the prediction error increased significantly. On the other hand, the total spikes from ab2 sensory hair supported predictions with higher error rates for a wide range of

49

integration window durations. Neither of these two sensory channels, when considered in isolation could support rapid decision making (< 100 ms) with low prediction error. However, the prediction error when spiking responses from both ab2 and ab3 channels were simultaneously considered, the prediction error became less sensitive to the integration window length. Furthermore, as can be expected, the combinatorial approach could achieve the lowest prediction error among all three cases within the first 50 ms after response onset. Since flies are capable of making decisions rapidly (within 100 ms)(Bhandawat et al., 2010; Steck et al., 2012), as might be needed for an escape response, these results further support the need for a readout scheme based on spiking information from multiple sensory channels.

Taken together, our result suggests that a perceptron-like "summation and thresholding" model, in which a linear combination of information from multiple ORN types can robustly explain the behavioral response.

a

b

●	Ethly Acetate
●	Hexanol
●	Ethyl Butyrate
●	Ethyl-3-Hydroxybutyrate
●	Methyl Hexanoate
●	Methyl Acetate
●	2, 3-Butanedione

○ · ● ●

10^{-8} 10^{-8} 10^{-4} 10^{-2}

c

Cross Validation

— ab2 only
— ab3 only
— ab2, ab3 combined
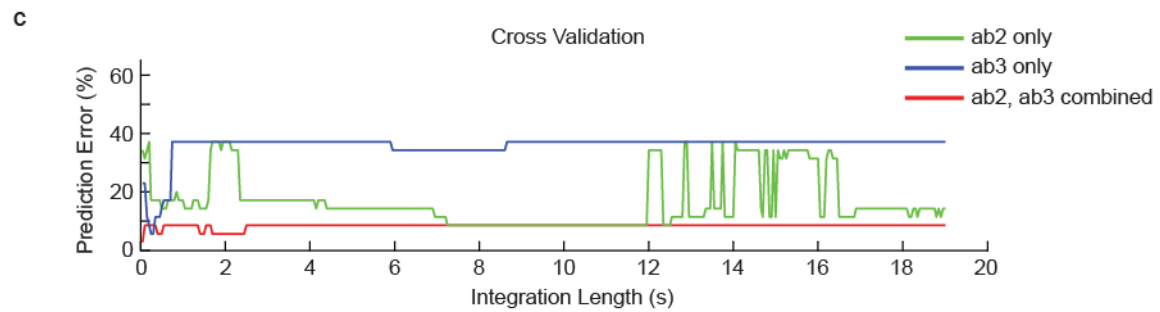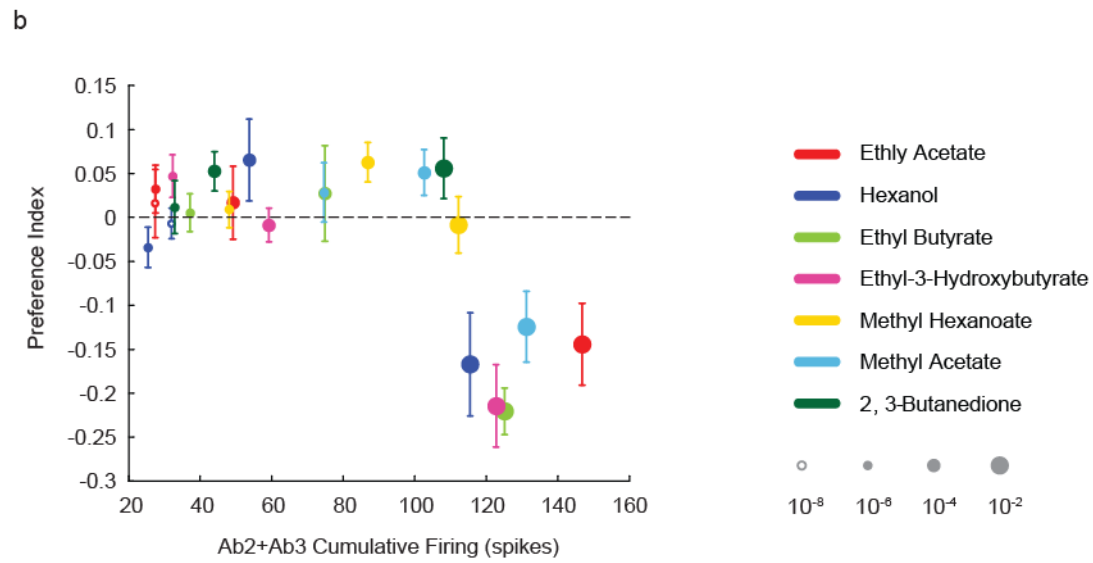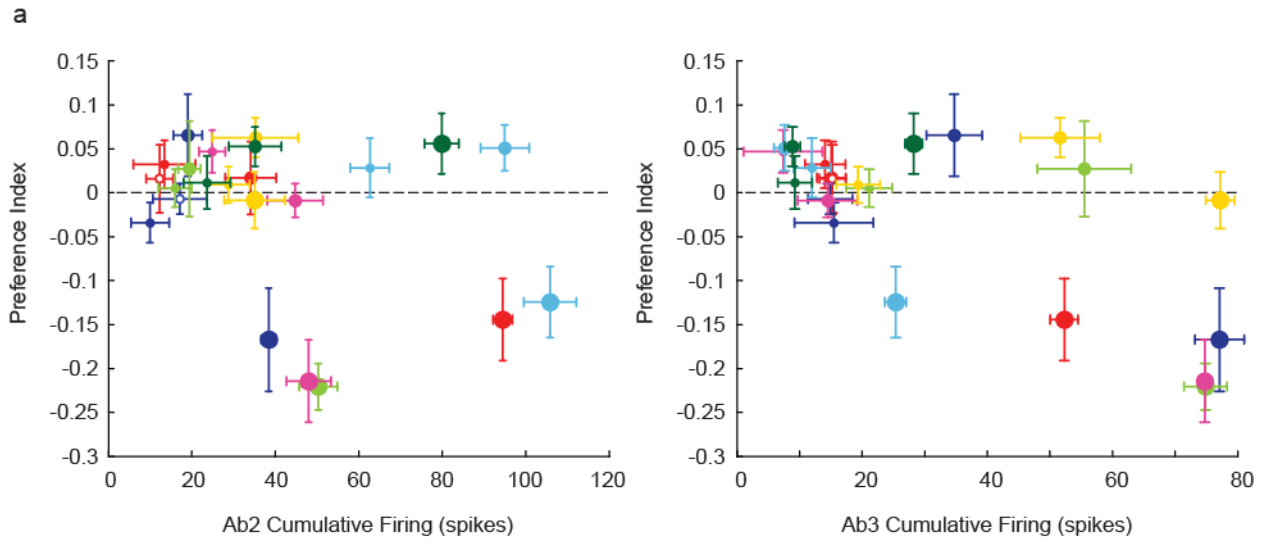
Figure 2.6: Predicting behavioral preference from receptor neuron responses

a, Behavioral preference for each odorant at each intensity (y-axis) is plotted against cumulative spike counts (500 ms integration window since response onset) is shown for both ab2 (left panel) and ab3 (right panel) sensillum. The mean±s.e.m for spiking activity and the behavioral preference values for each stimulus used in the study are shown. The size, fill and color of the marker uniquely identify odor identity – intensity combination. In both panels, note that a single threshold firing rate that reliably separated repulsive odors from non-repulsive ones did not exist.

b, Behavioral preference plotted against the sum of cumulative firing (500ms) from both ab2 and ab3 sensilla are shown. Note that stimuli that evoke less than 110 cumulative spikes/s in these two channels were non-repulsive, whereas those odor-intensity combinations that evoked more than this threshold repelled flies strongly.

c, Performance characterization of an optimal linear classifier is shown for three different cases: (i) using spiking information from ab2 sensilum alone (green) (ii) using spiking information from ab3 sensillim alone (blue), and (iii) using information from both these channels (red). The prediction error is shown for different values of the integration window used to summate the spikes. A leave-one-odor-out cross-validation scheme was used to quantify performance in this plot.
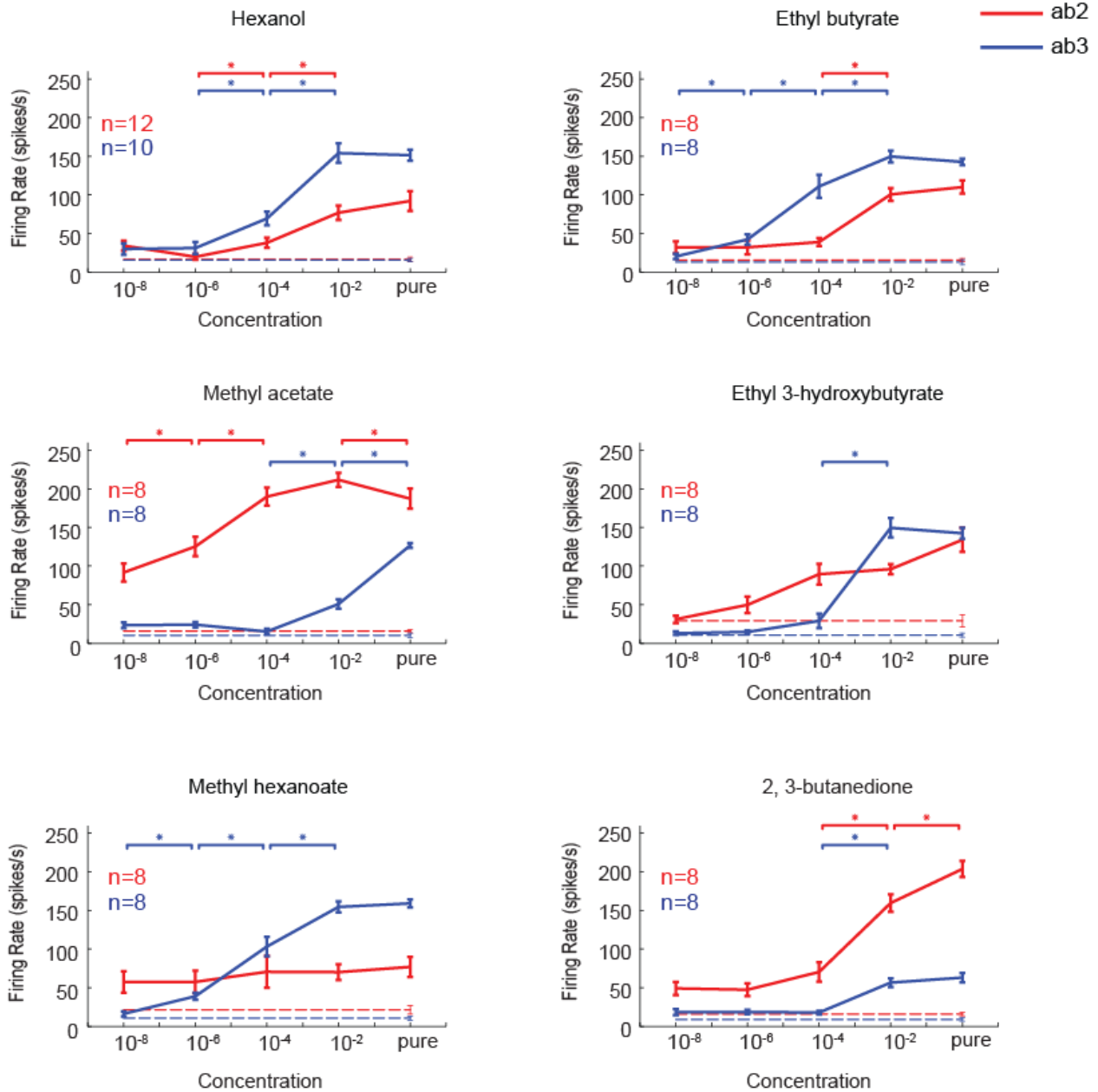
Figure 2.6.1: Dose response curves for both ab2 (red) and ab3 (blue) sensillum is shown for all six odorants used in this study. Asterisks indicate significant increase in firing rate compared with the neighboring lower concentration (p<0.05, paired t-tests). The dashed line indicates firing rate when presenting paraffin oil alone (i.e. the solvent used for diluting the odorants).

2.5 Discussion

The volatile nature of chemosensory cues transduced by the olfactory system indicates that it is well suited to serve as a first responder capable of informing an organism about potential environmental hazards. However, to generate an early warning signal two additional requirement need to be considered. First, given that the set of chemical stimuli that are harmful to an organism may be broad, a more general encoding strategy (many inputs–to–one behavioral outcome) may be required. Second, the sensory cues must be mapped onto a behavioral response that will help avoid such threats (i.e. repulsion). Our results indicate that the Drosophila olfactory system does indeed use a general strategy based on total spikes from multiple sensory channels to encode such information. Furthermore, dose-dependent odor-evoked repulsion observed in many organisms including fruit flies may help avoid such environmental threats.

We found that exposures to most volatile organic chemicals beyond a certain threshold intensity repelled fruit flies. This was true even for those considered to be food odorants(Laissue and Vosshall, 2008; Stensmyr et al., 2003). Exposures beyond this threshold were unviable to flies, and those performing geotaxis during such exposures were anesthetized and fell from the walls of the climbing tubes. To understand how the information regarding odorants were encoded as their intensities was altered from innocuous to threatening for flies, we recorded from olfactory receptor neurons housed in large basiconic sensory hairs on the antenna. Our results indicate that when information from select few receptor neurons in ab2 and ab3 sensillum were combined, we could robustly predict which odorant at what intensity became repellant and therefore not suitable for flies.

To test the robustness of our results and conclusions, we performed a similar classification analyses but using another published dataset(Hallem and Carlson, 2006b). We compared the

54

performances of three different integration strategies to predict the behavioral outcome: (i) combine inputs from all receptor neurons irrespective of which type of sensory hair they are housed in (Figure 2. 6.2a), (ii) integrating spiking responses of all antennal basiconic type ORNs (Figure 2. 6.2b), and (iii) combining signals from select neurons in ab2 and ab3 sensillum (Figure 2. 6.2c; similar to the analysis presented in Figure 2. 6). As a general rule, we found that the classification performance increased monotonically with the number of pooled ORN types (Figure 2. 6.2). However, when the antennal basiconic neurons were exclusively combined classification performance increased much faster and reached higher asymptotic success rates than the 'all ORN strategy' (Figure 2. 6.2b vs. Figure 2. 6.2a). Alternately, when select neurons in ab2 and ab3 sensilla were integrated, again good discrimination between innocuous and repulsive cues were observed. These results further provide an independent corroboration of our findings and suggest that either integration from a sub-type of receptor neurons (i.e. all housed in basiconic type sensory hairs), or from a select few sensory channels provide effective approaches to translate sensory inputs into behavioral outputs.

Previous work on odor-evoked repulsion in flies either using stress-related odorants(Suh et al., 2004) or unsuitable food sources(Stensmyr et al.) suggested a labelled line approach for the transformation of sensory input onto an avoidance response. In this work, our results suggest a combinatorial approach for generating the same motor response. Although these results may potentially be seen at odds with each other, it is quite possible that multiple mapping schemes from stimulus space to behavior could co-exist. Alternately, the combinatorial input from receptor neurons may be transformed to activate labelled lines in the downstream neural circuits that could then evoke repulsion.

These sensory-motor transformations could alternately be viewed from the perspective of metabolic costs. Since spiking is metabolically expensive(Laughlin et al., 1998), the increase in total spiking activities indicate an expensive operation. A previous study using Drosophila larvae found that odorants that evoked more inhibition were also more likely to be repulsive(Kreher et al., 2008). Therefore, a sigmoidal sensory-motor transformation that maps too much or too few spiking (extremes of metabolic costs) onto repulsion seems to account for results reported here by us and elsewhere by others(Kreher et al., 2008). Whether this result is merely correlational or is metabolic costs an important variable that can shape behavioral outcomes needs to be systematically determined.

Finally, we found that at extremely high stimulus intensities, the clearly resolvable spiking activity in individual neurons transformed into oscillatory field potential activity with power in the high-gamma frequencies. We found that this abrupt transition in spiking behavior is largely due to changes in neural excitability and can be abolished with TTX or induced with current injections. Further, such oscillatory activities can be observed when multiple cues, which by themselves do not generate such a response, are combined. Indeed, we found that olfactory mixtures reported in another pioneering study on non-synaptic inhibition between co-housed receptor neurons did indeed evoke oscillatory field potentials of varying amplitudes similar to those reported here. Therefore, we conclude that complex changes in spiking behavior of receptor neurons can simply be induced due neural excitability modulations and without any coupling between them.

What then might be the need for such high activity regimes, given the strong synapses between the receptor neurons and their downstream targets in the antennal lobe(Wilson, 2013), and the recent report that behavioral response can be generated with modest number of spikes(Bell and

Wilson, 2016)? It is possible that such responses may be an unavoidable consequence of having high sensitivity to food-related odorants. While responses to extremely low concentrations may guarantee sustenance, a compensatory mechanism might be needed to avoid the same odorants

when they become unsuitable.
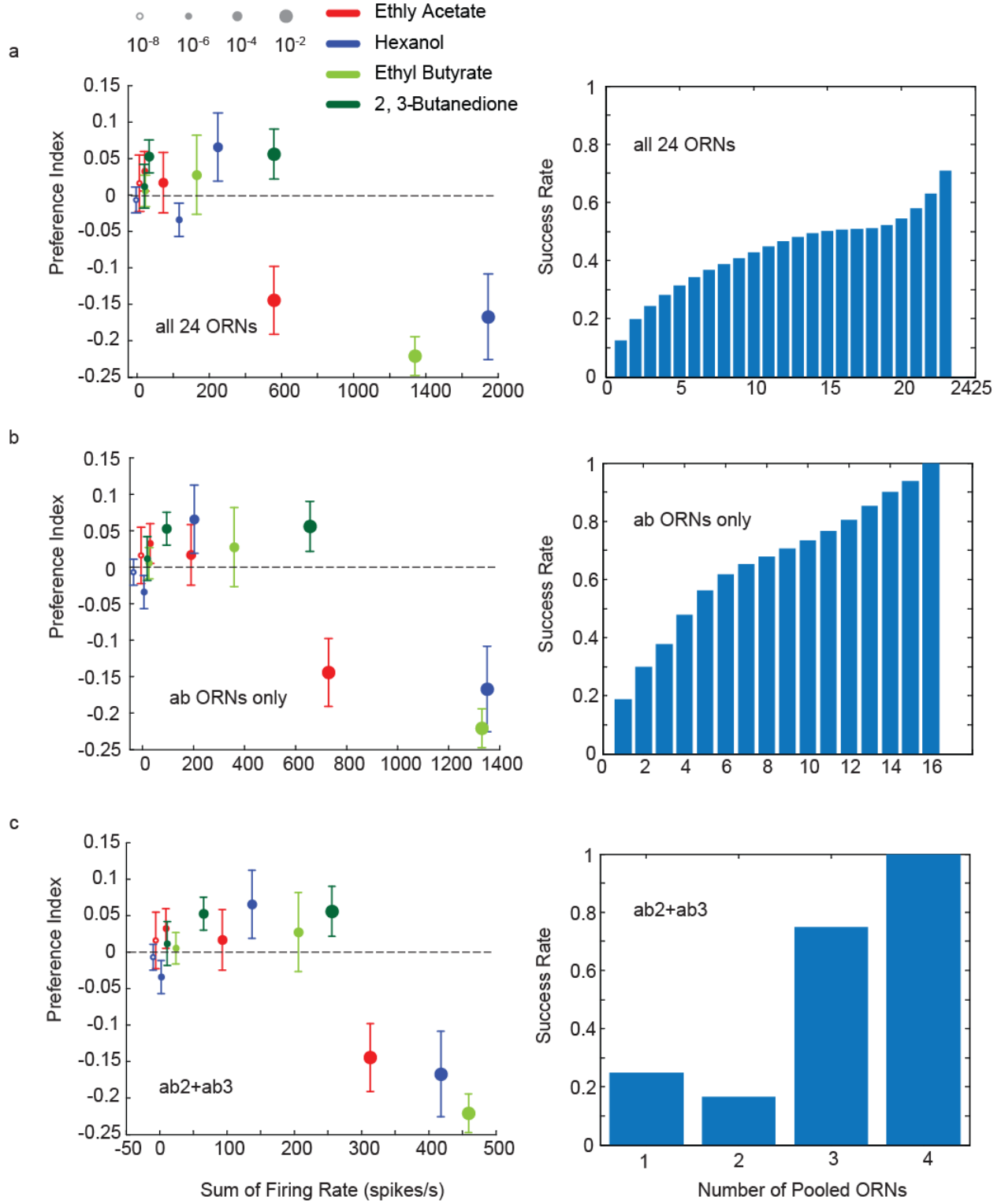
Figure 2.6.2: Independent validatiion of our results using a published dataset

a, Similar plots as in **Figure 2. 6** but plotting the behavioral preference indices obtained in our T-maze experiments against cumulative spike counts of 24 different types of receptor neurons published in Hallem and Calrson (2006). Right panel reveals that monotonic increase in performance (i.e. correct recognition of the repulsive stimuli) as the number of neurons pooled for the analysis was systematically increased. Mean performance across different combinations of realizing a particular number of ORNs is shown along with SEM (i.e. 24 choose 'n' for any n ORN combination).

b. Similar plot as in panel a, but revealing prediction performance when selectively combining spiking activities of all ORNs housed in antennal basiconic type sensilla is shown.

c. Repeat of analysis in Figure 2. 6b but using Hallem and Carlson (2006) data. Note that the analysis was limited to four odorants used in both our work and in the previous study.

2.6 References:

1   Bronson, F. H. The Reproductive Ecology of the House Mouse. *The Quarterly Review of Biology* **54**, 265-299 (1979).

2   Aron, C. Mechanisms of control of the reproductive function by olfactory stimuli in female mammals. *Physiological Reviews* **59**, 229-284 (1979).

3   Wyatt, T. D. Pheromones and animal behaviour: communication by smell and taste. (Cambridge University Press, 2003).

4   Reinhard, J., Srinivasan, M. V. & Zhang, S. Olfaction: scent-triggered navigation in honeybees. *Nature* **427**, 411-411 (2004).

5   Stensmyr, Marcus C. *et al.* A Conserved Dedicated Olfactory Circuit for Detecting Harmful Microbes in Drosophila. *Cell* **151**, 1345-1357, doi:10.1016/j.cell.2012.09.046.

6   Zhang, Y., Lu, H. & Bargmann, C. I. Pathogenic bacteria induce aversive olfactory learning in Caenorhabditis elegans. *Nature* **438**, 179-184, doi:http://www.nature.com/nature/journal/v438/n7065/suppinfo/nature04216_S1.html (2005).

7   Stensmyr, M. C., Giordano, E., Balloi, A., Angioy, A. M. & Hansson, B. S. Novel natural ligands for Drosophila olfactory receptor neurones. *The Journal of experimental biology* **206**, 715-724 (2003).

8   Couto, A., Alenius, M. & Dickson, B. J. Molecular, anatomical, and functional organization of the Drosophila olfactory system. *Current biology : CB* **15**, 1535-1547, doi:10.1016/j.cub.2005.07.034 (2005).

9   Hallem, E. A. & Carlson, J. R. Coding of odors by a receptor repertoire. *Cell* **125**, 143-160 (2006).

10   Poucher, W. A. *Perfumes, Cosmetics and Soaps*. 7 edn, (Chapman and Hall, 1974).

11   Yoshida, K. *et al.* Odour concentration-dependent olfactory preference change in C. elegans. *Nature Communications* **3**, 739, doi:10.1038/ncomms1750 http://www.nature.com/articles/ncomms1750#supplementary-information (2012).

12   Knaden, M., Strutz, A., Ahsan, J., Sachse, S. & Hansson, B. S. Spatial representation of odorant valence in an insect brain. *Cell reports* **1**, 392-399, doi:10.1016/j.celrep.2012.03.002 (2012).

13   Semmelhack, J. & Wang, J. W. Select *Drosophila* glomeruli mediate innate olfactory attraction and aversion. *Nature* **459**, 218-223 (2009).

14   Duchamp-Viret, P., Duchamp, A. & Chaput, M. A. Peripheral odor coding in the rat and frog: quality and intensity specification. *The Journal of neuroscience : the official journal of the Society for Neuroscience* **20**, 2383-2390 (2000).

15   Rubin, B. D. & Katz, L. C. Optical imaging of odorant representations in the mammalian olfactory bulb. *Neuron* **23**, 499-511 (1999).

16   Asahina, K., Louis, M., Piccinotti, S. & Vosshall, L. B. A circuit supporting concentration-invariant odor perception in Drosophila. *Journal of Biology* **8**, 9, doi:10.1186/jbiol108 (2009).

17   Suh, G. S. B. *et al.* A single population of olfactory sensory neurons mediates an innate avoidance behaviour in Drosophila. *Nature* **431**, 854-859, doi:http://www.nature.com/nature/journal/v431/n7010/suppinfo/nature02980_S1.html (2004).

18   Laissue, P. P. & Vosshall, L. B. in *Brain Development in Drosophila melanogaster* (ed Gerhard M. Technau) 102-114 (Springer New York, 2008).

19   Turner, S. L. & Ray, A. Modification of CO2 avoidance behaviour in Drosophila by inhibitory odorants. *Nature* **461**, 277-281, doi:http://www.nature.com/nature/journal/v461/n7261/suppinfo/nature08295_S1.html (2009).

20   Nagel, K. I. & Wilson, R. I. Biophysical mechanisms underlying olfactory receptor neuron dynamics. *Nat Neurosci* **14**, 208-216, doi:http://www.nature.com/neuro/journal/v14/n2/abs/nn.2725.html#supplementary-information (2011).

21   Su, C.-Y., Menuz, K., Reisert, J. & Carlson, J. R. Non-synaptic inhibition between grouped neurons in an olfactory circuit. *Nature* **492**, 66-71, doi:http://www.nature.com/nature/journal/v492/n7427/abs/nature11712.html#supplementary-information (2012).

22   Bhandawat, V., Maimon, G., Dickinson, M. H. & Wilson, R. I. Olfactory modulation of flight in Drosophila is sensitive, selective and rapid. *The Journal of experimental biology* **213**, 3625-3635, doi:10.1242/jeb.040402 (2010).

23   Steck, K. *et al.* A high-throughput behavioral paradigm for Drosophila olfaction - The Flywalk. *Scientific Reports* **2**, 361, doi:10.1038/srep00361 http://www.nature.com/articles/srep00361#supplementary-information (2012).

24   Laughlin, S. B., de Ruyter van Steveninck, R. R. & Anderson, J. C. The metabolic cost of neural information. *Nat Neurosci* **1**, 36-41 (1998).

25   Kreher, S. A., Mathew, D., Kim, J. & Carlson, J. R. Translation of sensory input into behavioral output via an olfactory system. *Neuron* **59**, 110-124, doi:10.1016/j.neuron.2008.06.010 (2008).

26   Wilson, R. I. Early olfactory processing in Drosophila: mechanisms and principles. *Annual review of neuroscience* **36**, 217-241, doi:10.1146/annurev-neuro-062111-150533 (2013).

27   Bell, Joseph S. & Wilson, Rachel I. Behavior Reveals Selective Summation and Max Pooling among Olfactory Processing Channels. *Neuron* **91**, 425-438, doi:http://dx.doi.org/10.1016/j.neuron.2016.06.011 (2016).

28   Dobritsa, A. A., van der Goes van Naters, W., Warr, C. G., Steinbrecht, R. A. & Carlson, J. R. Integrating the Molecular and Cellular Basis of Odor Coding in the Drosophila Antenna. *Neuron* **37**, 827-841, doi:https://doi.org/10.1016/S0896-6273(03)00094-1 (2003).

Chapter 3: Functional Organization of the Olfactory Circuits and the Temporal Evolution of Stimulus Encoding

3.1 Introduction

Most neuronal networks consist of many sub-types of neurons that interact through different microcircuits and actively reorganize the information they receive. To fully understand the information processing carried out, at a bare minimum three pieces of information are essential. First, it is necessary to understand the input received by the network. Second, to understand what computations arise from which microcircuit, it is necessary to follow this input signal as it propagates from one processing compartment to the next. And, third, it is necessary to understand how different neuronal sub-types that are present in these circuits contribute to the information processing. An additional layer of investigation could be added by comparing how information is represented by equivalent circuits in different individuals. This would allow us to understand what are the generic rules of signal processing and information transformation, and help identify any idiosyncratic features that may be utilized in different individuals. Understanding such idiosyncrasies in neural encoding can arguably help us better understand a source of variance in behavioral outcomes observed across individuals. Here, we dissect how odor signals are organized and processed as it propagates through the fruit fly (*Drosophila melanogaster*) antennal lobe neural network.

In the fruit fly olfactory system, vapors from volatile chemicals are transduced into neural responses by olfactory receptor neurons (ORN) present in the antenna that then transmit this information to a region called the antennal lobe (analogous to the mammalian olfactory bulb).

The ORNs of the same type, i.e. expressing the same receptor–co-receptor gene combination, send their axons to either one or two spherical structure of neuropil called glomeruli in the antennal lobe(Couto et al., 2005b; Fishilevich and Vosshall, 2005). The ORN activity drives responses in three major types of neurons in the antennal lobe: GABAergic local neurons (LNs), cholinergic projection neurons (excitatory PNs or ePNs) and GABAergic projection neurons (inhibitory PNs or iPNs). The local neurons are diverse(Chou et al., 2010), and play important roles in how sensory signals are processed within the antennal lobe(Olsen and Wilson, 2008; Yaksi and Wilson, 2010b) . However, LNs do not send their processes outside the antennal lobe, and thus only the activity ePNs and iPNs constitute the outputs from this olfactory neuronal network.

Notably, the ePNs and iPNs differ in how they receive inputs and transmit their output. The ePN dendrites innervate a single glomerulus and therefore receive input from a single ORN type(Couto et al., 2005b). The ePNs project their axons onto both mushroom body (a center associated with learning and memory(Debelle and Heisenberg, 1994; Heisenberg et al., 1985)) and lateral horn (a region with putative role in driving innate behavior(Gupta and Stopfer, 2012; Heimbeck et al., 2001). In contrast, iPNs dendrites are multi-glomerular and therefore integrate information distributed across several different ORN types. The iPN axons are also exclusively sent to the lateral horns. The ePNs and iPNs can influence each other's activity through chemical synapses(Shimizu and Stopfer, 2017). While the importance of the ePN and iPN activity for odor recognition is well established(Ahsan et al., 2017; Parnas et al., 2013; Strutz et al., 2014) , how the ePN and iPN activities are spatially organized and patterned over time to facilitate odor recognition remains poorly understood.

In this study, we used an *in vivo,* light-sheet, volumetric, calcium-imaging technique to examine this issue with high spatial and temporal resolution. We monitored the odor-evoked signals at the ORN axons entering the antennal lobe (input), the responses they drive in ePNs dendrites located within the antennal lobe, and ePN and iPNs axons (output) entering mushroom body calyx and lateral horn (iPNs only project to the latter). Using this approach, we examined how odorants-evoked responses are patterned over space and time in each of these neural population. We examined the functional mapping between dendritic and axonal compartments to understand the antennal lobe input-output relationships, and how feed-forward excitation and feed-forward inhibition converge onto lateral horn. Lastly, comparison across flies helped understand generic odor coding principles and how they might arise from idiosyncratic processing mechanisms utilized within the antennal lobe network.

3.2 Methods

3.2.1 Fly strains and culture conditions/Fly stocks

Flies were raised on a standard cornmeal diet. Vials were kept at 25°C with 12h:12h light-dark cycle. Females 2~6 days after eclosion were used for experiments.

The following fly genotypes were used:

A series of crosses were conducted among

w[1118]; P{y[+t7.7] w[+mC]=20XUAS-IVS-GCaMP6f}attP40

T(2;3)ap[Xa]/CyO; TM6, Sb

 w[*]; P{w[+mC]=UAS-mCD8::GFP.L}LL5/CyO; P{w[+mW.hs]=Orco-RFP.K}10D

and their hybrid progenies to obtain UAS-GCamp6f; Orco-RFP flies, which were used for

crosses with the olfactory neuron tagging GAL4 lines respectively:

w[*]; P{w[+mC]=Orco-GAL4.W}11.17; TM2/TM6B, Tb[1] (Orco-GAL4)

y[1] w[1118]; P{w[+mW.hs]=GawB}GH146 (GH146-GAL4)

Pin/CyO;GAL4-MZ699/TM6B (Mz699-GAL4)

The resulting progenies expressed GCamp6f under the control of neuronal-population-specific

drivers (Orco for ORNs, GH146 for ePNs, Mz699 for iPNs) along with RFP expressed in Orco

neurons.

3.2.2 Dissection procedure

The fly was cold-anaesthetized and tethered onto a custom made plexiglass block modified from

an earlier work(Silbering et al., 2012). The antennae were kept underneath the tape film, exposed

to the air flow, while the dorsal side of the fly head was immersed in external saline containing

(in mM): 103 NaCl, 3 KCl, 5 N-tris(hydroxymethyl) methyl-2- aminoethane-sulfonic acid, 8

trehalose, 10 glucose, 26 $NaHCO_3$, 1 NaH_2PO_4, 1.5 $CaCl_2$, and 4 $MgCl_2$ (osmolarity adjusted to

270-275 mOsm) (Badel et al., 2016; Jeanne et al., 2018). Dorsal cuticle was removed. Trachea

and stray tissue were cleaned with 5sf forceps (Fine Science Tools). Muscle 16 was cut to

stabilize the brain.

3.2.3 Odor Stimulation

Chemicals were diluted in paraffin oil. In each odor bottle, 20 ml of diluted odor solution (vol/vol) was added. Each batch of odor stimulus was used for no more than 10 days. Stimuli were delivered via a custom-made 16-channel olfactometer. Control signals to the solenoid valves were coupled with microscope control signals. For all experiments carried out in this study, the odor stimulus was 4 s in duration. The onset of an odor stimulus was aligned with the onset of an image stack acquisition. The main air tube was directed at the fly, about 2 cm from the fly. A funnel connected to a vacuum line was placed about 5 cm from the fly block to remove odor residuals.

Stimuli were presented in blocks. The first block comprised of 2~5 trials, during which only spontaneous activities were recorded. To minimize the adaptation and stimulus history related interference that arose due to high neural activities, the odor panel at the lower dilution (10^{-4} v/v) stimuli were pseudorandomized and presented first. Inter-block interval was a minimum of three minutes. Subsequently, a block of odor presentations where each stimulus was delivered at the higher concentration (10^{-2} v/v). The odorants were delivered in the same sequence in both low and high concentration blocks. Then, we again alternated between the low and high concentration blocks at least once more in each fly. Typically, the inter-trial interval within in block was 1 minute. However, for few odorants like 1o30, larger ITI (~1.5 – 2.5 min) were given after stimuli to minimize their interference on the subsequent trial.

3.2.4 *In vivo* light-sheet imaging

A custom-made light sheet microscope(Greer and Holy, 2019) was used to record imaging data. The microscope has two channels, which we used for recording GCaMP6f and RFP signals simultaneously.

We imaged at $\times 20$ magnification, which provided sufficient resolution for reliable identification of the target neural structures. The typical image size was 1260×60pixels, with pixel size being $0.325\mu m \times 0.325\mu m$. The centers of neighboring planes are about 8 μm apart on average. Note each "plane" is in fact a thin volume, as the light sheet kept sweeping through the tissue during the short camera exposure. At most 1 μm (upper bound) may be missed between two optical planes, which is smaller than the neural structures of interest.

Each brain volume was sampled at 4 Hz. For ePN and iPN recordings, a volume of ~190 μm thickness were scanned through along the axis of piezo movement (z-axis) to cover both the antennal lobe and calyx/lateral horn as these regions reside in different optical planes. The data from iPN dendrites were discarded from subsequent analysis due to the extremely low GCamp6f signal in the region. Calcium signals from a volume of ~80 μm thickness was recorded for monitoring responses at the ORN axonal terminals in the antennal lobe.

488 nm and 561 nm lasers were used to excite both the GCamp6f and RFP, respectively. The timings of the two lasers were synchronized to ensure the RFP images were acquired at the same time instances as GCamp signals. The lasers were only turned on during the camera exposure to reduce photobleaching.

During imaging experiments, external saline oxygenated with $95\%O_2/5\%CO_2$ (Airgas), was perfused at 2mL/min. Only flies that showed some change in calcium signals during a paraffin

oil puff or 10^{-4} odor test pulse were chosen for formal recording. Data acquisition began at least 5 min after the end of the test pulse.

3.2.5 Motion correction

We pre-processed the imaging data to correct for motion artifacts during acquisition. As the functional imaging movies generally contain flashing activities of neural response, it's difficult to obtain static reference template. We found that most of the motion artifacts, if present, in our datasets were due to translational displacements. To remove these artefacts, we used two different strategies to account for motion artifacts in the antennal lobe and in the lateral horn. In antennal lobe, we first corrected the motion using simultaneously acquired anatomical imaging data (RFP labeled ORN axons). Using the anatomical dataset, we found the translation correction matrix that maximized the correlation value between the target frame and template frame. Then we used this translation matrix to function recordings in the antennal lobe and obtained motion corrected imaging data. In the lateral horn, we learned the translation matrix by focusing on the less responsive regions (neural tracts). The obtained translation matrix was used to correct for the overall motion artifacts in the whole image.

3.2.6 Identifying response regions of calcium imaging data

We identified regions of interest (ROIs) by applying a constrained nonnegative matrix factorization (Pnevmatikakis et al., 2016). The spatiotemporal calcium activity can be expressed as a product of a spatial basis matrix A and a temporal matrix C.

$$Y = AC + E \tag{1}$$

Y represents spatiotemporal calcium responses, where each column represents vectorized calcium image in a time frame and each row represents a pixel value across time frames, and *E* indicates the observation noise. The factorization procedure is similar to regular nonnegative matrix factorization, requiring spatial matrix *A* and temporal matrix *C* being nonnegative. Moreover, the spatial component matrix is endowed with additional sparsity constraint to extract more compact and regularized spatial response regions as ROI masks. The problem can be succinctly summarized as the following optimization problem:

$$\min_{A,C} \|Y - AC\| \qquad\qquad\qquad (2)$$

$$\text{s.t.} \quad A, C \geq 0$$

$$\|A\|_1 \leq \epsilon$$

We optimized the spatial component and temporal component by alternating such that a new estimate of *A* is obtained by use of the last estimate of *C* and vice versa. As both subproblems are convex, there exists a variety of methods to solve it. We solved the spatial subproblem by a nonnegative least-angle regression (LARS) algorithm and temporal subproblem by nonnegative least squares. We used different degrees of spatial constraints (ϵ) to account for various responses statistics in antennal lobe and lateral horn. Similar to(Pnevmatikakis et al., 2016), at the end of each iteration, we merged overlapping components with high temporal correlation and removed components with low signal-to-noise ratio.

3.2.7 Initialization of CNMF using local correlation map

Even though the individual sub-problems are convex, the overall optimization problem listed above is non-convex. The quality of solution is highly sensitive to the initialization. Exploration

of initialization methods is time consuming and computationally expensive. Additionally, often requires a preset number of spatial components need to be identified during initialization (i.e. number of columns of matrix A). In this study, we used a local correlation map based approach to initialize the response regions (i.e. matrix A). The correlation value in each pixel is obtained by computing correlation coefficients between the temporal trace of that pixel and the mean temporal trace of surrounding four pixels (i.e. one above, one left, one right and one down). After we obtain the local correlation map, we apply a median filter and morphological closing to obtain the initial response regions (columns of matrix A). Compared to other initialization methods, this approach was computationally more efficient and the number of spatial components required for factorization was automatically determined based on the imaging dataset.

3.2.8 Correction of exponential signal drifts within each trial and calculation of $\Delta F/F$

First, the camera bias, a constant value, was subtracted from all signals acquired. A robust estimation of the baseline F at each time instance is essential to the reliable calculation of $\Delta F/F$. However, three common phenomena made this task challenging: 1. Intra-trial baseline drift, an approximately exponential decay within each trial (intra-trial drift), possibly due to photobleaching. 2. inter-trial baseline drift, the baseline may drift between trials, possibly due to some slower cellular processes. 3. Noisy spontaneous signals, instead of a "real baseline", the observable signals are the results of random fluctuations or spontaneous activities being superimposed on the underlying baseline.

To tackle these problems, we devised an approach to model the spontaneous fluorescence signals based on two basic assumptions: 1. The "true baseline" underlying the observed signals is a constant value for a given trial. Meanwhile, given the inter-trial baseline drift, the "true baseline" is trial dependent. 2. The observed signals are a result of superimposing an exponential decay on top of the "true baseline", and the rate of this exponential decay for a given ROI is fixed.

Hence, the observed spontaneous signal F_t' at time instance t in a trial can be described by formula

$$F_t' = F + a \cdot e^{b \cdot t} \qquad (1),$$

where F is the "true baseline" of the given ROI in that trial, and $a \cdot e^{b \cdot t}$ is the exponential term describing the intra-trial signal decay. To remove the contribution of uncorrelated noise observed in different trials, the exponential term was modeled as the "mean" exponential decay of all the trials for a given ROI.

To obtain the data for exponential term estimation, for each ROI, we pooled the pre-stimulus signals (first 2.5 s excluded) and the very last 1 s from each trial, which resulted in a $m \times n$ matrix, with 'm' indicating the total number of trials and 'n' indicating the total number of sampled time points. We computed the standard deviation of each column. Values out of the ± 1.5 std range in the column are discarded as outliers. Then we parameterized the formula

$$F' = a \cdot e^{bx} + c$$

by fitting it to the remaining data points within the pool while minimizing the mean squared error (MSE). Note, at this step, our goal was to obtain the mean intra-trial exponential decay term. Constant c describes some sort of the ROI's "mean baseline" across trials. Now for a given trial we have the "true baseline"

$$\tilde{F} = F_t' - a \cdot e^{\{b \cdot t\}},$$

where the exponential term is already known. Next, to obtain a trial's F, we simply parameterize $\tilde{F}$ by minimizing the MSE between formula (1) and that trial's spontaneous signals.

The baseline correction approach resulted in a small fraction of ROIs having near zero or even negative baselines values. Since this could result in unrealistically large $\Delta F/F$, we dealt with this issue in the following fashion.

To minimize the amount of baseline correction, these ROIs also had to meet a set of criteria to ensure it's ΔF and $\Delta F/F$ are indeed outliers of the population and the baseline value must be under an empirically determined threshold. For such an ROI, we substituted its baseline with the mean baseline across all other ROIs on the same plane. Note that in cases where the corrected baseline was smaller than the original baseline F_i, the original baseline was retained.

3.2.9 ROI cleaning

The ROI masks were projected back to the raw image movies. ROIs that does not belong to the target structures were removed after visual inspection.

Given some ROIs in the antennal lobe can span more than one planes and possible errors made by the detection algorithm, we sought to remove the duplicates. Candidate duplicate ROIs were identified by running a hierarchical clustering analysis on following response features:

- cosine distance between high-dimensional vectors of calcium signals recorded during this whole trial [34.5 s total: -9.5 s before odor onset to 25 s after odor onset; ~ 138 dimensional vectors]
- cosine distance between calcium signals recorded during a 15 s post-stimulus period [10 s after stimulus onset to +25 s after odor onset; ~ 60 dimensional vectors]

- Euclidean distance between a 15 s post-stimulus time periods across different trials [10 s after stimulus onsest to +25 s after odor onset; ~60 dimensional vectors].

The resulting candidate set was the intersection of the candidate sets generated by the independent hierarchical clustering.

Finally, the candidates were mapped back to the anatomical space, and re-examined through visual inspection. A candidate ROI was labeled as duplicate, only if it were clustered together with another ROI and was anatomically juxtaposed to it.

3.2.10 Quantification of ROI functional distance

An ROI's response to a stimulus was represented by its mean $\Delta F/F$ observed during the odor presentation window. Therefore, for a given ROI, its tuning was represented by a 12-dimensional vector, since the odor panel used in the study included six odorants each delivered at two different intensities [i.e. 12 stimuli]. The functional distance between an arbitrary pair of ROIs (ROI A, ROI B) was defined as the cosine similarity, defined as:

$$\text{cosine similiarity}(A, B) = \frac{A \cdot B}{||A|| \times ||B||}$$

between their 12-D tuning vectors. The spatial distance between two ROI's was calculated as the Euclidean distance between their centroids in the physical space.

The functional and spatial distances between pairs of ROIs were calculated and pooled across individual flies. The relationship between the two distances was determined using a linear regression. The degree of "linearity" between these two parameters was quantified using the R-squared value of the best-fit linear model, e.g. the amount of variance that can be explained by the model.

3.2.11 Functional embedding and the projection onto anatomical space

To visualize the relationship between the ROI "tuning" and the spatial organization, one intuitive approach is to represent an ROI as a point using its centroid coordinates in the 3D anatomical space, and assign similar colors to these points that have similar stimulus preference or tuning. Namely, for an arbitrary pair of ROIs, if their functional distance is small (i.e. similar tuning), colors that represent them should be close to each other in the RGB color space as well. Given that the RGB color space is essentially a 3D space, we used multidimensional scaling (MDS) to translate the pairwise functional distance into Euclidean distance in the 3D RGB color space. The pairwise functional distances of all ROI pairs were precomputed as a "dissimilarity" matrix and fed into the parametric MDS algorithm. The resulting 3D coordinates of the ROIs were normalized to unit scale by the following procedure:

Let X be the set of all x-axis values of the MDS output. Let X_{ceil} be the 95% quantile value of X and X_{floor} be the 5% quantile value.

We have the normalized value $x' = \frac{x - X_{floor}}{X_{ceil} - X_{floor}}$. If x' is out of the range [0,1], it was clipped to either 0 or 1, whichever was closer. This procedure was repeated on values corresponding to the other two MDS axes.

Note the max and min values were defined as the values at the 95% and 5% quantiles, respectively, for robustness. Then the normalized coordinate values were used as RGB values.

In addition, several landmark tuning vectors were artificially constructed and added to the dataset to facilitate interpretation. Sharing the same 12-dimensional format as the real ROI tuning

vectors, these landmark tuning vectors had 1s indicating excitation, 0s indicating no response, and -1s indicating inhibition instead.

To avoid numerical stability issues, ROIs that were barely activated by any of the odorants in the panel were not considered for this analysis. Less than 1% of the ROIs were neglected due to this criterion.

3.2.12 Regression Analysis of ePN input and output relation

We regarded the AL spatiotemporal response as the input to the regression model, which was a $t \times n$ matrix X, where n is the number of AL ROIs and t is the total number of time points (note that responses between 0 to +12s in different trials were concatenated to form a super long column vector). The CL and LH responses from the recording were regarded as the target matrix. Thus, the target matrix Y was a $t \times m$ matrix, where m is the total number of CL and LH ROIs. We have the generic form of linear regression:

$$Y = XW + \varepsilon,$$

where W is the $n \times m$ weight matrix that transforms AL response into CL/LH response, while minimizing the error ε. Since direct least-squares regression to determine W was not feasible, we used a multi-task lasso regression (MTLR). Optimal W was obtained by minimizing a slightly modified objective function:

$$\frac{1}{2t}\left|\left|Y - XW\right|\right|_F^2 + \lambda \sum_{i=1}^{n} \sqrt{\sum_{j=1}^{m} w_{ij}^2},$$

where $||Y - XW||_F^2$ is the Frobenius norm of the residual matrix with $||a||_F^2 = \sqrt{\sum_{i=1}^{n} \sum_{j=1}^{m} |a_{ij}|^2}$,

e.g. the square root of the residual sum of squares of each element. Note the regularization term is essentially a l_1-norm of l_2-norms, scaled by the hyper-parameter λ.

To determine the optimal hyper-parameter, we performed a grid search, adopting a K-fold cross-validation scheme that leaves one stimulus group (both concentrations of the same odorant) out each time.

3.2.13 Analysis of temporal coding

To quantify the pattern similarity between a stimulus pair as a function of time (**Fig. 6**), we first aligned trials with respect to stimulus onset. Then we computed the cosine similarity between the two population response vectors at the same reference time point (i.e.cosine (a_t, b_t) where a_t and b_t are the at time t following introduction of stimulus a or b, respectively). By computing the similarity at different points in time after odor onset, we characterized how similarity between pairs of odorants evolve as a function of time.

Since the odor panel comprised of six odorants each delivered at two concentrations, we calculated similarity between 66 unique stimulus pairs in total.

For the visualization of cosine similarity distributions, kernel density estimation was performed using a Gaussian kernel with the bandwidth determined by the Scott rule(Scott, 17 August 1992).

3.2.14 Analysis of ON-OFF response

The neural activities during the 4 s stimulus presentation period was defined as the "ON response," whereas activities during a 4 s time window after the stimulus termination were taken as the "OFF response". The one second period immediately following the termination of the odorant was excluded as it included both ON and OFF responses.

We used a MDS dimensionality approach to visualize the ON or OFF response vectors (Fig. 4.1). The MDS analysis was done independently for data collected from each individual fly.

To quantify the diversity of the ON and OFF response patterns, principal component analysis was performed on the same data. The number of principal components (PCs) needed to account for at least 90% of the variance in activity patterns was used to measure the pattern diversity, as more diverse patterns would require more PCs to capture the majority of the data variance, and vice versa (**Fig. 8D**).

To compute the mean angle between the ON and OFF activity patterns, for each stimulus, mean activity pattern vectors were computed for the ON and OFF time windows. For a given stimulus pair, the angles between the ON and OFF activities were calculated and averaged across individual flies (**Fig. 8C**).

3.3 Results

3.3.1 Light-sheeting imaging of odor evoked neural activity

We used a custom-built light-sheet imaging setup (Greer and Holy, 2019) to monitor calcium signals (GCamp6f) from olfactory sensory neurons expressing the *orco* co-receptor (ORNs), and their two downstream targets excitatory GH146 projection neurons (ePNs) and inhibitory Mz699 projection neurons (iPNs) (**Figure 3.1A - C**). In each fly, one of these three neural population was labeled, and neural responses from all optical planes was near-simultaneously recorded (see **Methods**; **Figure 1D**). While the axonal outputs alone were monitored for ORNs and iPNs (as GCamp6f expression levels were weak in the antennal lobe for the Mz699 line), both dendritic and axonal calcium signals were monitored for ePNs (GH146 line). This approach allowed us to relate the dendritic inputs in the antennal lobe with the functional signals reaching the two downstream targets: mushroom body calyces and lateral horns.

We probed the responses of ORNs, ePNs and iPNs to a panel of six odorants, each delivered at two concentrations. The odor panel was chosen to ensure diversity in functional groups, behavioral valence, activation patterns and concentrations(Badel et al., 2016; Knaden et al., 2012b; Strutz et al., 2014) . For example, benzaldehyde (*Bzald*) was reported to be repulsive(Ahsan et al., 2017; Strutz et al., 2014) and activate ventral glomeruli strongly compared with other stimuli(Badel et al., 2016) , whereas ethyl acetate (*EA*) is regarded as an attractive cue that generates strong input to dorso-medial glomeruli(Ahsan et al., 2017). The light-sheet images acquired were segmented using an unsupervised non-negative matrix factorization method(Pnevmatikakis et al., 2016) (see **Methods** for details). Note that the ROIs corresponded to glomeruli for Orco-ORN axons and ePN dendrites **(Figure 3.2A;** top row), and

ePN and iPN axonal boutons in calyx (CX) and lateral horn (LH) (**Figure 3.2A**; bottom row). A

quick summary of the number of ROIs extracted from each fly is listed in **Figure 1C** (also refer

Figures 1.1-1.5 for ROI masks that were extracted for each plane and in each fly).

A

Laser

Objective

Saline

Odor Delivery

B

Calyx (CL)   Lateral Horn (LH)

3. ePN-cl (axons)

4. ePN-lh (axons)

5. iPN-lh (axons)

Antennal Lobe (AL)

2 ePN-al (dendrites)

iPN-al (dendrites)

1. ORN-al (axons)

C

#ROIs

ORN-al   ePN-al   ePN-cl   ePN-lh   iPN-lh
line-region

D

| | Depth 1 | Depth 2 | Depth 3 | Depth 1 | Depth 2 | Depth 3 |

Lateral / Dorsal / Anterior

AL, Orco - Fly 1

AL, GH146 - Fly 7

CL, GH146 - Fly 7

LH, GH146 - Fly 7

LH, Mz699 - Fly 13

Bzald02   EB02

80

Figure 3.1: Light-sheet imaging for volumetric in vivo characterization of odor-evoked responses at the input and outputs of the antennal circuitry.

(A) A schematic of the experimental setup. The fly is mounted on a custom mounting block with its antennae exposed to air stream and brain immersed in saline. At each scanning step, a whole brain plane is illuminated by a light-sheet with two wavelengths (488 nm and 561 nm). The fluorescent signals are collected by the objective and the downstream optical components.

(B) Fly lines labeling any one of the following three distinct neural populations were used in our experiments: cholinergic ORNs expressing Orco co-receptor (ORNs), cholinergic projection neurons (ePNs) and GABAergic projection neurons (iPNs). For ORNs and iPNs, axonal activity alone was monitored. For ePN both dendritic responses in the antennal lobe and axonal responses transmitted onto mushroom body calyx and lateral horns were near simultaneously monitored.

(C) The number of region of interest(ROI) extracted by a constrained non-negative matrix factorization algorithm is shown for different regions. Both the median and the interquartile ranges (IQR, 50%) are shown. Whisker lengths are 1.5 IQR past the low and high quartiles. Points out of this range were regarded as outliers.

(D) Maximum responses observed during the Bzald0202 presentation window are shown for each optical plane. Each row shows changes in calcium activity from a labeled neural population at an anatomical location. Each column shows responses monitored at one depth of imaging stacks.

(E) Similar plots as shown in panel D but now showing responses to EB02.
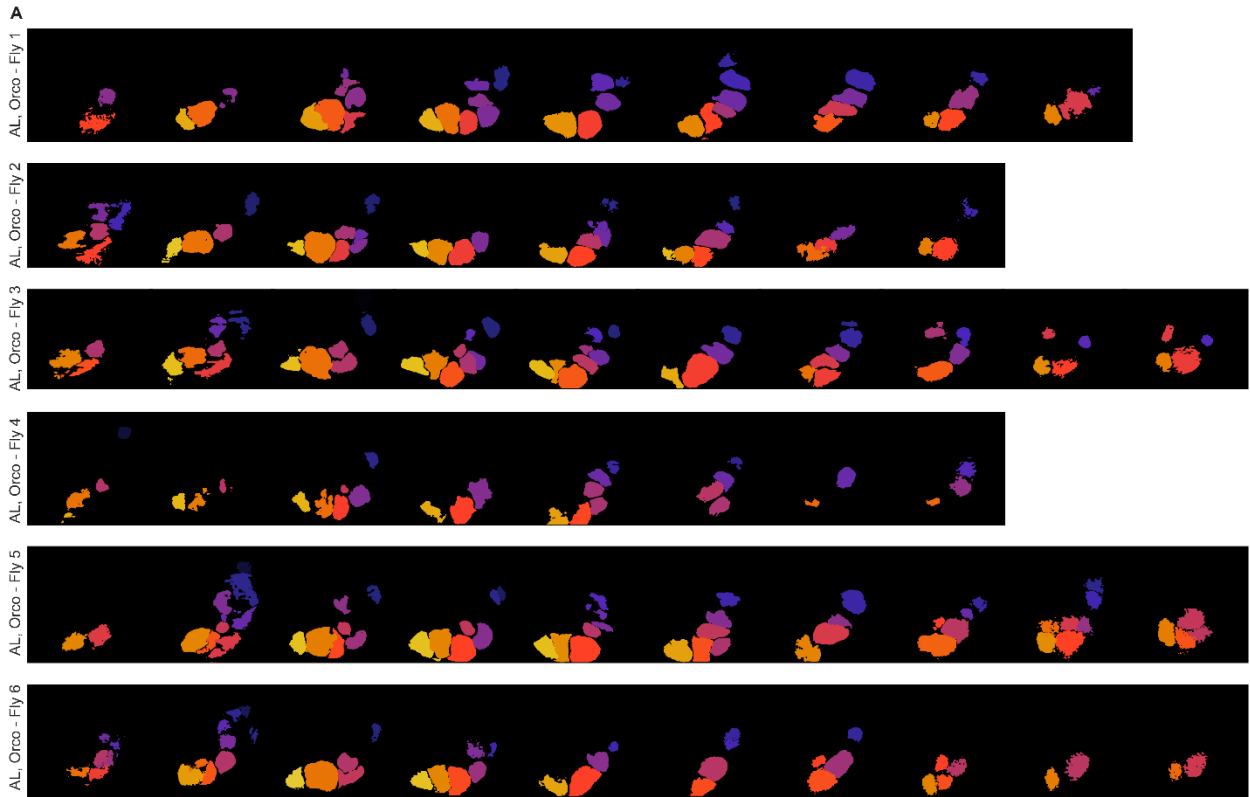
Figure 3.1.1: ROI masks extracted to segment axonal responses in flies expressing calcium indicators in ORN axons.

ROI masks extracted for each plane and in each Orco labeled fly are shown. Each row shows ROIs across different planes for an individual fly. Left most panel shows ROI masks in dorsal regions and right most panel shows ROIs in more ventral regions. In each plane, different ROIs are labelled using different colors. In total, ROI masks for all six flies used in the study are shown in different rows.
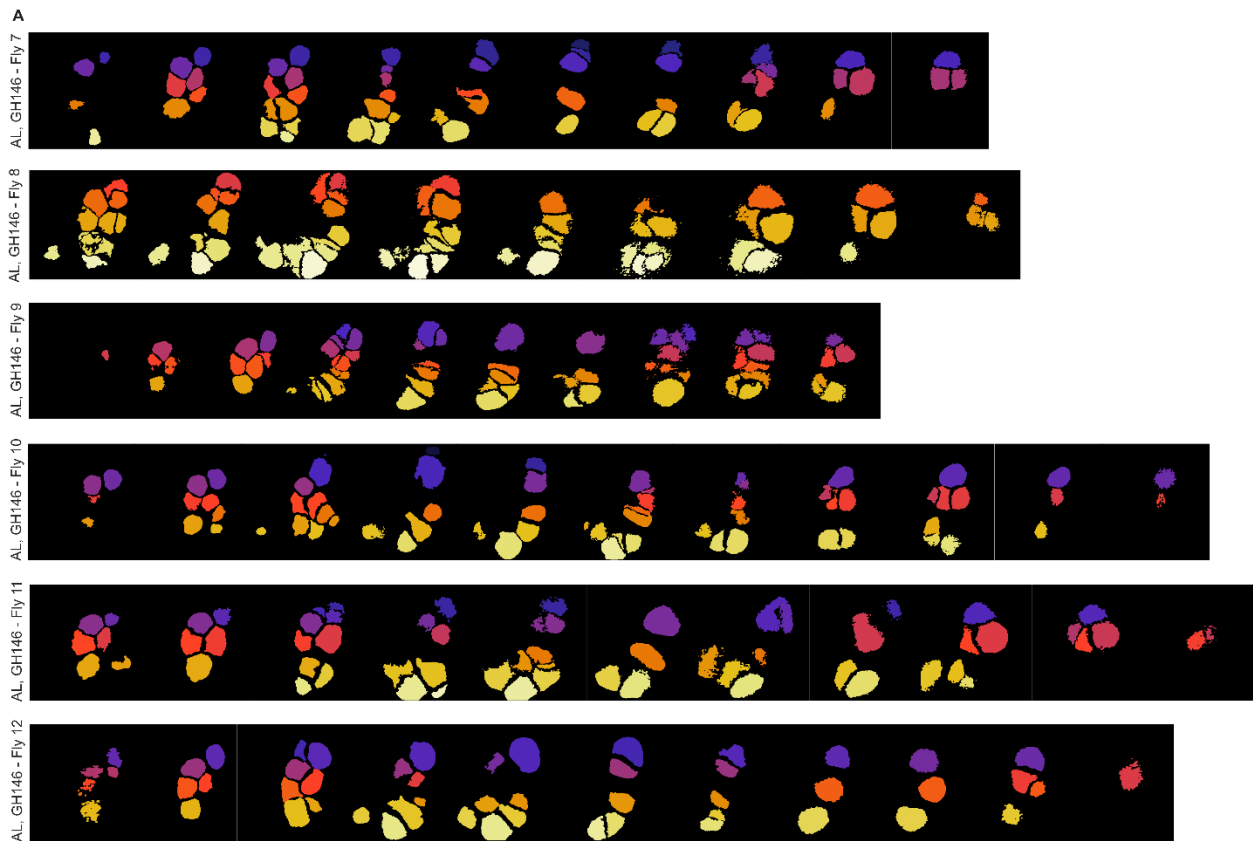
Figure 3.1.2: ROI masks extracted that segment ePN dendritic activity in the antennal lobe.

Similar to Figure 3.1.1, but ROI masks for GH146 flies with ePNs labeled with GCamp6f. ROI masks extracted are shown for each plane and in each fly antennal lobe i.e. to segment dendritic responses.
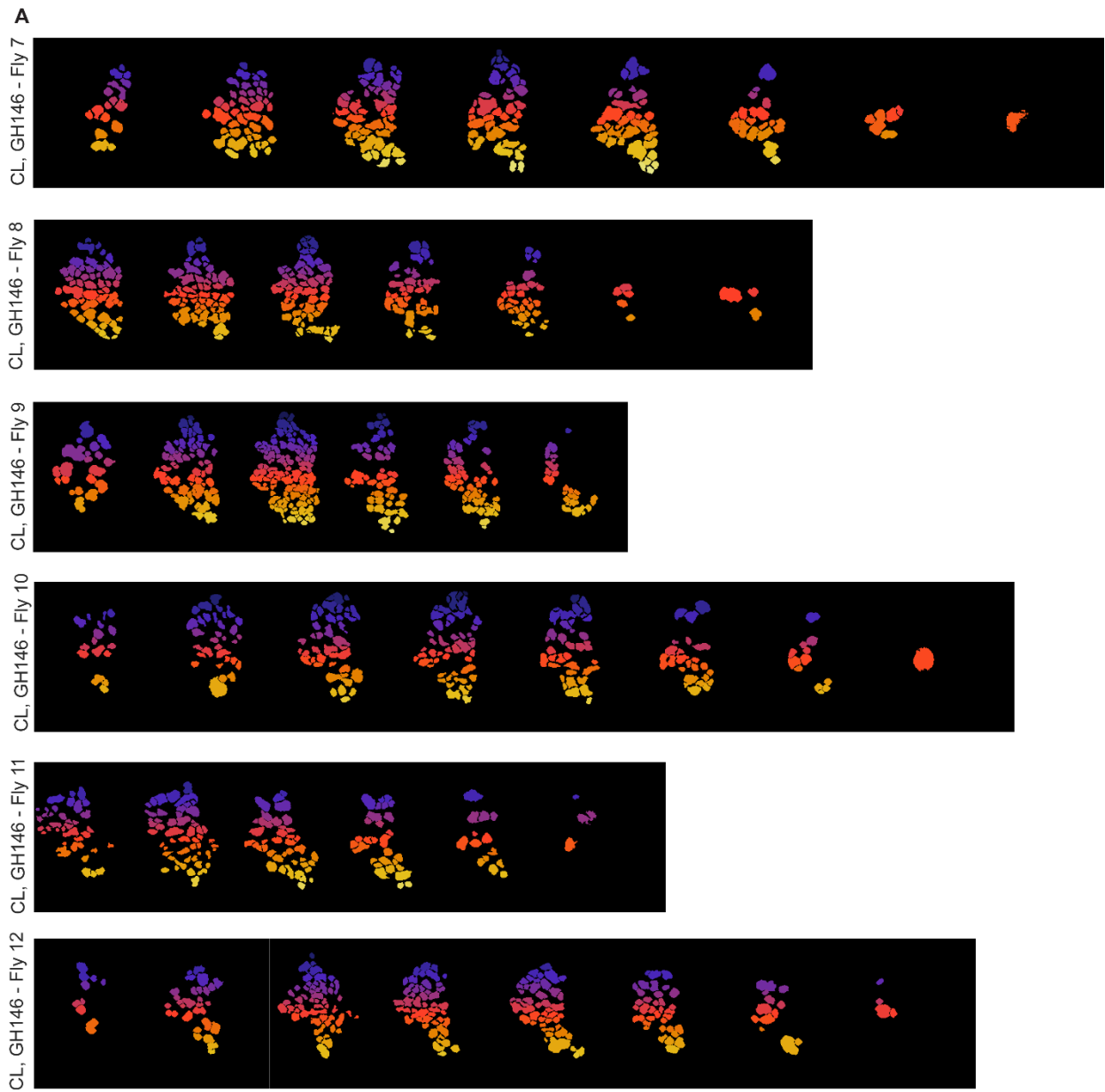
Figure 3.1.3: ROI masks extracted to segment ePN axonal responses in the mushroom body calyx.

Similar to Figure 3.1.1, but ROI masks to segment ePN axonal responses that are transmitted to the mushroom body calyx are shown for each plane and in each fly.
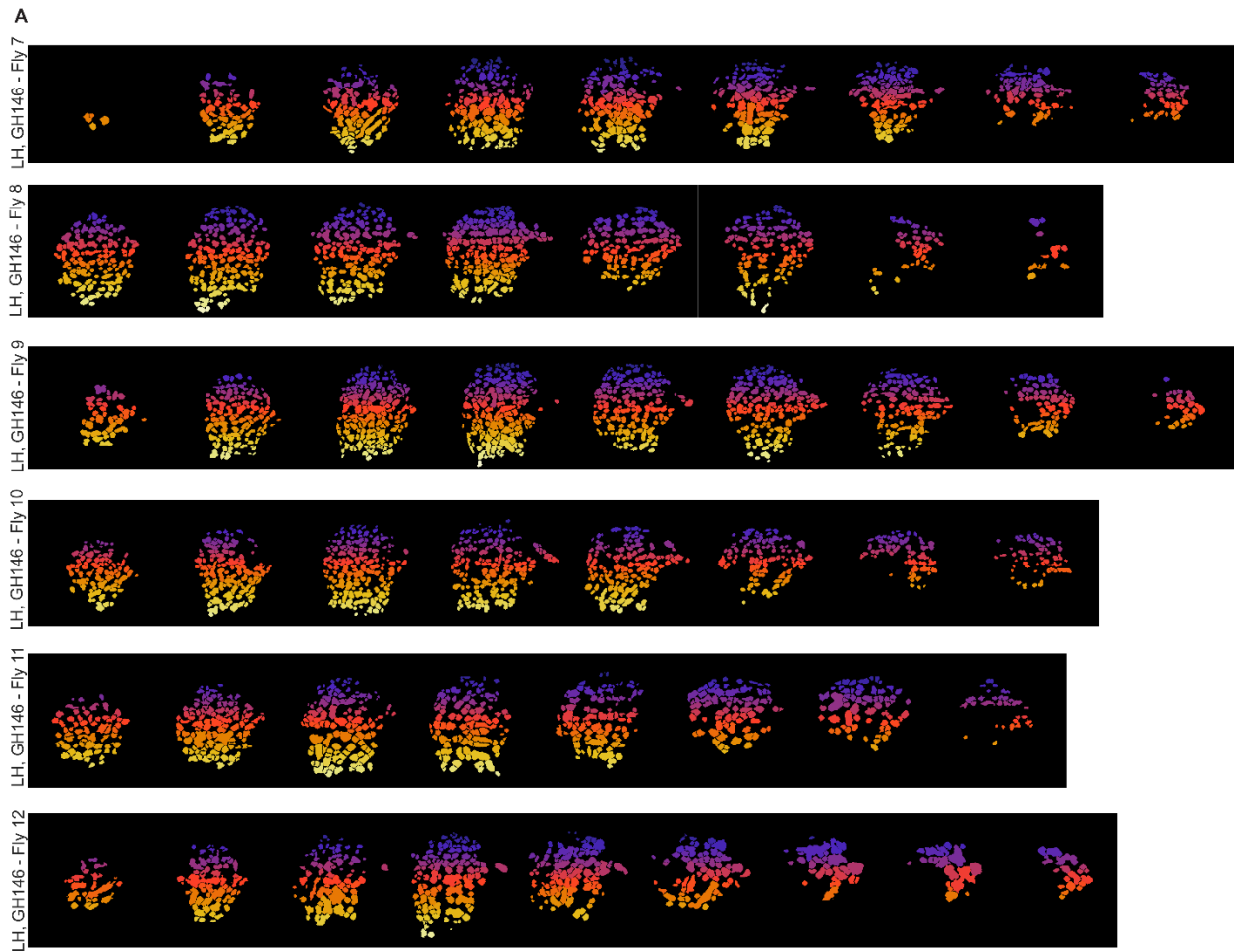
Figure 3.1.4: ROI masks extracted to segment ePN axonal responses in the lateral horn.

Similar to Figure 3.1.1, but ROI masks extracted to segment GH146 ePNs axonal responses in the lateral horn are shown for each plane and in each fly.
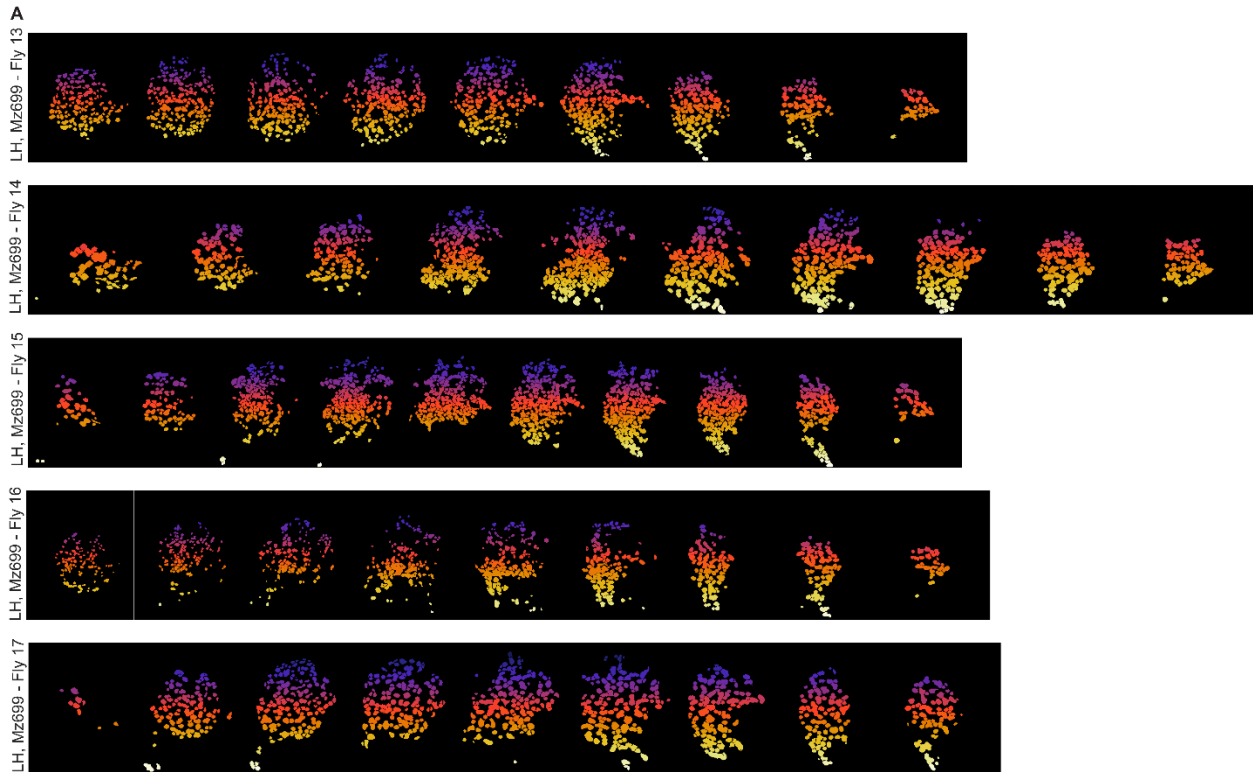
Figure 3.1.5: ROI masks extracted to segment iPN axonal responses in the lateral horn.

Similar to Figure 3.1.1, but ROI masks extracted to segment Mz699 iPNs axonsal responses in the lateral horn extracted are shown for each plane and in each fly.

In addition to large spatial coverage, we also acquired images rapidly (4 Hz sampling rate) to characterize odor-evoked, spatiotemporal response dynamics across the entire population of a specific type of olfactory neuron **(Figure 3.2)**. Consistent with earlier reports(de Bruyne et al., 2001), we found that each odorant activated a unique combination of ORNs. For most ORNs, the sensory input lasted the duration of the odor response, and for certain odorant-ORN combinations, the unabated response persisted and outlasted the stimulus duration **(Figure 3.2B**;

for example, *1o3ol04* and *Acet04*). In a few ORNs, substantial reduction in calcium signals were also evident during the odor presentation (ethyl acetate (*EA*) and ethyl butyrate (*EB*), **Figure 2.1**). Prolonged excitatory responses, and inhibition that persisted after stimulus termination were pronounced at higher intensities (*MH02*; see **Figure 2.2**). As the intensity was increased, additional ORNs were recruited for all odorants (**Figure 3.2.2**).

In the downstream antennal lobe level, ePN dendrites showed richer response dynamics for all odorants (**Figure 3.2c**). Increase in calcium signals after stimulus termination (i.e. 'OFF responses') were observed in many glomeruli. Consistent with prior results(Bhandawat et al., 2007), we also observed that odorants that evoked weak ORN inputs had amplified responses at the level of ePN dendrites (e.g. *Bzald04*). We also found the ePN signals attenuated more rapidly. More importantly, the mean response overlap between pairs of odorants did not increase as signals propagated downstream but appeared to remain consistent in all five fly-lines/regions examined (**Figure 3.2.3**). Increasing odor intensity, recruited activity in additional glomeruli, and resulted in more complex changes in the response timing (**Figure 3.2.2**).

As noted earlier, ePNs send axons to both the mushroom calyces and lateral horns, whereas iPNs project only to lateral horns. We found that activation patterns of ePN and iPN axons entering these higher centers were broadly distributed across several boutons. The ePN and iPN axonal responses tended to be more transient than even those observed at the level of ePN dendrites (**Figure 3.2.1**). In most flies, the ordering of odorants based on strength of activation differed between the ePN dendritic and axonal compartments (**Figure 3.2.4, 2.5**). Together, these results suggest that active signal transformation occurs between input and output compartments of these neurons. The activation became stronger for all odorants at higher

intensity, but nevertheless remained highly transient and attenuated rapidly **(Figure 3.2.2)**. These

observations remained consistent when data from across the flies were compared.

Note that these observations indicate that the light sheet imaging data allowed us to probe the

spatial and temporal aspects of olfactory processing with greater resolution. Primarily, we sought

to understand how sensory signals are represented and transformed at the input and output of the

antennal lobe.

89
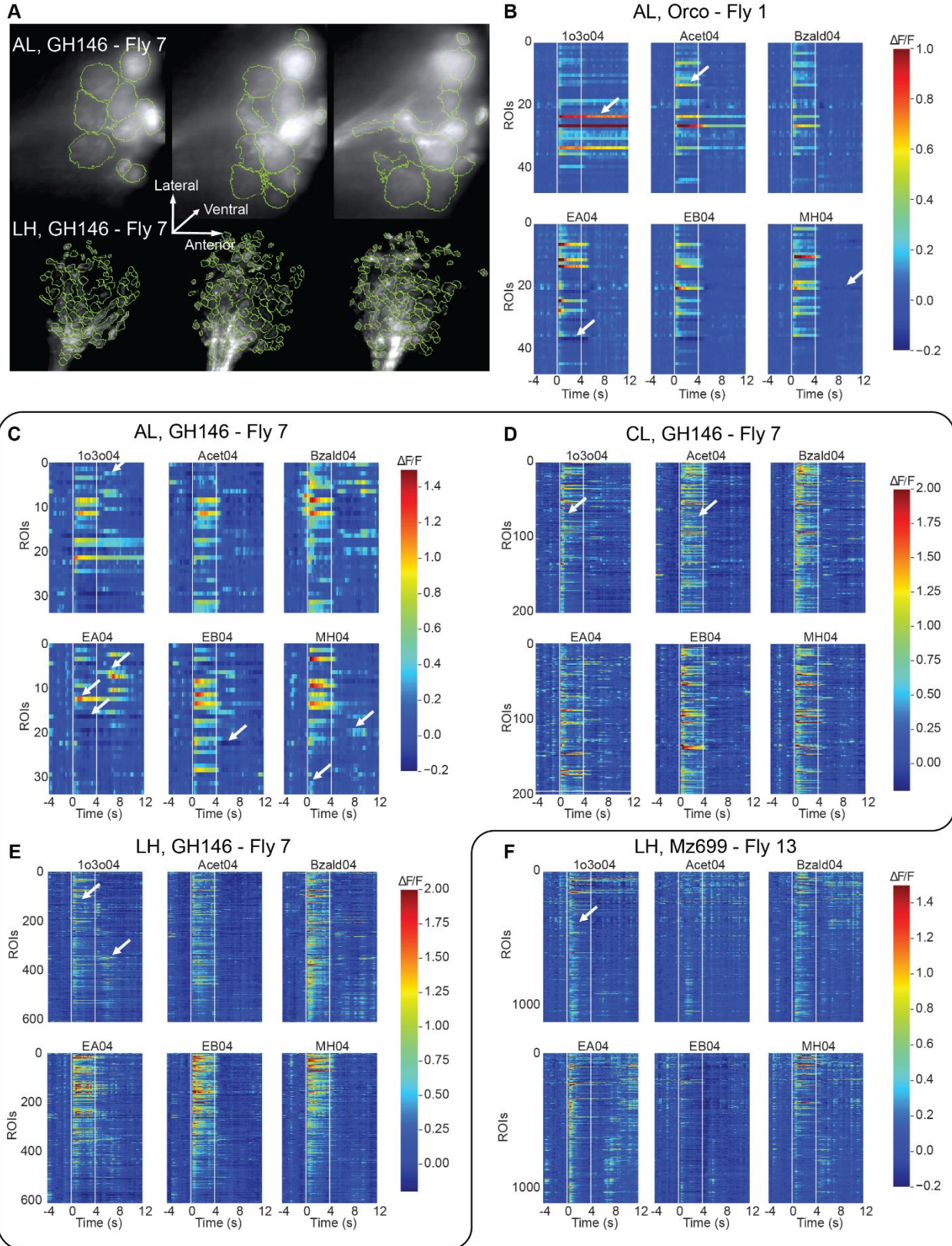
Figure 3.2: Extraction of spatial and temporal patterns of odor-evoked neural activity.

(**A**) Region-of-interest (ROI) masks extracted by an unsupervised non-negative matrix factoriztion method are overlaid on top of raw calcium signals recorded from ePN dendrites in the antennal lobe (top panel) and ePN axons entering the lateral horn (bottom panel). Three panels are shown characterizing odor-evoked responses and ROI masks extracted at three different depths. Note the mask contours match the anatomical structures (glomeruli and axonal boutons) in both regions very well.

(**B** through **F**) Representative responses to a panel of six odorants are shown as a data matrix. Calcium signals from individual ROIs extracted in each fly line/region are shown: olfactory receptor neurons in the antennal lobe (**B**); excitatory projection neuron dendrites in the antennal lobe (**C**); excitatory projection neurons axons in the mushroom body calyx (**D**); excitatory projection neuron axons in the lateral horn (**E**); inhibitory projection neuron axons in the lateral horn (**F**). Warmer color indicates stronger excitation, whereas cooler colors indicates inhibition. In each panel, each row represents temporal response of one ROI arranged in the order from dorsal to ventral. All the ROIs across different depths were pooled together and shown in the plot (from dorsal at the top to ventral planes at the bottom of each data matrix). Y-axis indicates the ROI numbers. White arrows annotate the typical response dynamics (see text for details).
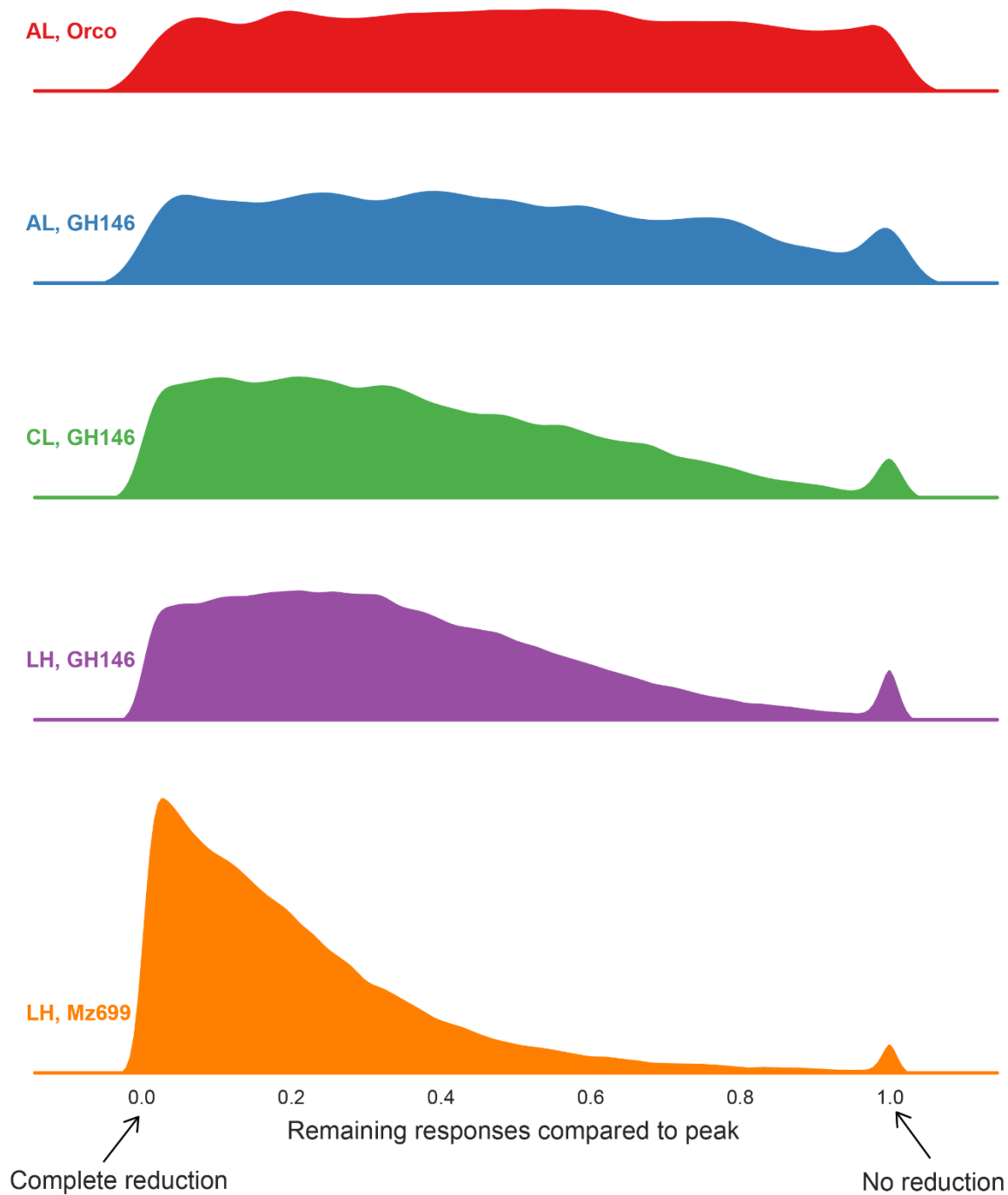
Figure 3.2.1: Odor-evoked temporal response dynamics.

The response distribution showing the activity levels of ROIs relative to their peak responses at the end of the odor pulse (i.e. prior to termination; 3.75 s after odor onset). To account for excitatory and inhibitory responses, the absolute values of the signals were used for this analysis.

The peak response is defined as the maximum absolute value during the odor presentation window. Each row is one fly line/region. The x-axis indicates the fraction of ROIs showing a particular level of activity and y-axis indicates the density.
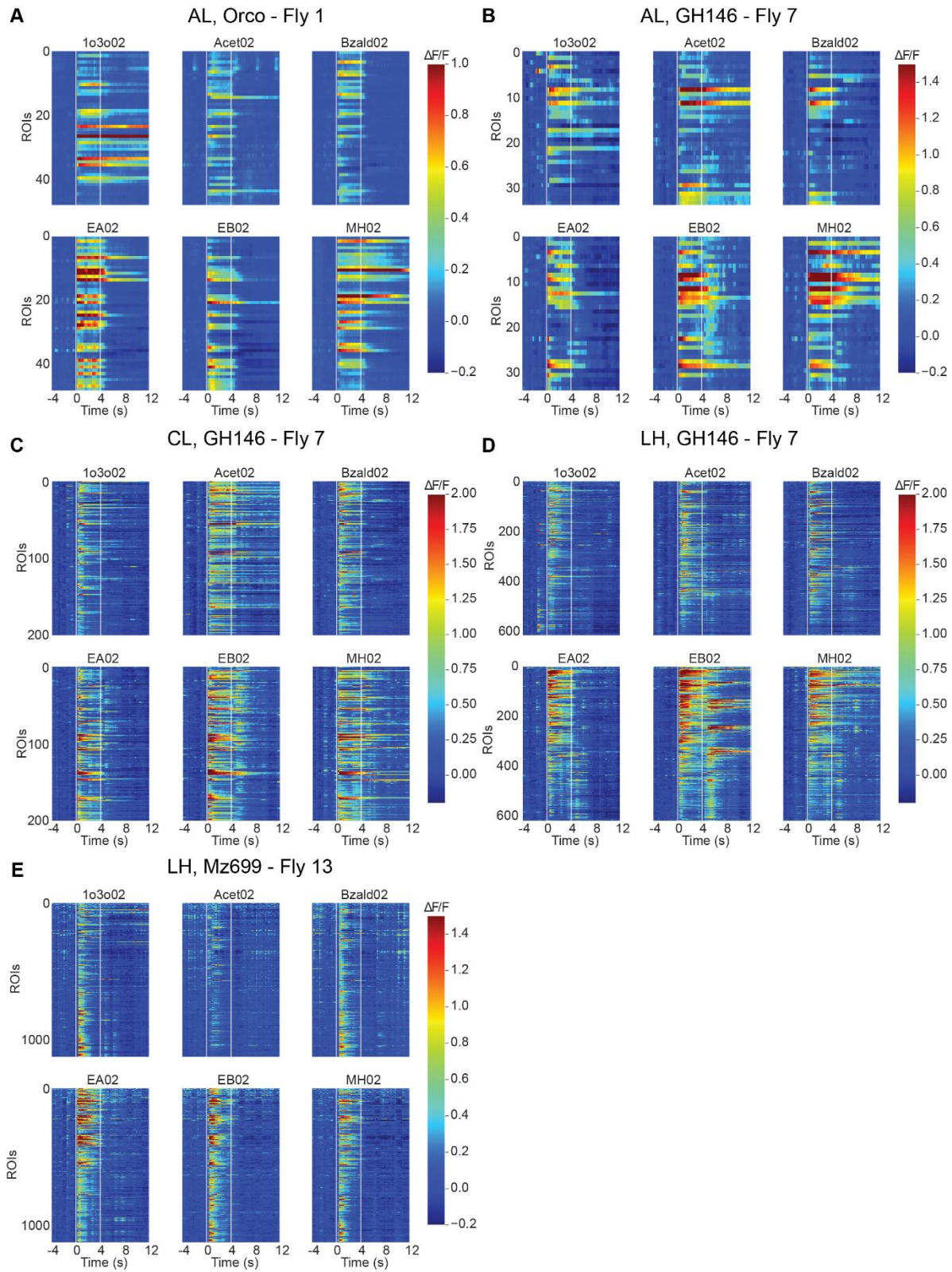
Figure 3.2.2: Temporal responses in higher concentrations.

(A to **E)** Similar to **Figure 2 (B** to **F)** Representative responses to the same six stimuli but delivered at a higher concentration are shown.
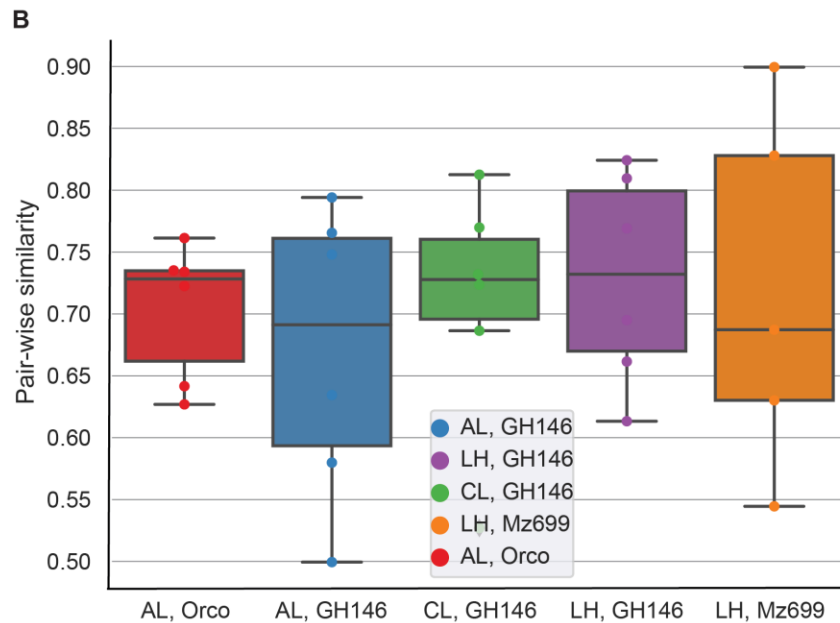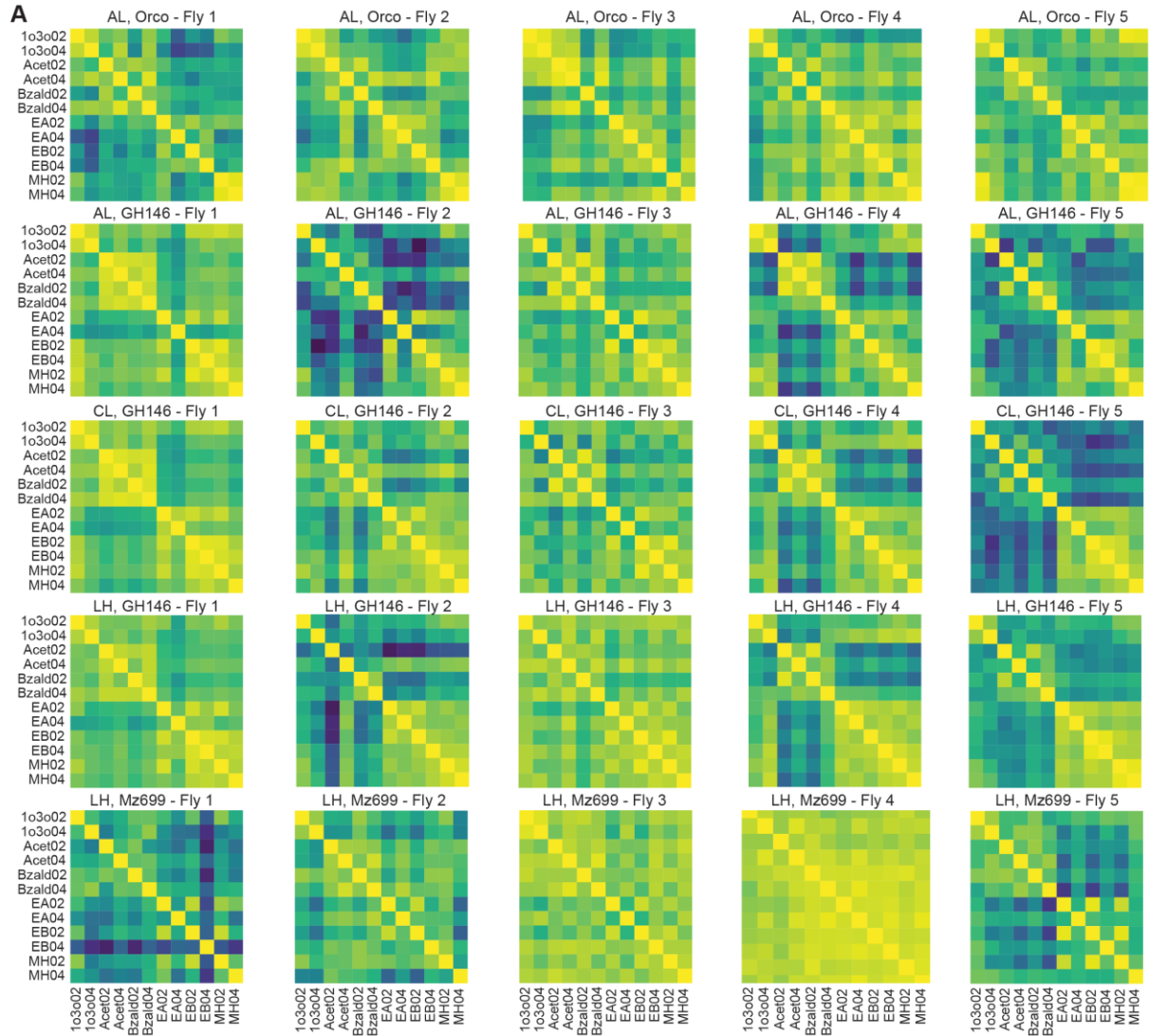
Figure 3.2.3: Pair-wise odor response similarities.

(A) Representative heatmaps showing similarity between odor-evoked responsese evoked by all stimulus pairs. Each row is a fly line/region and different columns correspond to different individual flies. In each heatmap, each grid is the cosine similarity between a pair of stimuli indicated by the corresponding labels. To calculate the similarity between a stimulus pair, every ROI's response was represented by its mean response during odor presentation, and the responses across all ROIs were regarded as a high-dimensional vector. The cosine distance between these two response vectors evoked by the two odorants were computed and plotted as a heatmap. Warmer color means higher similarity.

(B) Mean pairwise similarities between odorants was computed for each fly line/region and summarized as a box plot. The y-axis indicates the mean cosine similarity between a pair of odorants.
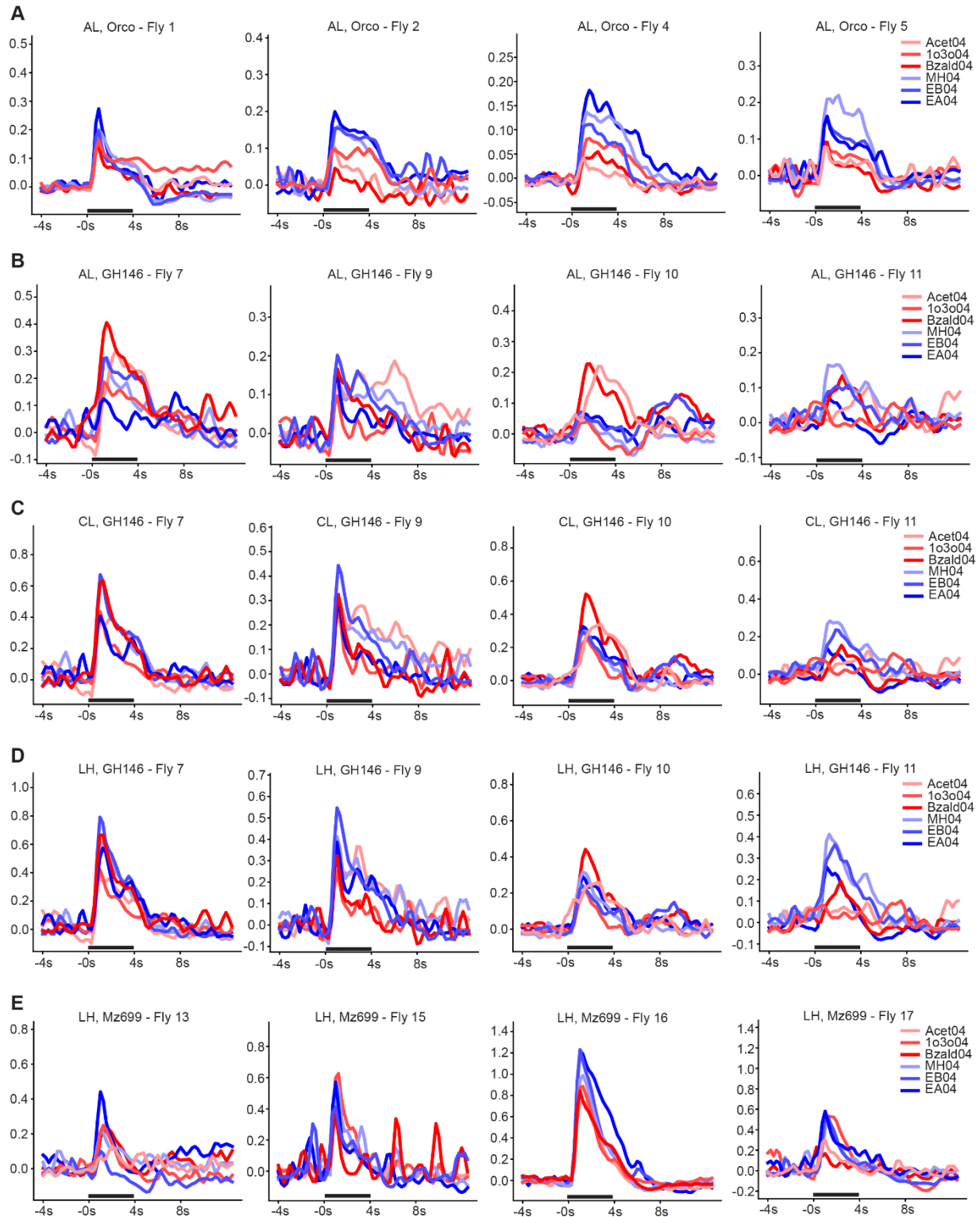
Figure 3.2.4: PSTHs characterizing overall responses evoked by the odor panel at lower concentration.

(A) Mean firing rates across all ORN axon ROIs are shown for four representative flies. In each panel, responses to 6 different stimuli delivered at their lower concentrations are shown. Red color are used to indicate PSTHs evoked by putative repulsive odorants and blue colors label PSTHs evoked by attractive ones. The 4-s odor stimulation period is shown as a black bar along the x axis.

(B) Similar as panel **(A)**, but mean firing rates across all ePN dendritic ROIs in the antennal lobe are shown.

(C) Similar as panel **(A)**, but mean firing rates across all ePN axonal ROIs in the calyx are shown.

(D) Similar as panel **(A)**, but mean firing rates across all ePN axonal ROIs in the lateral horn are shown.

(E) Similar as panel **(A)**, but mean firing rates across all iPN axonal ROIs in the lateral horn are shown.
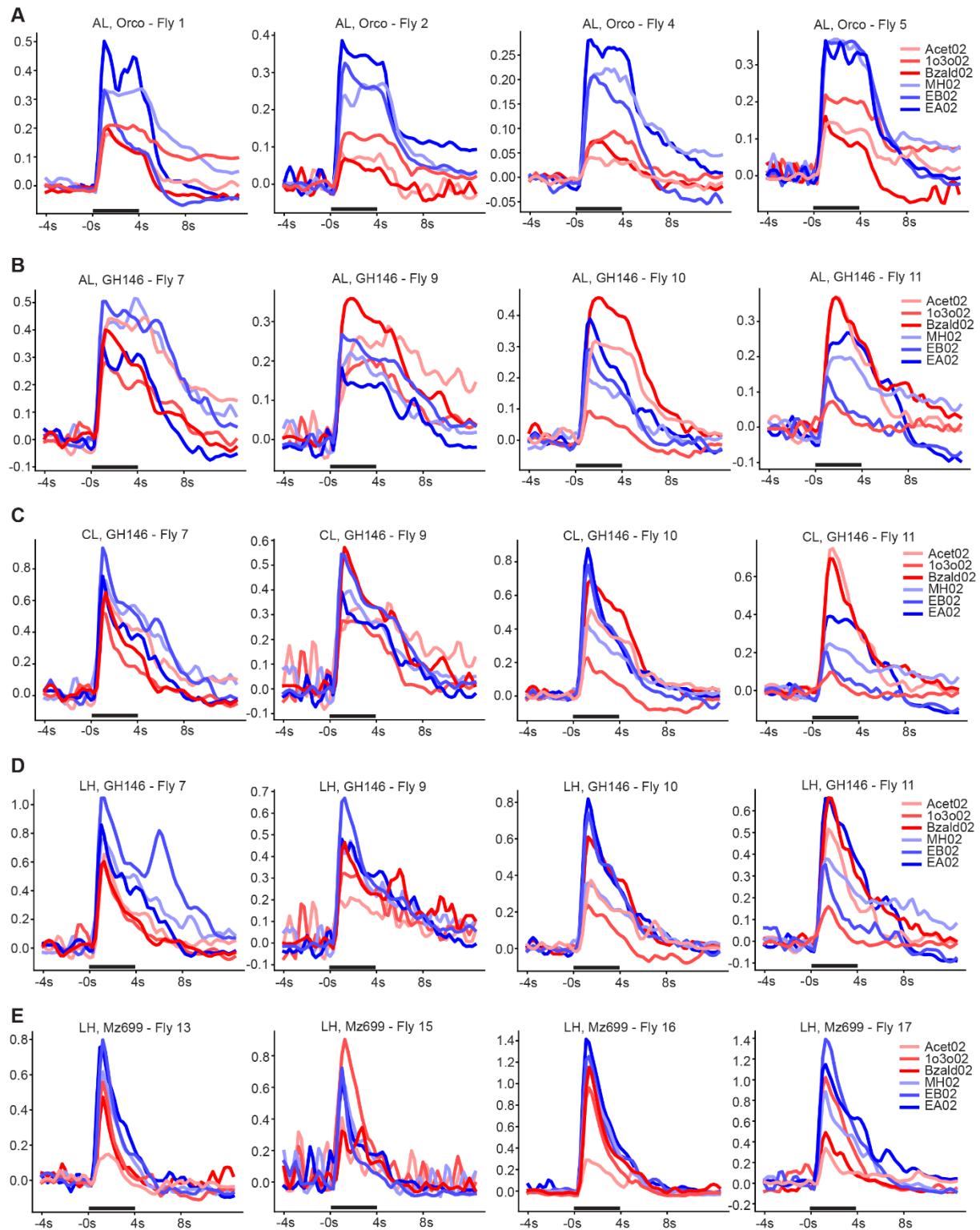
Figure 3.2.5: PSTHs characterizing overall responses evoked by the odor panel at lower concentration.

Similar as Figure 3.2.4, but mean firing rates for the same panel of odorants delivered at a higher concentration are shown.

3.3.2 Spatial organization of neural processes within the antennal lobe, calyx and lateral horn

How are functional units (ROIs) organized within each processing stage? Do ROIs that are spatially closer respond to odorants in a similar fashion? To examine this, we represented the response tuning of each ROI using a 12-dimensional vector, with each vector-component being the ROI's mean response to an odorant (**Figure 3.3A**). Next, for every pair of ROIs, we computed response similarity (i.e. cosine of the angle between their 12-D tuning vectors) and plotted it as a function of spatial distance between them (i.e. distance between the two ROI's centroids; **Figure 3A**). Note that a response similarity of 1 indicates that the two ROIs have very similar odor-evoked responses, whereas negative values indicate response tunings that are opposite.

Our results indicate that for all three neural populations examined (ORNs, ePNs and iPNs), there was a weak but general trend that spatially near-by ROIs were similar in their odor tuning (**Figure 3.3B**). Notably, the 'space vs. tuning' distributions were different between ORN axons and ePN dendrites in the antennal lobe, and between ePN and iPN axons innervating the lateral horn. The former result indicates active transformation of sensory signals as it propagates through the glomerular microcircuits in the antennal lobe, while the later observation suggests that ePN and iPN innervations in the lateral horn follow different organization principles.

100

However, in all flies examined, there was barely linear spatial organization in the calyx (**Figure 3.3B** 3rd column).

Taken together, these results indicate that, similar to results in the mouse olfactory bulb(Ma et al., 2012), the spatial organization of odor representation in fly antennal lobe is weak. Notably, this organizational feature was present in all flies examined (**Figure 3.3C-D**).

3.3.3 Characterizing spatial organization of odor tuning across neural populations and across flies

To better understand the spatial organization of ROIs in different regions, we positioned each ROI based on its XYZ co-ordinates in the fly brain and colored it based on its odor response tuning. As mentioned earlier, the specificity or tuning of each ROI was defined using a 12-D vector (each vector component to indicate the response elicited by each of the twelve stimuli used; **Figure 4A**). The 12-D ROI tuning vectors were dimensionality reduced to a 3D space using multiscale scaling (MDS) algorithm (**Figure 3.4a**). Each 3-D MDS vector was then assigned a color using a 3-D RGB color scale (see **Methods**). Note that ROI's with similar tuning profiles were assigned similar colors. Furthermore, to create suitable points of reference or 'tuning landmarks', a few artificial templates were generated, and the colors that each one of these templates was assigned is also shown (**Figure 3.4B; Figure 4.1** shows colors that were assigned to a more elaborate set of reference vectors/templates).

Using this odor tuning-based coloring approach, we visualized each ROI and compared their stimulus specificities (**Figure 3.4C**). Note that red through dark purple/dark blue colors identify ROIs that were strongly activated by attractive odorants (*EA04*, *EB04* and *MH04*;

Figure 4B), where the green through yellow colors identify ROIs that responded to the repulsive ones (*Bzald04*, *1o3o04*, *Acet04*; **Figure 4B**).

In *orco*-labeled flies (**Figure 3.4C**; first row), we found that dorso-medial and ventro-medial glomeruli were activated strongly by attractive odorants (*EA04*, *EB04* and *MH04*; blue/purple colored ROIs). Whereas glomeruli in ventro-lateral regions tended to respond more to the repulsive odorants (green ROIs). It is worth noting that the attractive odorants evoked strong responses and activated more glomeruli at the level of sensory neuron axons.

In comparison, at the level of ePN dendrites (**Figure 3.4C**; second row), the odor tuning maps changed. First, the extent of activation of the attractive odorants was restricted to fewer glomeruli located in the dorso-medial and ventro-medial regions. Response to the repulsive odorants, that were weaker at the level of Orco sensory neuron axons, became stronger and spread to more glomeruli in the ventro-lateral regions (note that the response amplification to *Bzald*, *Acet* and *1o3o* is also evident in ePN PSTH's shown in **Figure 2.4, 2.5**).

In the calyx, we found that the ROIs in the core region differed in tuning from the ROIs that bordered them and formed the outer-rim. Attractive odorants strongly activated the outer-rim, whereas ePN axons entering the core strongly responded to repulsive odorants. These results are again consistent with pure anatomical studies that have examined how a few glomeruli in the dorso-medial region of the antennal lobe innervate the calyx(Tanaka et al., 2004).

Finally, in the lateral horn too we found that both ePN and iPN axons were spatially organized based on their odor tuning. While all repulsive odorants evoked strong responses at the level of ePN axons in the lateral horns, iPN axons only weakly responded to some of those odorants (for example iPN axonal responses to *Acet04* were weaker in all flies; refer **Figure 2.4,**

2.5). Intriguingly, a stereotyped region in the dorso-lateral lateral horn received ePN and iPN axons that matched in their response selectivity (blue-purple region indicating response to attractive odorants). While in the rest of the lateral horn, the ePN and iPN differed in their response tuning. This suggests that matched feed-forward excitation and inhibition may compete in the lateral horn regions receiving inputs regarding attractive odorants, while interactions

between mismatched excitatory and inhibitory inputs may occur in other regions.
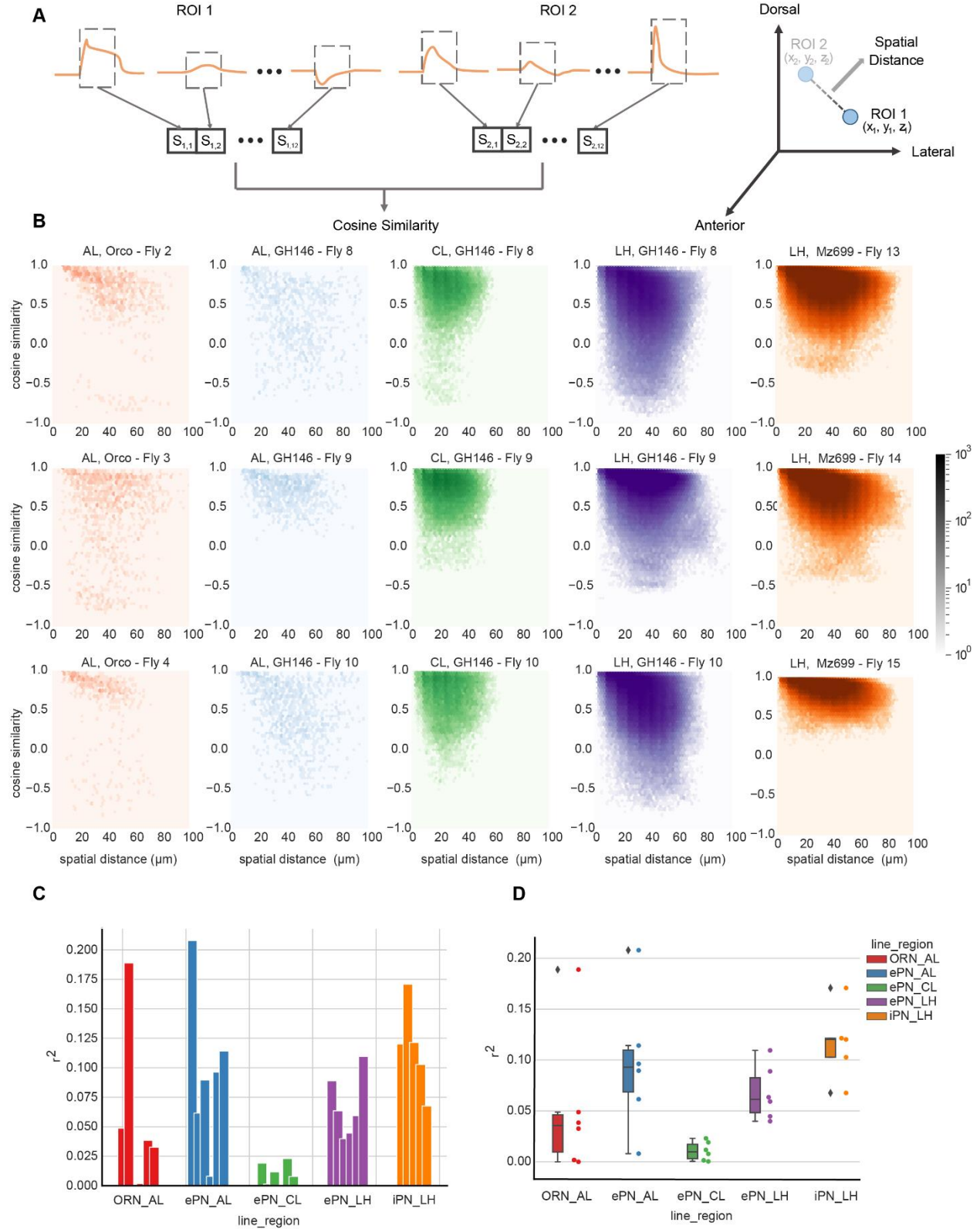
Figure 3.3: Functional distance vs. spatial distance.

(A) A schematic illustrating how functional distances (left) and spatial distances right) were calculated. For each ROI, its tuning vector consists of twelve elements. Each vector component represents its mean response (over time) to one odor stimulus. Functional distance was calculated as the cosine similarity between two ROI's response vectors. Spatial distance between a pair of ROIs was calculated as the Euclidean distance between two ROIs spatial location as shown in the right panel.

(B) A scatter plot showing relationship between functional distance (y-axis) vs. spatial distance (x-axis) for all ROI pairs. Each column indicates an anatomical region. Results from three representative flies are show for each line (three rows). For all three lines, there was a weak but general trend that spatially near-by ROIs have higher correlation between their odor-tuning vectors.

(C) The linearity of functional vs spatial distance relationship was quantified (coefficient of determination or r^2) and shown. Each bar indicates the r^2 value of a linear regression model, with spatial distance as independent variable and functional distance as dependent variable for one region and from one fly. Colors correspond to different regions matching the color scheme shown in **panel b**).

(D) Same as **panel c**, but coefficient of determination summarized as box plots.

A

ROIs

Tuning Profile

ROI 1 | $S_{1,1}$ $S_{1,2}$ $S_{1,3}$ ... $S_{1,11}$ $S_{1,12}$

ROI 2 | $S_{2,1}$ $S_{2,2}$ $S_{2,3}$ ... $S_{2,11}$ $S_{2,12}$

ROI 3 | $S_{3,1}$ $S_{3,2}$ $S_{3,3}$ ... $S_{3,11}$ $S_{3,12}$

ROI n-1 | $S_{n-1,1}$ $S_{n-1,2}$ $S_{n-1,3}$ ... $S_{n-1,11}$ $S_{n-1,12}$

ROI n | $S_{n,1}$ $S_{n,2}$ $S_{n,3}$ ... $S_{n,11}$ $S_{n,12}$

MDS

x, y, z in MDS Space

$D_{1,1}$ $D_{1,2}$ $D_{1,3}$

$D_{2,1}$ $D_{2,2}$ $D_{2,3}$

$D_{3,1}$ $D_{3,2}$ $D_{3,3}$

$D_{n-1,1}$ $D_{n-1,2}$ $D_{n-1,3}$

$D_{n,1}$ $D_{n,2}$ $D_{n,3}$

Color Mapping to RGB Space

B

Color | Tuning Pattern

Excitation / No Response

1o3o02, 1o3o04, Acet02, Acet04, Bzald02, Bzald04, EA02, EA04, EB02, EB04, MH02, MH04

C

AL, Orco - Fly 1 | AL, Orco - Fly 2 | AL, Orco - Fly 3 | AL, Orco - Fly 5

AL, GH146- Fly 8 | AL, GH146 - Fly 9 | AL, GH146 - Fly 10 | AL, GH146 - Fly 11

CL, GH146 - Fly 8 | CL, GH146 - Fly 9 | CL, GH146 - Fly 10 | CL, GH146 - Fly 11

LH, GH146 - Fly 8 | LH, GH146 - Fly 9 | LH, GH146 - Fly 10 | LH, GH146 - Fly 11

LH, Mz699 - Fly 13 | LH, Mz699 - Fly 14 | LH, Mz699 - Fly 15 | LH, Mz699 - Fly 17

106

Figure 3.4: Spatial organization of extracted ROIs.

(A) An ROI's tuning profile is again summarized as a 12-dimension vector as in **Figure 3a**. To obtain the 3D color space, we used multidimensional scaling (MDS) to map the pairwise 12-D functional distance in the tuning space onto a 3D color space. Then the color of each ROI was assigned based on the coordinates in the 3D color space where each axis corresponded to red/green/blue colors **(Methods)**.

(B) The correspondence between tuning profiles and colors are shown. Color bar on the left indicates the color correspondence of the 'artificial landmark' tuning profiles shown on the right (same row). Green/Yellow colors indicate ROIs that are more responsive to aversive odorants (1o3o, Acet and Bzald). On the contrary, Red/magenta colors show ROIs tuning preference to attractive odors (EA, EB and MH).

(C) ROIs are shown in their actual 3D spatial locations across different regions/fly lines (4 representative flies are shown for each region). Each ROI is also labeled by the color obtained from MDS analysis indicating tuning properties.

Figure 3.4.1: A more elaborate set of reference vectors/templates.

(A) The mapping between tuning vectors onto the 3D color space is illustrated with a more elaborate set of reference vectors/templates. Each row corresponds to a mapping between a reference template and the color assgined.

(B) Similar to **Figure 4(B)**, ROIs are shown in actual spatial locations across different regions but for two additional flies in each line/region.

3.3.4 Relating dendritic ePN inputs with their axonal outputs to higher centers

Next, we investigated the relationship between the ePN responses in the antennal lobe (dendrites) and those transmitted to mushroom body calyx and lateral horn (axons). Previous connectomic studies had shown that each ePN project its axonal terminals to a limited number of locations in the calyx and lateral horn (Zheng et al., 2018). This wiring pattern would suggest that each ePN may simply send its output to a spatially restricted region downstream, and may have only a minimal influence on functional signals reaching the other spatial loci. Since we acquired data from ePN dendrites and axons near simultaneously from each fly, we examined if this was indeed the case.

We performed a regression analysis to understand the functional relationship between ePN input and output compartments (see **Methods; Figure 5A**). In this approach, we used linear combination of ePN dendritic responses to predict the responses at each individual axonal bouton. Note that each row of the regression weights matrix **(Figure 3.5B)** indicates how the regression weights from multiple antennal lobe ROIs were linearly combined to map onto each calyx or lateral horn ROI. Alternately, each column of the weight matrix show in **Figure 5B**, can

be interpreted as the contribution each antennal lobe ROI makes in generating axonal responses in the two downstream regions.

Contrary to our expectations, each ePN dendritic activity showed a more global contribution downstream (**Figure 3.5C, D**). As can be noted, most columns have both hot (positive influence) and cool (negative influence) colored vector components indicating that majority of antennal lobe ROIs had a mixed influence in calyx and lateral horns axonal responses (i.e. positive influence in some regions and negative influence in others). Only a few antennal lobe ROIs had predominantly positive or negative influences on the downstream regions. Note that, for some antennal lobe ROIs, the ratio of positive to negative influence also varied between calyx and lateral horn (**Figure 3.5C;** 3rd column). This observation implies that the input from the antennal lobe is restructured differently between the two downstream targets.

To understand the spatial distribution of how each antennal lobe ROI contributed to downstream activity, we mapped the vector of regression weights onto the spatial locations of each axonal bouton (**Figure 3.5C**). The antennal lobe ROIs had diverse functional relationships with the ePN axonal responses observed in the calyx and lateral horn. Nevertheless, the regression weights from a single antennal lobe ROI appeared to be spatially organized, with regions of positive and negative influences occurring in spatially contiguous regions juxtaposed next to each other. This spatial arrangement was much clearer in the lateral horns and to a lesser extent also observed in the calyx. Interestingly, antennal lobe ROIs that were spatially close to one another had functional innervation patterns that were markedly different from one another (**Figure 3.5C;** columns 1 vs column 5 shows functional mapping of inputs from two ROIs in the dorso-medial antennal lobe)

To quantitatively compare the influence different antennal lobe ROIs had on the two downstream regions, for each ROI, we plotted the fraction of positive influence/weights versus the fraction of negative influence/weights (see Methods; **Figure 5D**). Note that ROIs that were close to the two axes had predominantly either positive (closer to y-axis) or negative (closer to the x-axis) influence. Most ROIs had a mixed influence and were positioned away from both these individual axes in these plots. Notably, a similar distribution of ePN antennal lobe ROI weights were observed in both calyx and lateral horns, and across different flies. In sum these results indicate that the functional relationships between responses observed in the dendritic and axonal ePN compartments are complex, and diverse.
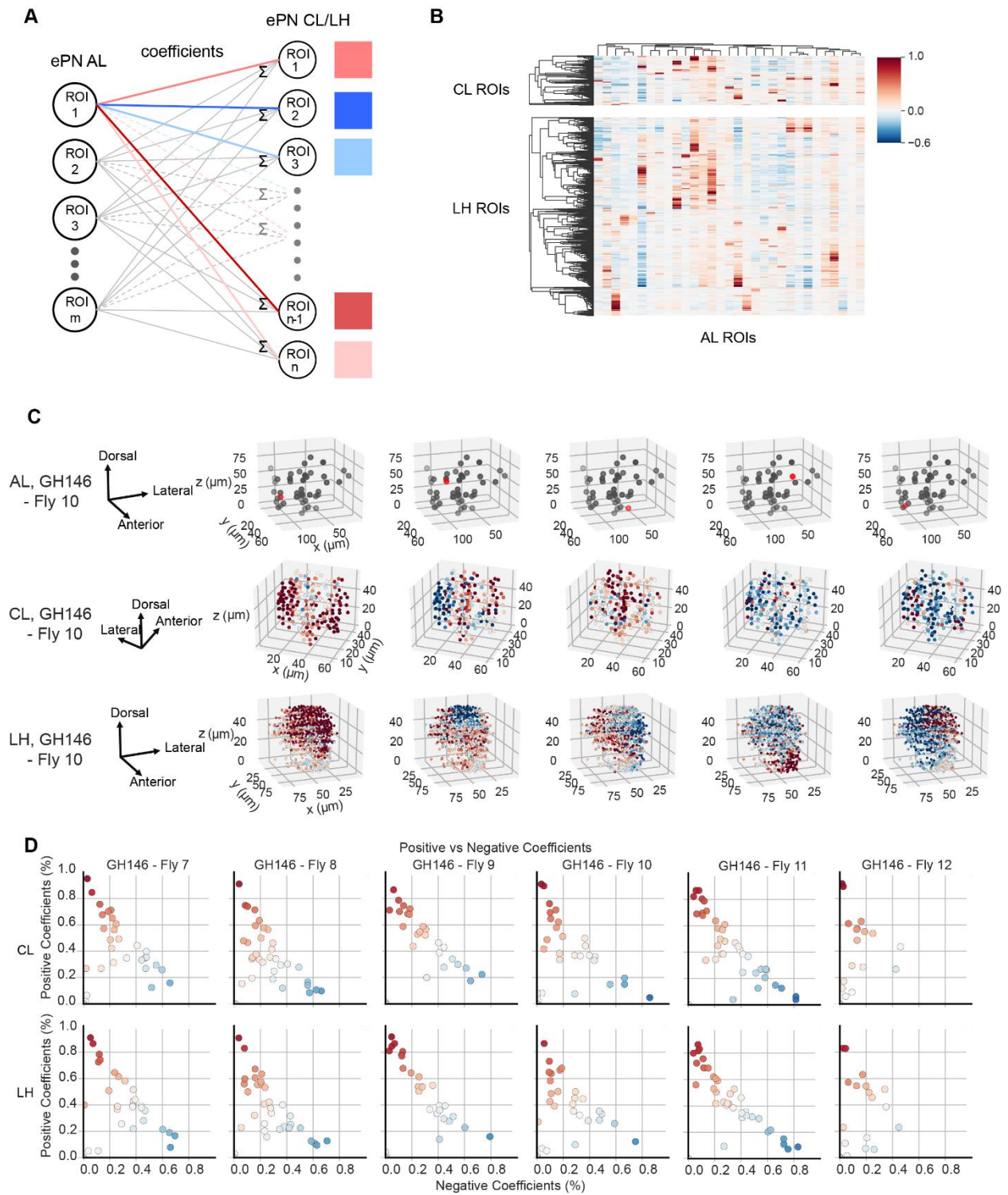
Figure 3.5: Linking dendritic inputs of ePNs with their axonal outputs (I/O mapping).

(**A**) The schematic shows how linear regression was performed to obtain the coefficients relating responses in two regions (input – antennal lobe; output – calyx/lateral horn). Responses over time of each axonal bouton/ROI in the lateral horn/calyx regions were predicted using a linear combination of ePN dendritic responses. Regression weights were learned using a multi-task lasso regression (see methods).

(**B**) The regression coefficients learned from a representative fly are shown. Each column corresponding one ROI in AL as regressors. Each row shows the weights that were assigned to different ePN dendritic ROIs used to predict response a single ROI in the LH/CL. Only non-zero columns are shown here. Warmer color indicates stronger positive influences and cooler color shows stronger negative influences.

(**C**) 3D scatter plots showing single antennal lobe ROI's functional influence on the ePN axonal responses observed in the calyx and lateral horn. The first row shows the spatial location of the specific ROIs in the antennal lobe (ROI labeled in red). Rows two (calyx) and three (lateral horn) show ROIs in these locations colored using the regression coefficients obtained. Each column identifies the AL ROI (first row) and its influence in calyx and lateral horn (rows two and three, respectively). The orientations of each imaged region are indicated on the left panel.

(**D**) The percentage of significant positive (Y-axis) and negative coefficients (X-axis) assigned for each antennal lobe ROI are plotted against each other. Color encodes the net difference between the positive/negative coefficient percentages; for instance, warmer colors represent that the antennal lobe ROI had more positive coefficients than the negative ones. Results from 6 experiments/flies are shown in different columns. Top row shows regression weight distribution in the mushroom body calyx, and the bottom row reveals similar results but in the lateral horn.

3.3.5 Temporal patterning of odor-evoked responses

So far, we have examined how odor-evoked responses are spatially distributed at the level of

ORN axons and how these responses map onto the two downstream neural populations (ePNs

and iPNs). Next, we sought to examine how these odor-evoked responses are patterned over

time. Our results indicate that spatial patterns of activity in the antennal lobe, both at the level of

Orco axons (**Figure 3.6.1**) and ePN dendrites (**Figure 3.6A**), were highly similar immediately

after the onset of the odorants. However, over time these spatial patterns of neural activity

evolved to become more distinct.

To quantify this observation, we computed the cosine similarity between responses evoked by

different odorants at specific time point during stimulus presentation (**Figure 3.6B**; see

Methods). As can be observed, the responses evoked by different odorants at all five neural

processes (Orco axons, ePN dendrites, ePN axons entering calyx and lateral horn, iPN axons

entering lateral horn) had high correlation immediately after the onset of stimulus. However,

over time these correlations reduced and responses evoked by different odorants became more

distinct from each other (i.e. lower correlations/similarity).

These observations were further corroborated when pairwise similarities between odorants across

flies were examined (**Figure 3.6C**). Note that pairwise similarities between most odorants

immediately after onset were high in all three lines examined (tick marks shown below the

probability density functions in **Figure 6C**). The pre-stimulus activity before onset of any two

stimuli showed wide dispersion of cosine similarity values with a mode near zero indicating

randomness in signals recorded during this time period. Immediate after odor onset, the distributed shifted right indicating an increase in odor similarity across pairs of odorants and observed in all flies examined. With progression of time, the distribution of pairwise cosine similarities shifted leftwards (i.e. towards lower values) indicating decorrelation of odor-evoked responses.

The evolution of mean pair-wise correlation across odorants over time showed variable reduction rates in each individual fly examined (**Figure 3.6D**). As can be expected, in all three neural populations, low concentration stimuli decorrelated faster and more than responses to the same set of stimuli evoked at a higher concentration (**Figure 3.6E**). Interestingly, only in the ePN axonal projections the speed of response decorrelation was comparable at both low and high concentrations. This result directly suggests that some additional modification of response patterns occurred in this neural population to rapidly make the neural activity evoked by each odor more distinct from others (**Figure 3.6E**).

Taken together, these results indicate that the odor-evoked response patterns and the discriminatory information needed for selective recognition evolve over time in the early fly olfactory circuits. Consistent with findings from other model systems(Friedrich and Laurent, 2001; Gschwend et al., 2015; Raman et al., 2010), the observed temporal patterning made odor-evoked response patterns to become different from the initial stimulus-evoked activity but also

more distinct when compare to other odorants.
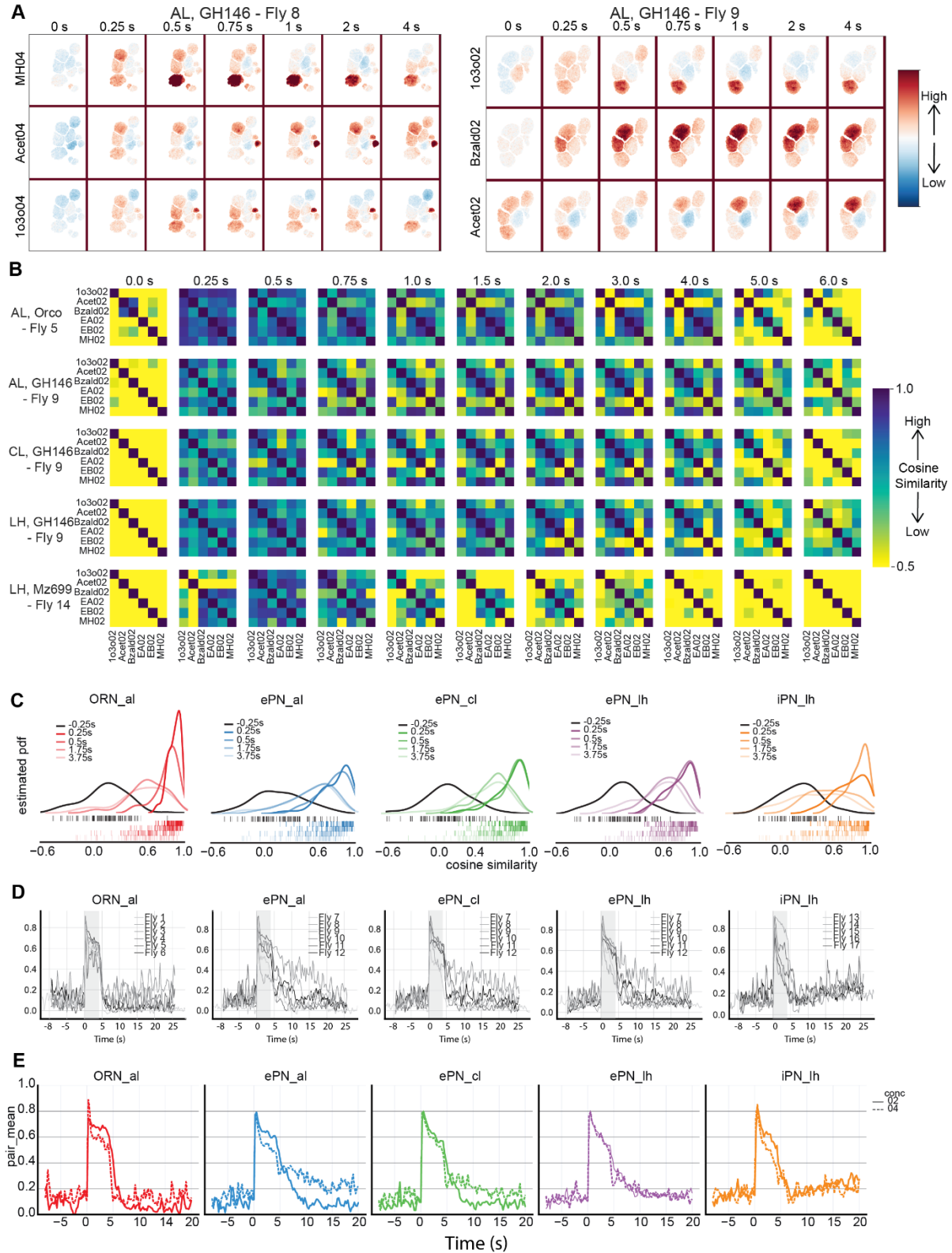
Figure 3.6: Odor-evoked responses decorrelate over time

(A) Change in fluorescence signals ($\Delta F/F$) for a few representative ROIs on single optical plane in the antennal lobe are shown as a function of time since odor onset (shown at the top of the panel). Each row reveals responses evoked by an odorant. Right panel show evolution of odor-evoked responses in the antennal lobe ePN dendrites observed in another fly.

(B) Pattern similarity matrices for a representative fly for each labeled fly line/region are shown. Each element in the matrix is the cosine similarity value between a pair of odorants. Hot colors indicate stronger similarity, and cooler colors indicate weaker similarity. Each row reveals how pairwise odor similarities evolve over time. Again, time since odor onset is indicated at the top of the panel. In total, pairwise similarity matrices at eleven time points are shown. Odor stimulus was presented from 0.0 sec to 4.0 sec. Note that similarity matrices with higher pattern similarities (cooler/blue colors) at the start of response and gradually decorrelate over time (hotter/yellow colors). This can be observed in all five rows corresponding to responses observed in ORNs, ePN dendrites, ePN axons in the calyx, ePN axons in the lateral horn and iPN axons in the lateral horn.

(C) Distributions of pairwise pattern similarity (cosine distance) obtained using kernel density estimation (see **Methods**) are shown. Each curve shows pairwise pattern similarity distribution at one time point. In each panel, response similarity distributions are shown for five different time points before and during stimulus presentation. Tick marks shown below the distributions represent pairwise similarity between every pair of odorants and across flies. Ticks are color coded following the same scheme used for the distributions shown on the top.

(D) Mean pair-wise cosine similarity in each region is shown as a function of time. Each trace shows the mean cosine similarity value across all odor pairs for each individual fly. Color bar

indicates the 4 s duration when the odorant was presented. Five panels are shown to illustrate results from the three fly lines used in the study.

(E) Mean pair-wise cosine similarity as a function of time is shown. Two traces, corresponding to the two concentrations of odorants used, are shown tracking changes in mean cosine similarity across odorants/flies.
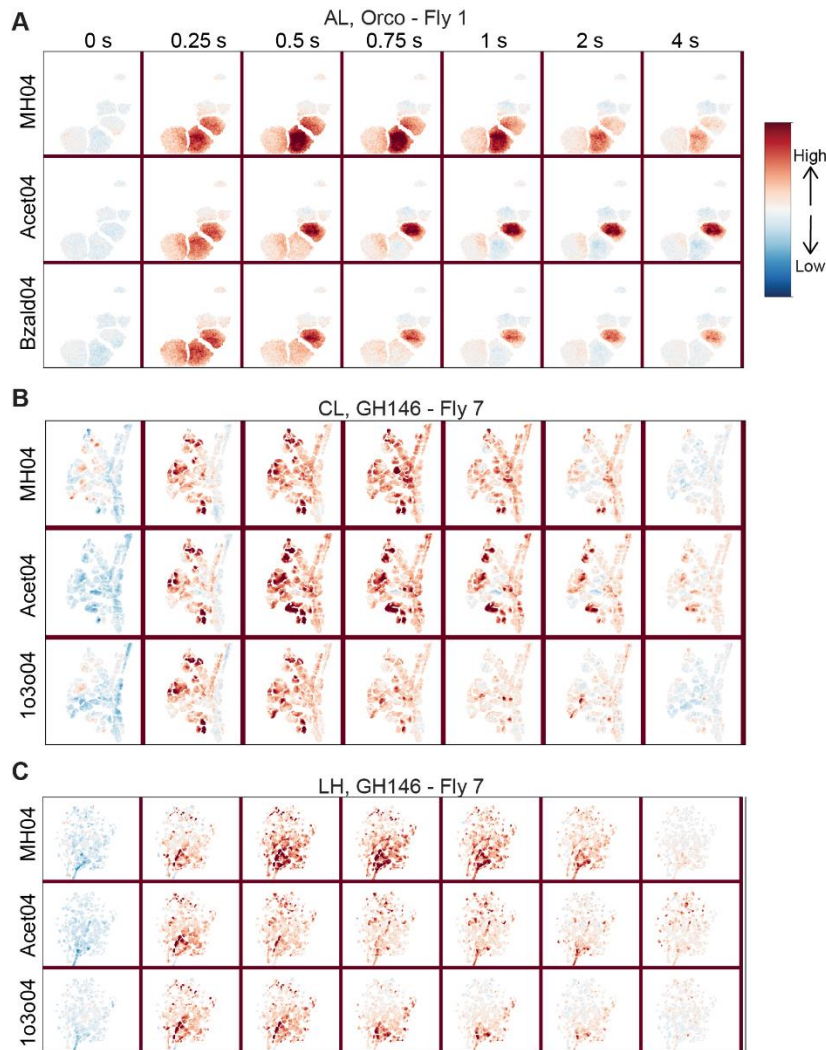
Figure 3.6.1: Time evolution of spatial responses in ORNs and ePN axons

(**A** to **C**) Similar plot as shown in **Figure 6(A)**, but showing spatial distribution of activity at the level of ORN axons in the antennal lobe, and ePN axons entering the calyx and the lateral horns.

Time since odor onset is shown at the top of each panel: 0 s indicates start of odor stimulus and stimulus lasts for 4 seconds. Response to three representative odorants are shown in the three rows.

3.3.6 Idiosyncratic processing underlies how odorants are segregated over time

Given that the initial olfactory circuits have been reported to be stereotyped across flies(Fishilevich and Vosshall, 2005; Jefferis et al., 2007; Vosshall et al., 2000; Vosshall, 2008), it would be reasonable to expect the variability across flies in these peripheral neural circuits to be low. However, our results (**Figure 3.6D**) indicate that decorrelation of odor-evoked responses occur at different rates in different flies. To further examine this issue, we compared how similarity between pairs of odorants evolved over time in different flies (**Figure 3.7A**). Note that the hot colors indicate high correlations/similarity and cool colors indicate negative correlations. Also, clearly observable in the correlation plots shown for the two representative flies is the initial vertical band of high correlation immediately after odor onset. However, note that correlation between different stimulus pairs transformed rapidly. Bands of highly-correlated responses observed immediately after odor onset (show using hotter colors) transitioned to dissimilar responses (less hot colors) at varying points in time. More importantly, the pairwise odor correlation patterns differed between flies indicating that although the odor responses

119

became more distinct, which pairs of odorants became separable at which point in time depended not only on the odorants but also varied from one fly to another.

To further quantify this result, we computed and plotted the standard deviation in pairwise odor response correlations across flies (**Figure 3.7B**). High standard deviation would identify pairs of odorants that were decorrelated differently in different flies. Our results indicate that some odor pairs were indeed processed in a relatively conserved manner across flies (identified using arrowheads), whereas many differed starting from the activity they evoked at the level of ORN axons. The standard deviation between flies were relatively less at the level of ePN axons compared to their dendritic activity, whereas the multiglomerular iPNs had the higher levels of variability even though they integrated inputs from multiple different ORNs. These results indicate that while odor-evoked response patterns decorrelated to become more distinct over time in all flies, this computation was performed in an idiosyncratic fashion.

To illustrate the variability across flies, for each stimulus pair we plotted the median response similarity (**Figure 3.7C;** median over time and each row shows variance across flies for each odor-pair). Our results indicate that the attractive odorants (indicated using arrowheads at the bottom of the panel) were more reliably represented across flies and evoked less variable responses in ORNs and ePNs. Overall, the variability was reduced at the level of ePN axonal responses in calyx and lateral horns. In sum, these results indicate that odor-evoked responses,

even in the early olfactory circuits are not stereotyped for most odorants.
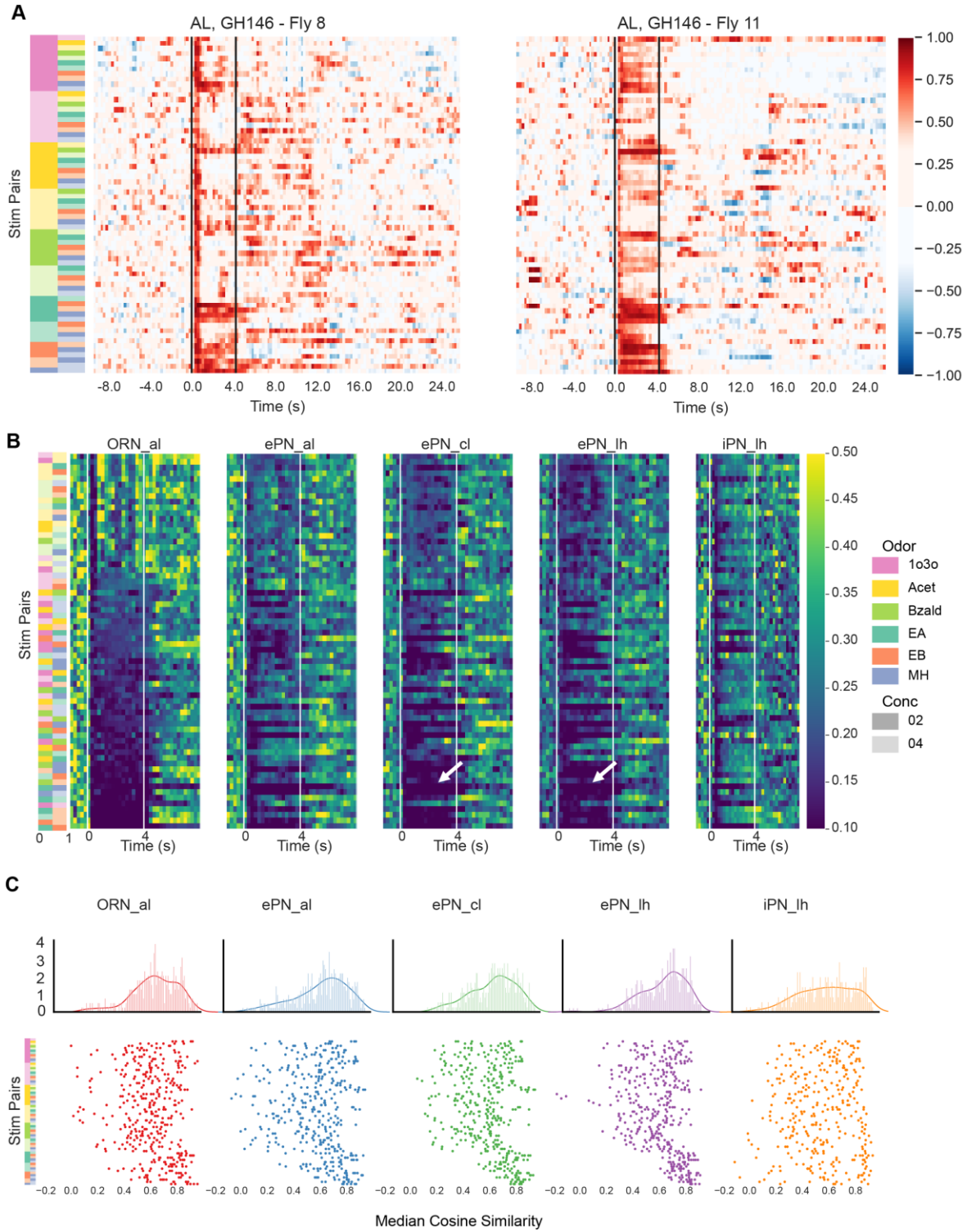
Figure 3.7: Pairwise odor similarities vary across flies

(A) Pairwise cosine similarities of ePN dendritic responses and how they evolve as a function of time are shown as a heatmap. Each row tracks response similarity between one odor pair, and each column represents one time point. The identity of each stimulus pair tracked in a given row is indicated using a color bar on the left of the heatmap. The four second window when the odorant was presented in indicated using black vertical lines. Hotter colors indicate more similarity and cooler colors indicate less similarity. Panel of the right, shows evolution of pairwise cosine similarity for the same pairs of odorants (ordered as shown on the left panel) but in a different fly.

(B) For each odor-pair, the standard deviation in pairwise odor similarity across individuals were calculated and plotted as a function of time. Hot regions in the heatmap show the standard deviation of the cosine similarity across individual fly was greater (i.e. more variability across flies). Similar plots, but characterizing variation in pairwise odor similarity in the five fly line/regions studied are shown. The color bar on the left identifies the odor pair tracked in each row. Note that the rows are sorted in descending order based on standard deviation values observed in the ORN level.

(C) The median cosine similarity during the 4s stimulation period for each stimulus pair, and for each fly, is shown as a scatter plot (bottom). Therefore, each marker represents median pairwise odor similarity observed in a single fly, and each row tracks variation across flies. The identity of the odor pairs corresponding to each row is indicated using the color bar on the left. Tighter packing of individual markers along a single row indicates responses observed across individual flies were highly reliable. The overall distribution across odor pairs and flies is shown on the top.

3.3.7 Stimulus evoked ON and OFF responses

Finally, we examined how stimulus-evoked responses were patterned after the stimulus termination (i.e. the stimulus-evoked OFF responses). We found that at the level of ORNs two types of responses were observed after stimulus termination: continuation of the ON response and inhibition in new ROIs that did not have an ON response. Excitatory responses only during the OFF period were seldom observed at the level of sensory neuron responses (**Figure 3.8A**).

In comparison, the OFF responses observed at the level of ePN dendrites and ePN/iPN axons showed response patterns that were more orthogonal with respect to the ON responses (**Figure 3.8A; Figure 8.1**). ROIs that were active during ON period returned to baseline activity levels or even below baseline level responses (i.e. inhibition) in many ROIs. Whereas, ROIs that were not activated by stimulus exposure or even inhibited during the ON periods, tended to have a strong OFF response.

To understand how dissimilar were the neural responses observed during and after stimulus termination, we performed a cross-correlation analysis. A snapshot of activity across all ROIs was regarded as a high-dimensional vector. The similarity between each response vector with every other response vector that was observed over time was computed and shown succinctly as a correlation matrix (**Figure 3.8B**). Hot colors were used to indicate high correlation/similarity and cool colors to indicate negative correlation/dissimilarity. Note that while response vector observed during odor presentations (i.e. the ON responses) were well correlated amongst themselves, the responses observed after odor termination (i.e. the OFF

responses) poorly correlated with these ON responses (arrow head). This relationship between the ON and the OFF responses was observed in all three neural populations and in every fly studied.

To quantify how much the OFF patterns deviated from the ON patterns, we computed the angles between the mean population vectors during the ON and OFF periods (**Figure 3.8C**). Consistent with interpretation of the correlation plots, for most odorants, the ON and OFF response vectors evoked by the same odorant had an angular similarity in the 60°– 100°range (closer to 0° indicates similar responses and 90° indicates orthogonal responses).

Finally, we examined whether the response patterns evoked after odor termination are as diverse as those observed during stimulus presence. To compare pattern diversity, we used the number of principal components that were required to capture 90% of the total variance of the data (can also be thought of as a measure of intrinsic dimensionality of the dataset; **Figure 8D**). Surprisingly, compared to the ON responses, our results indicate that the OFF patterns were more diverse and needed more principal component to capture the same amount of variance in the response patterns observed.

In sum, our results indicate that for most odorants, another round of diverse response patterns were observed following stimulus termination. More importantly, these response patterns were dissimilar to the odor-evoked ON responses, and were a common encoding feature in all three neural response populations and all flies studied.
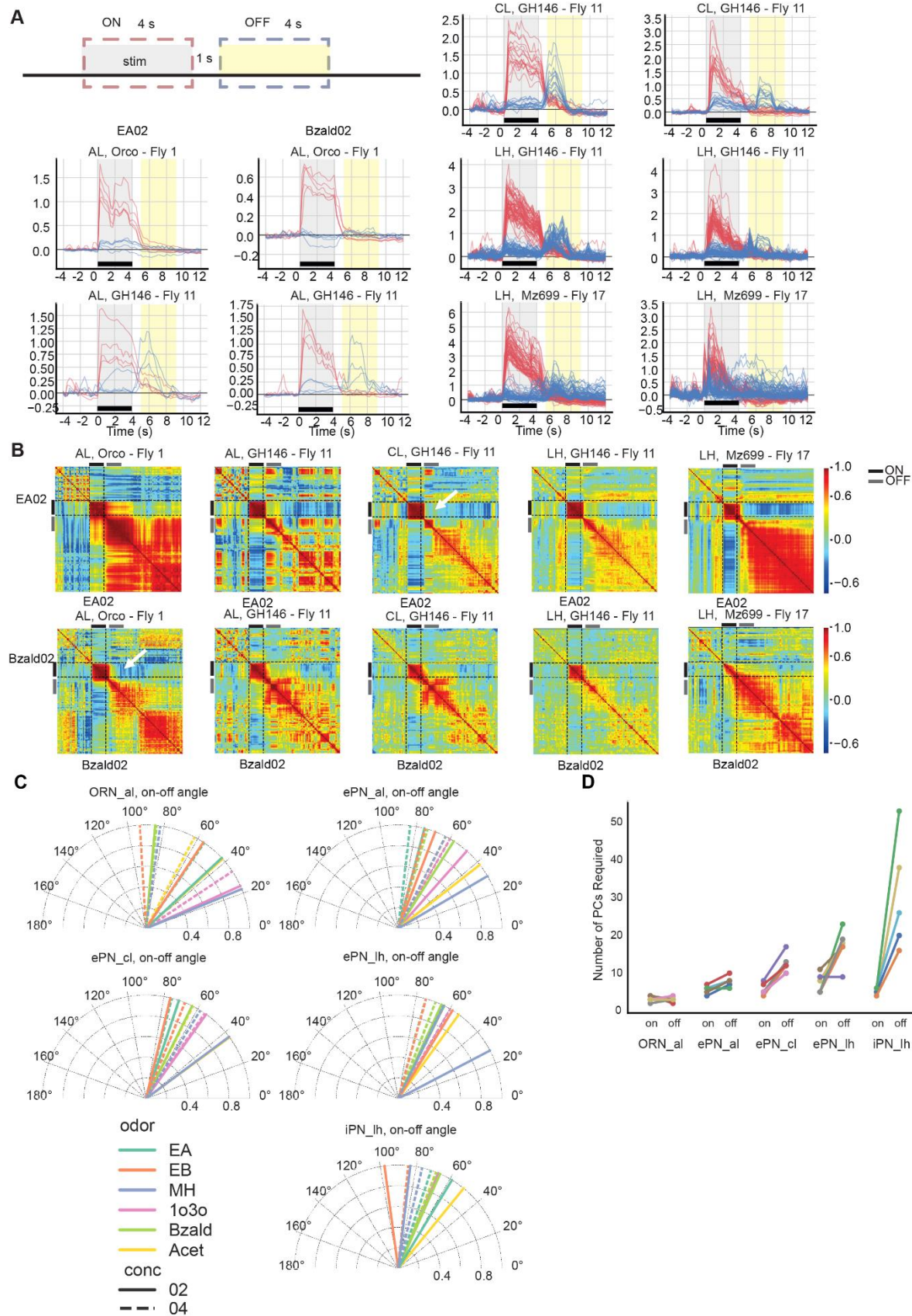
Figure 3.8: Odor evoked ON vs. OFF responses

(A) The top and bottom 5% of traces sorted by the mean amplitude during stimulus are shown, with the top 5% in red, and the bottom 5% in blue. The ON and OFF response windows are schematic schematically identified in the plot. Responses evoked by two representative odorants in each of the five fly line/region combinations are shown.

(B) Evolution of correlation between neural activity before, during and after odor exposure are shown as a heatmap. The black bar on the left and top indicates the time period when the stimulus was delivered. Hot colors indicate high similarity and cool colors indicate low similarity. Note that each non-diagonal pixel represents similarity between ensemble ROI activities in one time bin versus those in another time bin. One row or column represents the correlation between one ensemble ROI activity vector with all other ensemble ROI vectors. Correlation heatmaps for two representative stimuli are shown for all three fly lines and five locations imaged.

(C) Angle between mean ON and OFF response patterns evoked by each odorant is shown. Different colors represent different stimuli and the line style represents the two concentration levels.

(D) The number of principal components needed to account for 90% of the data variance during ON and OFF response periods are plotted as a pair of points for each fly line/regions. Colors indicate individual flies.
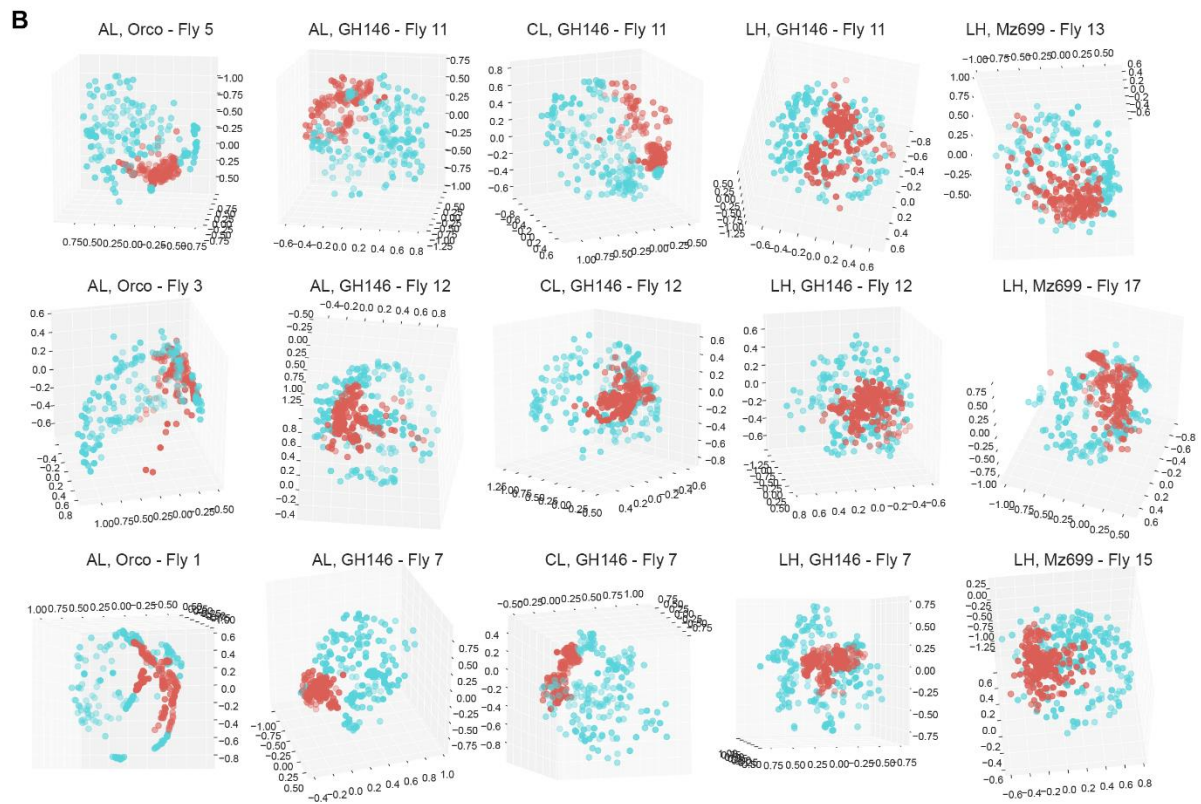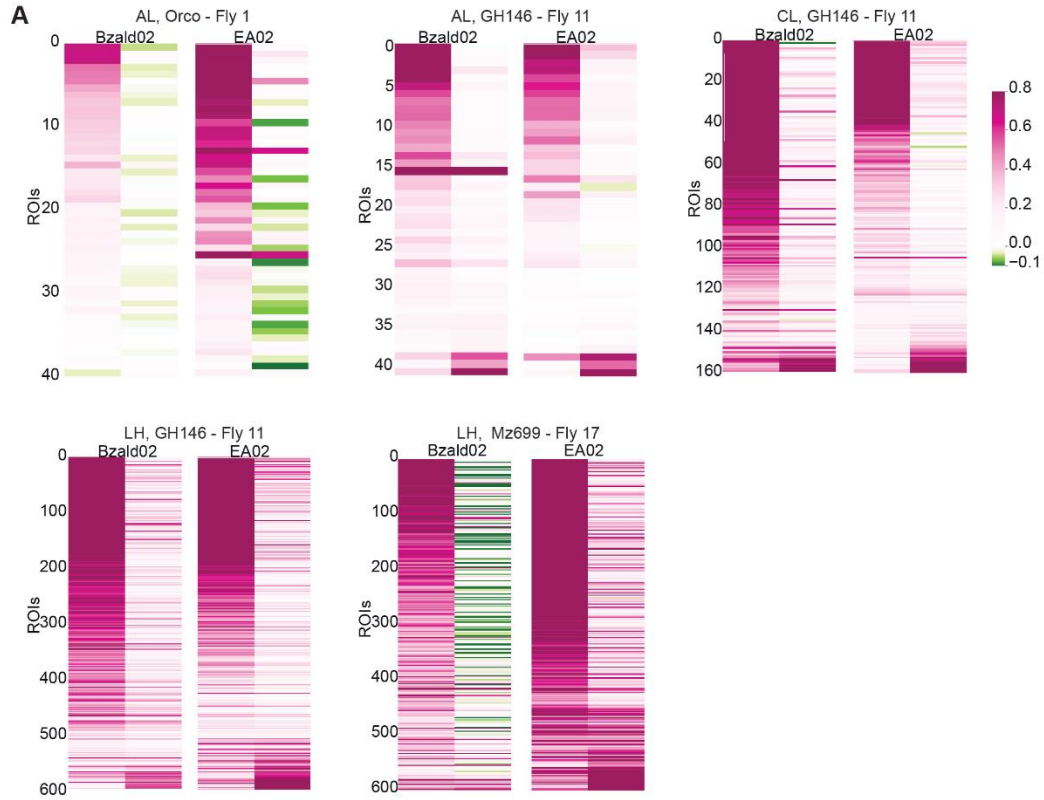
Figure 3.8.1: Odor evoked ON vs. OFF responses.

(A) The average responses across all ROIs during the ON and OFF response periods are stacked next to each other and shown as a color bar. In each panel, left column indicates ON responses (peak activity during 4s ON window) and right column shows the OFF responses (peak activity during 4s window after termination of the stimulus). Each row represents one ROI.

(B) ON vs OFF response pattern comparison following visualization using a multi-dimensional scaling (MDS) approach. The ensemble responses at each time point during the ON and OFF period were regarded as high-dimensional vectors, and were plotted in a 3D plot after MDS dimensionality reduction. Response vectors evoked when odorants were presented are labeled in red and the response vectors during the after stimulus termination are shown in cyan. Results from three representative flies for each line/region is shown.

3.4 Discussion

We sought to understand how sensory input from olfactory receptor neurons are spatially and temporally reformatted by two different downstream neural populations: ePNs and iPNs. While ePNs are cholinergic and receive input from a single glomerulus (Couto et al., 2005b) , iPNs are mostly GABAergic and multiglomerular (Wang et al., 2014). Further, while ePNs project to both calyx and lateral horn, iPN axons only innervate the lateral horns (Strutz et al., 2014). So, given the differences in the nature of input received (from one vs. many types of ORNs), and the downstream centers they feed onto, it is reasonable to expect that the ePNs and iPNs use different transformations to reformat sensory information received. However, our data reveal that

several spatial and temporal aspects of odor-evoked responses were strikingly similar in both these neural populations.

3.4.1 Spatial Organization of ePN and iPN processes

Our results indicate that both ePN and iPN axons were organized in the lateral horns such that nearby spatial regions had similar odor tuning. Though this relationship was weak, it was still significantly higher than the spatial organization of ePN axons in the calyx. More importantly, our results indicated that in lateral horn, ePNs and iPNs axons with similar stimulus tuning spatially overlapped. Since the iPN axons in different regions of lateral horn were differentially tuned to different odorants, our results indicate that this neural population may provide feed-forward inhibition in an odor specific manner.

In the antennal lobe, the ePN dendrites again showed a weak correlation between odor tuning and spatial location. Notably, the tuning vs distance relationship varied between flies. The weak spatial organization of antennal lobe neural activity in flies are qualitatively similar to results reported in the mice olfactory bulb(Ma et al., 2012). In the calyx, the ePN axons were organized such that the attractive odorants strongly activated the periphery, whereas the repulsive odorants were driving responses in the core regions. This organizational structure was found in all the flies, and is consistent with anatomical studies that revealed that dorso-medial glomeruli innervate the outer rim of the calyx and the ventral glomeruli send processes to the inner core regions(Tanaka et al., 2004). Note that this organization of ePN axons in the calyx is indeed non-linear, and therefore was not picked up in the linear correlation measures we used to quantify the relationship between ROI location and tuning. Taken together, these results indicate that the observed differences in the organizational logic between dendritic and axonal compartments of

ePNs was observed in all flies examined, arguably may indicate that different computations (global vs. local) that may be performed in these centers.

We also examined whether a single antennal lobe region had a one-to-one, local or global influence on the downstream centers. Note that the activity observed in the axonal boutons entering calyx and lateral horns incorporates the feedforward input from the antennal lobe ePNs and any recurrent pre-synaptic inhibition that is recruited in the target region. Although our results were obtained from a linear statistical analysis with a sparsity constraint, it indicates that each antennal lobe ROI contributes globally. Furthermore, most ROIs appeared to have both positive and negative influence in the downstream regions indicating that ePN activity is further transformed as it reaches calyx and lateral horns. These results were again replicated in different flies indicating that this is a generic organizing principle in the fly olfactory system.

In the lateral horn, a sterotyped, dorso-lateral region that was activated by all putative attractive odorants were detected. A prior study had identified a similar region in the lateral horn for the iPN axons(Strutz et al., 2014). Our results reveal that this lateral horn region is not only innervated by feed-forward inhibition (i.e. iPN axons), but also by feed-forward excitatory inputs (i.e. ePN axons) from the antennal lobe as well. Such overlapping odor tunings for ePN and iPN inputs suggest possible counter-balancing interactions that could theoretically implement a high-pass filter(Parnas et al., 2013) in this local region (when ePN input > iPN input). However, in other lateral horn regions, the iPN and ePN odor response tuning mismatched. Understanding how such mismatched feed-forward excitation and inhibition interact and to carry out what computations would need further examination.

3.4.2 Temporal organization of ePN and iPN responses

In addition to the spatial reorganization of activity, our results indicate that the odor-evoked responses were dynamic and evolved over time at the level of sensory neurons and in both ePNs and iPNs. The initial responses immediately after the stimulus onset were strong but did not have much discriminatory information. Over time, neural activity patterns evoked by different stimuli became more odor-specific. This decorrelation of odor-evoked responses over time was observed in all three neural populations examined. However, the trends observed (which odor pair became distinct when) observed varied even between the dendritic and axonal compartments of the same neural populations, and between flies. This result indicates that a generic computational function can be achieved in an idiosyncratic fashion in flies, and that the information transmitted to the calyx and lateral horns may be qualitatively different.

The decorrelation result is strikingly similar to what has been reported in other model organisms, particularly in zebra fish(Friedrich and Laurent, 2001), with one caveat. We found that decorrelation already happens at the ORN level and gets accelerated downstream.

 However, it is in stark contrast with a recent hypothesis put-forth for odor recognition that suggests initial responses carry information odor identity(Wilson et al., 2017). One possible explanation for the lack of odor-specificity at the stimulus onset could be that the neural activity immediately following stimulus presentation indicates stimulus presence and help with localization. Such localization signals have been reported in many other sensory systems(Bekesy, 2017). We note that the responses immediately following this localization signal may still be extremely important for the fly to recognize the odorant.

Extraction of odor specific information may happen in two different ways. First, the information may be refined in a systematic manner, such that the initial responses recognize odor groups and

additional features are extracted to allow precise recognition (Odor present -> fruity -> tropical -> pineapple; analogous to a decision tree). In this case, a snapshot of activity during later time point is sufficient to recognize the stimulus, while the initial responses may be utilized for other sensory computations. The second possibility is that features are extracted in a serial fashion but the later responses need not be the most unique features. This latter scenario is analogous to serial parsing of words (r·e·a·d· vs. r·e·e·l· vs. r·a·i·l· vs. m·e·e·t·). While the initial letters are still important for word recognition, the subsequent letters extracted are necessary but in isolation are not sufficient to allow precise recognition. In this case, an integration of all the features extracted might be necessary for stimulus recognition. Our results indicate that temporal patterning observed in the fly antennal lobe may be more analogous first scenario (i.e. pairwise similarity smoothly reducing over time), but achieved in an idiosyncratic fashion, indicating multiple different solutions may exist to this problem.

It would important to point out that variations across different individuals could arise trivially due to unaccounted differences in experimental conditions between different experiments. However, our results reveal that not all results we observed varied across individual flies. First, as highlighted earlier, gross spatial features matched across individual flies (**Figure 3.4**). Further, even in the temporal dimension, certain pairs of odorants evoked responses that were highly consistent (**Figure 3.7**). Such robustness in spatial and temporal features, at least for a subset of odorants, indicate that the variations observed in our dataset cannot be attributed solely to trivial differences in experimental conditions. It would be worth pointing out that such variations in neural responses could underlie differences in behavioral preferences in individual flies(Honegger et al., 2020). What variations are important and therefore gets translated to

mediate idiosyncratic differences in odor preferences, and what variations are squashed to underlie robust recognition needs further examination.

Finally, our results indicate that the stimulus-evoked responses do not stop after stimulus termination. At the level of sensory neurons, these are persistence of activity, in some cases excitation and other inhibition, that was observed during the stimulus. However, in the ePN and iPN dendrites and axons, the responses often switched from one ensemble to another. Therefore, stimulus ON and OFF responses were orthogonal to each other, and was observed in all flies. These results are consistent with those reported in other sensory systems, and in particular the locust olfactory system(Nizampatnam et al., 2018).

What is the purpose of these elaborate OFF responses? In cockroaches, such responses were observed directly at the level of sensory neurons and were thought to indicate reduction in stimulus concentrations(Burgstaller and Tichy, 2011). Such dedicated ON and OFF neurons were not found in flies. A single ROI in any region was able to respond during either ON or OFF periods depending on the odor. In a different study, it was reported that these OFF responses may indicate 'unsensing' of a stimulus (analogous to a pause after a tone or space after word), and were found to be better predictors of termination of behavioral responses(Saha et al., 2017). Furthermore, our results here indicate that the response patterns observed after stimulus termination were stimulus specific and more diverse than those observed during the stimulus presence period. Further, when odorants are encountered in sequences, the OFF response of the first stimulus was found to contrast enhance the neural activity evoked by the second stimulus. While these results are similar to the findings observed in locusts, causal relationship between OFF responses and their behavioral contributions remains to be determined.

Acknowledgements

Author contributions

HR and BR conceived the study and designed the experiments/analyses. HR performed all the light-sheet experiments and collected the data. LZ motion corrected the raw calcium imaging movies and extracted ROIs in collaboration with HR. HR performed all the subsequent data analysis with LZ's assistance. HR, LZ and BR wrote the paper taking inputs from all the authors. YBS and TH advised on the selection of fly lines and light-sheet imaging, respectively. BR supervised all aspects of the work.

3.5 References:

Ahrens, M.B., Orger, M.B., Robson, D.N., Li, J.M., and Keller, P.J. (2013). Whole-brain functional imaging at cellular resolution using light-sheet microscopy. Nat Methods 10, 413-+.

Ahsan, J., Knaden, M., Strutz, A., Sachse, S., and Hansson, B.S. (2017). Spatial representation of odorant valence in an insect brain. Mech Develop 145, S115-S115.

Akalal, D.B., Wilson, C.F., Zong, L., Tanaka, N.K., Ito, K., and Davis, R.L. (2006). Roles for Drosophila mushroom body neurons in olfactory learning and memory. Learn Mem 13, 659-668.

Alberch, P. (1991). From genes to phenotype: dynamical systems and evolvability. Genetica 84, 5-11.

Aron, C. (1979). Mechanisms of control of the reproductive function by olfactory stimuli in female mammals. Physiological Reviews 59, 229-284.

Asahina, K., Louis, M., Piccinotti, S., and Vosshall, L.B. (2009). A circuit supporting concentration-invariant odor perception in Drosophila. Journal of biology 8, 9.

Averbeck, B.B., Latham, P.E., and Pouget, A. (2006). Neural correlations, population coding and computation. Nature Reviews Neuroscience 7, 358-366.

Azevedo, F.A.C., Carvalho, L.R.B., Grinberg, L.T., Farfel, J.M., Ferretti, R.E.L., Leite, R.E.P., Jacob, W., Lent, R., and Herculano-Houzel, S. (2009). Equal Numbers of Neuronal and Nonneuronal Cells Make the Human Brain an Isometrically Scaled-Up Primate Brain. J Comp Neurol 513, 532-541.

Badel, L., Ohta, K., Tsuchimoto, Y., and Kazama, H. (2016). Decoding of Context-Dependent Olfactory Behavior in Drosophila. Neuron 91, 155-167.

Bekesy, G.V. (2017). Sensory Inhibition.

Bell, Joseph S., and Wilson, Rachel I. (2016). Behavior Reveals Selective Summation and Max Pooling among Olfactory Processing Channels. Neuron 91, 425-438.

Benton, R., Vannice, K.S., Gomez-Diaz, C., and Vosshall, L.B. (2009). Variant Ionotropic Glutamate Receptors as Chemosensory Receptors in Drosophila. Cell 136, 149-162.

Bhalla, U.S., and Bower, J.M. (1997). Multiday recordings from olfactory bulb neurons in awake freely moving rats: Spatially and temporally organized variability in odorant response properties. J Comput Neurosci 4, 221-256.

Bhandawat, V., Maimon, G., Dickinson, M.H., and Wilson, R.I. (2010). Olfactory modulation of flight in Drosophila is sensitive, selective and rapid. The Journal of experimental biology 213, 3625-3635.

Bhandawat, V., Olsen, S.R., Gouwens, N.W., Schlief, M.L., and Wilson, R.I. (2007). Sensory processing in the Drosophila antennal lobe increases reliability and separability of ensemble odor representations. Nat Neurosci 10, 1474-1482.

Bronson, F.H. (1979). The Reproductive Ecology of the House Mouse. The Quarterly Review of Biology 54, 265-299.

Buehlmann, C., Graham, P., Hansson, B.S., and Knaden, M. (2015). Desert ants use olfactory scenes for navigation. Anim Behav 106, 99-105.

Burgstaller, M., and Tichy, H. (2011). Functional asymmetries in cockroach ON and OFF olfactory receptor neurons. J Neurophysiol 105, 834-845.

Bushdid, C., Magnasco, M.O., Vosshall, L.B., and Keller, A. (2014). Humans Can Discriminate More than 1 Trillion Olfactory Stimuli. Science 343, 1370-1372.

Carey, A.F., and Carlson, J.R. (2011). Insect olfaction from model systems to disease control. Proc Natl Acad Sci U S A 108, 12987-12995.

Caron, S.J., Ruta, V., Abbott, L.F., and Axel, R. (2013). Random convergence of olfactory inputs in the Drosophila mushroom body. Nature 497, 113-117.

Cedar, H., and Bergman, Y. (2009). Linking DNA methylation and histone modification: patterns and paradigms. Nat Rev Genet 10, 295-304.

Chen, T.W., Wardill, T.J., Sun, Y., Pulver, S.R., Renninger, S.L., Baohan, A., Schreiter, E.R., Kerr, R.A., Orger, M.B., Jayaraman, V.*, et al.* (2013). Ultrasensitive fluorescent proteins for imaging neuronal activity. Nature 499, 295-300.

Chen, X., Mu, Y., Hu, Y., Kuan, A.T., Nikitchenko, M., Randlett, O., Chen, A.B., Gavornik, J.P., Sompolinsky, H., Engert, F., and Ahrens, M.B. (2018). Brain-wide Organization of Neuronal Activity and Convergent Sensorimotor Transformations in Larval Zebrafish. Neuron 100, 876-890 e875.

Chou, Y.H., Spletter, M.L., Yaksi, E., Leong, J.C., Wilson, R.I., and Luo, L. (2010). Diversity and wiring variability of olfactory local interneurons in the Drosophila antennal lobe. Nat Neurosci 13, 439-449.

Clyne, P., Grant, A., O'Connell, R., and Carlson, J.R. (1997). Odorant response of individual sensilla on the Drosophila antenna. Invert Neurosci 3, 127-135.

Colomb, J., Reiter, L., Blaszkiewicz, J., Wessnitzer, J., and Brembs, B. (2012). Open Source Tracking and Analysis of Adult Drosophila Locomotion in Buridan's Paradigm with and without Visual Targets. Plos One 7.

Couto, A., Alenius, M., and Dickson, B.J. (2005a). Molecular, anatomical, and functional organization of the Drosophila olfactory system. Current biology : CB 15, 1535-1547.

Couto, A., Alenius, M., and Dickson, B.J. (2005b). Molecular, anatomical, and functional organization of the Drosophila olfactory system. Current Biology 15, 1535-1547.

de Bruyne, M., Clyne, P.J., and Carlson, J.R. (1999). Odor Coding in a Model Olfactory Organ: TheDrosophila Maxillary Palp. The Journal of Neuroscience 19, 4520-4532.

de Bruyne, M., Foster, K., and Carlson, J.R. (2001). Odor coding in the Drosophila antenna. Neuron 30, 537-552.

Debelle, J.S., and Heisenberg, M. (1994). Associative Odor Learning in Drosophila Abolished by Chemical Ablation of Mushroom Bodies. Science 263, 692-695.

Dobritsa, A.A., van der Goes van Naters, W., Warr, C.G., Steinbrecht, R.A., and Carlson, J.R. (2003). Integrating the molecular and cellular basis of odor coding in the Drosophila antenna. Neuron 37, 827-841.

Duchamp-Viret, P., Duchamp, A., and Chaput, M.A. (2000). Peripheral odor coding in the rat and frog: quality and intensity specification. The Journal of neuroscience : the official journal of the Society for Neuroscience 20, 2383-2390.

Dweck, H.K., Ebrahim, S.A., Khallaf, M.A., Koenig, C., Farhan, A., Stieber, R., Weissflog, J., Svatos, A., Grosse-Wilde, E., Knaden, M., and Hansson, B.S. (2016). Olfactory channels associated with the Drosophila maxillary palp mediate short- and long-range attraction. Elife 5.

Fishilevich, E., and Vosshall, L.B. (2005). Genetic and Functional Subdivision of the Drosophila Antennal Lobe. Current Biology 15, 1548-1553.

Friedrich, R.W., and Laurent, G. (2001). Dynamic optimization of odor representations by slow temporal patterning of mitral cell activity. Science 291, 889-894.

Gottfried, J., Hummel, T., and Welge-Lüssen, A. (2006). Taste and smell: An update. Chap Smell: Central nervous processing, Vol 63, pp 44–69) Hummel, T and Welge-Lüssen, A doi 10, 000093750.

Gotz, K.G. (1980). Visual guidance in Drosophila. Basic Life Sci 16, 391-407.

Greer, C.J., and Holy, T.E. (2019). Fast objective coupled planar illumination microscopy. Nat Commun 10.

Gschwend, O., Abraham, N.M., Lagier, S., Begnaud, F., Rodriguez, I., and Carleton, A. (2015). Neuronal pattern separation in the olfactory bulb improves odor discrimination learning. Nat Neurosci 18, 1474-+.

Gupta, N., and Stopfer, M. (2012). Functional Analysis of a Higher Olfactory Center, the Lateral Horn. J Neurosci 32, 8138-8148.

Hallem, E.A., and Carlson, J.R. (2004). The odor coding system of Drosophila. Trends Genet 20, 453-459.

Hallem, E.A., and Carlson, J.R. (2006a). Coding of odors by a receptor repertoire. Cell 125, 143-160.

Hallem, E.A., and Carlson, J.R. (2006b). Coding of odors by a receptor repertoire. Cell 125, 143-160.

Hallem, E.A., Ho, M.G., and Carlson, J.R. (2004). The molecular basis of odor coding in the drosophila antenna. Cell 117, 965-979.

Hansson, B.S., and Stensmyr, M.C. (2011). Evolution of insect olfaction. Neuron 72, 698-711.

Heimbeck, G., Bugnon, V., Gendre, N., Keller, A., and Stocker, R.F. (2001). A central neural circuit for experience-independent olfactory and courtship behavior in Drosophila melanogaster. Proc Natl Acad Sci U S A 98, 15336-15341.

Heisenberg, M., Borst, A., Wagner, S., and Byers, D. (1985). Drosophila mushroom body mutants are deficient in olfactory learning. J Neurogenet 2, 1-30.

Hettinger, T.P. (2011). Olfaction is a chemical sense, not a spectral sense. P Natl Acad Sci USA 108, E349-E350.

Hige, T., Aso, Y., Rubin, G.M., and Turner, G.C. (2015). Plasticity-driven individualization of olfactory coding in mushroom body output neurons. Nature 526, 258-262.

Honegger, K.S., Campbell, R.A., and Turner, G.C. (2011). Cellular-resolution population imaging reveals robust sparse coding in the Drosophila mushroom body. J Neurosci 31, 11772-11785.

Honegger, K.S., Smith, M.A.-Y., Churgin, M.A., Turner, G.C., and Bivort, B.L.d. (2020). Idiosyncratic neural coding and neuromodulation of olfactory individuality in Drosophila. PNAS 117, 23292-23297.

Hong, E.J., and Wilson, R.I. (2015). Simultaneous encoding of odors by channels with diverse sensitivity to inhibition. Neuron 85, 573-589.

Hubel, D.H., and Wiesel, T.N. (1959). Receptive fields of single neurones in the cat's striate cortex. J Physiol 148, 574-591.

Hutmacher, F. (2019). Why Is There So Much More Research on Vision Than on Any Other Sensory Modality? Front Psychol 10, 2246-2246.

Jayaraman, V., and Laurent, G. (2007). Evaluating a genetically encoded optical sensor of neural activity using electrophysiology in intact adult fruit flies. Frontiers in Neural Circuits 1.

Jeanne, J.M., Fisek, M., and Wilson, R.I. (2018). The Organization of Projections from Olfactory Glomeruli onto Higher-Order Neurons. Neuron 98, 1198-1213 e1196.

Jeanne, J.M., and Wilson, R.I. (2015). Convergence, Divergence, and Reconvergence in a Feedforward Network Improves Neural Speed and Accuracy. Neuron 88.

Jefferis, G.S., Potter, C.J., Chan, A.M., Marin, E.C., Rohlfing, T., Maurer, C.R., Jr., and Luo, L. (2007). Comprehensive maps of Drosophila higher olfactory centers: spatially segregated fruit and pheromone representation. Cell 128, 1187-1203.

Karunanithi, S., Georgiou, J., Charlton, M.P., and Atwood, H.L. (1997). Imaging of calcium in Drosophila larval motor nerve terminals. J Neurophysiol 78, 3465-3467.

Katz, B., and Miledi, R. (1968). The role of calcium in neuromuscular facilitation. J Physiol 195, 481-492.

Kay, L.M. (2005). Theta oscillations and sensorimotor performance. P Natl Acad Sci USA 102, 3863-3868.

Kay, L.M. (2015). Olfactory system oscillations across phyla. Curr Opin Neurobiol 31, 141-147.

Kay, L.M., Beshel, J., Brea, J., Martin, C., Rojas-Libano, D., and Kopell, N. (2009). Olfactory oscillations: the what, how and what for. Trends in Neurosciences 32, 207-214.

Kay, L.M., and Stopfer, M. (2006). Information processing in the olfactory systems of insects and vertebrates. Semin Cell Dev Biol 17, 433-442.

Kazama, H., and Wilson, R.I. (2009). Origins of correlated activity in an olfactory circuit. Nat Neurosci 12, 1136-1144.

Knaden, M., Strutz, A., Ahsan, J., Sachse, S., and Hansson, B.S. (2012a). Spatial representation of odorant valence in an insect brain. Cell Rep 1, 392-399.

Knaden, M., Strutz, A., Ahsan, J., Sachse, S., and Hansson, B.S. (2012b). Spatial Representation of Odorant Valence in an Insect Brain. Cell Reports 1, 392-399.

Kreher, S.A., Mathew, D., Kim, J., and Carlson, J.R. (2008). Translation of sensory input into behavioral output via an olfactory system. Neuron 59, 110-124.

Lai, S.L., Awasaki, T., Ito, K., and Lee, T. (2008). Clonal analysis of Drosophila antennal lobe neurons: diverse neuronal architectures in the lateral neuroblast lineage. Development 135, 2883-2893.

Laissue, P.P., and Vosshall, L.B. (2008). The Olfactory Sensory Map in Drosophila. In Brain Development in Drosophila melanogaster, G.M. Technau, ed. (New York, NY: Springer New York), pp. 102-114.

Larsson, M.C., Domingos, A.I., Jones, W.D., Chiappe, M.E., Amrein, H., and Vosshall, L.B. (2004). Or83b Encodes a Broadly Expressed Odorant Receptor Essential for Drosophila Olfaction. Neuron 43, 703-714.

Laughlin, S.B., de Ruyter van Steveninck, R.R., and Anderson, J.C. (1998). The metabolic cost of neural information. Nat Neurosci 1, 36-41.

Laurent, G. (2002). Olfactory network dynamics and the coding of multidimensional signals. Nat Rev Neurosci 3, 884-895.

Lin, H.H., Lai, J.S., Chin, A.L., Chen, Y.C., and Chiang, A.S. (2007). A map of olfactory representation in the Drosophila mushroom body. Cell 128, 1205-1217.

Linneweber, G.A., Andriatsilavo, M., Dutta, S.B., Bengochea, M., Hellbruegge, L., Liu, G., Ejsmont, R.K., Straw, A.D., Wernet, M., Hiesinger, P.R., and Hassan, B.A. (2020). A neurodevelopmental origin of behavioral individuality in the Drosophila visual system. Science 367, 1112-1119.

Lledo, P.M., Gheusi, G., and Vincent, J.D. (2005). Information processing in the mammalian olfactory system. Physiol Rev 85, 281-317.

Ma, L., Qiu, Q., Gradwohl, S., Scott, A., Yu, E.Q., Alexander, R., Wiegraebe, W., and Yu, C.R. (2012). Distributed representation of chemical features and tunotopic organization of glomeruli in the mouse olfactory bulb. Proc Natl Acad Sci U S A 109, 5481-5486.

Mao, T., O'Connor, D.H., Scheuss, V., Nakai, J., and Svoboda, K. (2008). Characterization and subcellular targeting of GCaMP-type genetically-encoded calcium indicators. PLoS One 3, e1796.

Marin, E.C., Jefferis, G.S., Komiyama, T., Zhu, H., and Luo, L. (2002). Representation of the glomerular olfactory map in the Drosophila brain. Cell 109, 243-255.

McGuire, S.E., Le, P.T., and Davis, R.L. (2001). The role of Drosophila mushroom body signaling in olfactory memory. Science 293, 1330-1333.

Menzel, R., and Muller, U. (1996). Learning and memory in honeybees: from behavior to neural substrates. Annu Rev Neurosci 19, 379-404.

Mittal, A.M., Gupta, D., Singh, A., Lin, A.C., and Gupta, N. (2020). Multiple network properties overcome random connectivity to enable stereotypic sensory responses. Nat Commun 11, 1023.

Mizunami, M., Weibrecht, J.M., and Strausfeld, N.J. (1998). Mushroom bodies of the cockroach: Their participation in place memory. J Comp Neurol 402, 520-537.

Murthy, M., Fiete, I., and Laurent, G. (2008). Testing odor response stereotypy in the Drosophila mushroom body. Neuron 59, 1009-1023.

Nagel, K.I., and Wilson, R.I. (2011). Biophysical mechanisms underlying olfactory receptor neuron dynamics. Nat Neurosci 14, 208-216.

Neher, E., and Sakaba, T. (2008). Multiple roles of calcium ions in the regulation of neurotransmitter release. Neuron 59, 861-872.

Nizampatnam, S., Saha, D., Chandak, R., and Raman, B. (2018). Dynamic contrast enhancement and flexible odor codes. Nat Commun 9, 3062.

Olsen, S.R., and Wilson, R.I. (2008). Lateral presynaptic inhibition mediates gain control in an olfactory circuit. Nature 452, 956-960.

Parnas, M., Lin, A.C., Huetteroth, W., and Miesenbock, G. (2013). Odor discrimination in Drosophila: from neural population codes to behavior. Neuron 79, 932-944.

Pigliucci, M. (2010). Genotype-phenotype mapping and the end of the 'genes as blueprint' metaphor. Philos T R Soc B 365, 557-566.

Pnevmatikakis, E.A., Soudry, D., Gao, Y.J., Machado, T.A., Merel, J., Pfau, D., Reardon, T., Mu, Y., Lacefield, C., Yang, W.J., *et al.* (2016). Simultaneous Denoising, Deconvolution, and Demixing of Calcium Imaging Data. Neuron 89, 285-299.

Poucher, W.A. (1974). Perfumes, Cosmetics and Soaps, 7 edn (Chapman and Hall).

Raman, B., Joseph, J., Tang, J., and Stopfer, M. (2010). Temporally Diverse Firing Patterns in Olfactory Receptor Neurons Underlie Spatiotemporal Neural Codes for Odors. J Neurosci 30, 1994-2006.

Reinhard, J., Srinivasan, M.V., and Zhang, S. (2004). Olfaction: scent-triggered navigation in honeybees. Nature 427, 411-411.

Rubin, B.D., and Katz, L.C. (1999). Optical imaging of odorant representations in the mammalian olfactory bulb. Neuron 23, 499-511.

Rusakov, D.A. (2006). Ca2+-dependent mechanisms of presynaptic control at central synapses. Neuroscientist 12, 317-326.

Rytz, R., Croset, V., and Benton, R. (2013). Ionotropic receptors (IRs): chemosensory ionotropic glutamate receptors in Drosophila and beyond. Insect Biochem Mol Biol 43, 888-897.

Sachse, S., and Krieger, J. (2011). Olfaction in insects. e-Neuroforum 2, 49.

Saha, D., Leong, K., Li, C., Peterson, S., Siegel, G., and Raman, B. (2013). A spatiotemporal coding mechanism for background-invariant odor recognition. Nat Neurosci 16, 1830-1839.

Saha, D., Li, C., Peterson, S., Padovano, W., Katta, N., and Raman, B. (2015). Behavioural correlates of combinatorial versus temporal features of odour codes. Nat Commun 6, 6953.

Saha, D., Sun, W., Li, C., Nizampatnam, S., Padovano, W., Chen, Z., Chen, A., Altan, E., Lo, R., Barbour, D.L., and Raman, B. (2017). Engaging and disengaging recurrent inhibition coincides with sensing and unsensing of a sensory stimulus. Nat Commun 8, 15413.

Sarafoleanu, C., Mella, C., Georgescu, M., and Perederco, C. (2009). The importance of the olfactory sense in the human behavior and evolution. J Med Life 2, 196-198.

Schultzhaus, J.N., Saleem, S., Iftikhar, H., and Carney, G.E. (2017). The role of the Drosophila lateral horn in olfactory information processing and behavioral response. J Insect Physiol 98, 29-37.

Scott, D.W. (17 August 1992). Multivariate Density Estimation: Theory, Practice, and Visualization (John Wiley & Sons, Inc).

Semmelhack, J., and Wang, J.W. (2009). Select *Drosophila* glomeruli mediate innate olfactory attraction and aversion. Nature 459, 218-223.

Shimizu, K., and Stopfer, M. (2017). A Population of Projection Neurons that Inhibits the Lateral Horn but Excites the Antennal Lobe through Chemical Synapses in Drosophila. Frontiers in Neural Circuits 11.

Silbering, A.F., Bell, R., Galizia, C.G., and Benton, R. (2012). Calcium Imaging of Odor-evoked Responses in the Drosophila Antennal Lobe. Jove-J Vis Exp.

Simpson, J.H. (2009). Mapping and Manipulating Neural Circuits in the Fly Brain. Adv Genet 65, 79-143.

Steck, K., Veit, D., Grandy, R., Badia, S.B.i., Mathews, Z., Verschure, P., Hansson, B.S., and Knaden, M. (2012). A high-throughput behavioral paradigm for Drosophila olfaction - The Flywalk. Scientific Reports 2, 361.

Stensmyr, Marcus C., Dweck, Hany K.M., Farhan, A., Ibba, I., Strutz, A., Mukunda, L., Linz, J., Grabe, V., Steck, K., Lavista-Llanos, S., *et al.* A Conserved Dedicated Olfactory Circuit for Detecting Harmful Microbes in Drosophila. Cell 151, 1345-1357.

Stensmyr, M.C., Giordano, E., Balloi, A., Angioy, A.M., and Hansson, B.S. (2003). Novel natural ligands for Drosophila olfactory receptor neurones. The Journal of experimental biology 206, 715-724.

Stern, S., Kirst, C., and Bargmann, C.I. (2017). Neuromodulatory Control of Long-Term Behavioral Patterns and Individuality across Development. Cell 171, 1649-1662 e1610.

Stocker, R.F. (1994). The organization of the chemosensory system in Drosophila melanogaster: a rewiew. Cell and Tissue Research 275, 3-26.

Stopfer, M., Bhagavan, S., Smith, B.H., and Laurent, G. (1997). Impaired odour discrimination on desynchronization of odour-encoding neural assemblies. Nature 390, 70-74.

Stopfer, M., Jayaraman, V., and Laurent, G. (2003). Intensity versus identity coding in an olfactory system. Neuron 39, 991-1004.

Strutz, A., Soelter, J., Baschwitz, A., Farhan, A., Grabe, V., Rybak, J., Knaden, M., Schmuker, M., Hansson, B.S., and Sachse, S. (2014). Decoding odor quality and intensity in the Drosophila brain. Elife 3.

Su, C.-Y., Menuz, K., Reisert, J., and Carlson, J.R. (2012). Non-synaptic inhibition between grouped neurons in an olfactory circuit. Nature 492, 66-71.

Suh, G.S.B., Wong, A.M., Hergarden, A.C., Wang, J.W., Simon, A.F., Benzer, S., Axel, R., and Anderson, D.J. (2004). A single population of olfactory sensory neurons mediates an innate avoidance behaviour in Drosophila. Nature 431, 854-859.

Tanaka, N.K., Awasaki, T., Shimada, T., and Ito, K. (2004). Integration of chemosensory pathways in the Drosophila second-order olfactory centers. Curr Biol 14, 449-457.

Tanaka, N.K., Ito, K., and Stopfer, M. (2009). Odor-evoked neural oscillations in Drosophila are mediated by widely branching interneurons. J Neurosci 29, 8595-8603.

Turner, S.L., and Ray, A. (2009). Modification of CO2 avoidance behaviour in Drosophila by inhibitory odorants. Nature 461, 277-281.

Venkatesh, S., and Naresh Singh, R. (1984). Sensilla on the third antennal segment of Drosophila melanogaster meigen (Diptera : Drosophilidae). International Journal of Insect Morphology and Embryology 13, 51-63.

Vosshall, L.B., Amrein, H., Morozov, P.S., Rzhetsky, A., and Axel, R. (1999). A spatial map of olfactory receptor expression in the Drosophila antenna. Cell 96, 725-736.

Vosshall, L.B., Wong, A.M., and Axel, R. (2000). An olfactory sensory map in the fly brain. Cell 102, 147-159.

Vosshall, P.P.L.L.B. (2008). The Olfactory Sensory Map in Drosophila. In Brain Development in Drosophila melanogaster, G.M. Technau, ed. (Springer-Verlag New York).

Wang, K.Y., Gong, J.X., Wang, Q.X., Li, H., Cheng, Q., Liu, Y.F., Zeng, S.Q., and Wang, Z.R. (2014). Parallel pathways convey olfactory information with opposite polarities in Drosophila. P Natl Acad Sci USA 111, 3164-3169.

Wang, Y., Guo, H.F., Pologruto, T.A., Hannan, F., Hakker, I., Svoboda, K., and Zhong, Y. (2004). Stereotyped odor-evoked activity in the mushroom body of Drosophila revealed by green fluorescent protein-based Ca2+ imaging. J Neurosci 24, 6507-6514.

Wilson, C.D., Serrano, G.O., Koulakov, A.A., and Rinberg, D. (2017). A primacy code for odor identity. Nature Communications 8.

Wilson, R.I. (2011). Understanding the functional consequences of synaptic specialization: insight from the Drosophila antennal lobe. Curr Opin Neurobiol 21, 254-260.

Wilson, R.I. (2013). Early olfactory processing in Drosophila: mechanisms and principles. Annu Rev Neurosci 36, 217-241.

Wilson, R.I., and Mainen, Z.F. (2006). Early events in olfactory processing. Annu Rev Neurosci 29, 163-201.

Wilson, R.I., Turner, G.C., and Laurent, G. (2004). Transformation of olfactory representations in the Drosophila antennal lobe. Science 303, 366-370.

Wright, G.A., and Schiestl, F.P. (2009). The evolution of floral scent: the influence of olfactory learning by insect pollinators on the honest signalling of floral rewards. Functional Ecology 23, 841-851.

Wyatt, T.D. (2003). Pheromones and animal behaviour: communication by smell and taste (Cambridge University Press).

Xu, P.S., Lee, D., and Holy, T.E. (2016). Experience-Dependent Plasticity Drives Individual Differences in Pheromone-Sensing Neurons. Neuron 91, 878-892.

Yaksi, E., and Wilson, R.I. (2010a). Electrical Coupling between Olfactory Glomeruli. Neuron 67, 1034-1047.

Yaksi, E., and Wilson, R.I. (2010b). Electrical Coupling between Olfactory Glomeruli (vol 67, pg 1034, 2010). Neuron 68, 801-801.

Yoshida, K., Hirotsu, T., Tagawa, T., Oda, S., Wakabayashi, T., Iino, Y., and Ishihara, T. (2012). Odour concentration-dependent olfactory preference change in C. elegans. Nature Communications 3, 739.

Zhang, Y., Chen, Y., Bressler, S.L., and Ding, M. (2008). Response preparation and inhibition: the role of the cortical sensorimotor beta rhythm. Neuroscience 156, 238-246.

Zhang, Y., Lu, H., and Bargmann, C.I. (2005). Pathogenic bacteria induce aversive olfactory learning in Caenorhabditis elegans. Nature 438, 179-184.

Zheng, Z.H., Lauritzen, J.S., Perlman, E., Robinson, C.G., Nichols, M., Milkie, D., Torrens, O., Price, J., Fisher, C.B., Sharifi, N*., et al.* (2018). A Complete Electron Microscopy Volume of the Brain of Adult Drosophila melanogaster. Cell 174, 730-+.

Chapter 4: Concluding Remarks

4.1 Relating ORN responses to intensity-induced behavior change

Studies in Chapter 2 present an alternative mechanism to link the early-stage neural activities to odor valence. Odor valence, the extent to which odor being attractive or repulsive to the animal, is thought to be encoded by the recruitment of "attractive/aversive channels" in flies. Flies exhibit varying preferences for different odors (odor identity). It's also known the preference for the same odorant can change as a function of its concentration (odor intensity), or even reverse when the concentration crosses a certain threshold. Considering the change in odor intensity does not usually lead to drastic changes in neural activation patterns as compared to the change in the odor identity, this phenomenon provides a unique perspective to study odor valence encoding. To understand the ecological significance of the intensity-induced valence switch, I developed a novel video-tracked behavior paradigm, monitoring the flies' spontaneous activities in exposure to odors at different concentrations. The repulsion induced by high concentrations seems to be a protective mechanism, as flies were able to cling onto the test tube's inner wall at lower concentrations but fell when exposed to pure odorants.

Electrophysiology recordings from ORNs showed the regular spiking activities can transition into oscillatory waveforms at high concentrations, which coincided with the flip in odor valence revealed by T-maze assays. Considering oscillations is found to play a role in neural coding in many organisms (Bhalla and Bower, 1997; Kay, 2005; Kay et al., 2009; Kay and Stopfer, 2006;

Laurent, 2002; Zhang et al., 2008), these oscillatory signals can potentially indicate a major change in the firing mode of the ORNs as well as the form of signals the AL may receive.

In flies, oscillatory waveforms in the sensillum recording are believed to be a result of ephaptic coupling between the two ORNs housed in the same sensillum. However, contrary to the ephaptic coupling hypothesis, the existence of a second ORN in the sensillum is not essential to produce the oscillatory waveforms. The "oscillations" can be produced by a single ORN after knocking out its counterpart in the same sensillum. Further, numerical modeling suggests that the phenomenological observations of "oscillations" can be directly explained by the ORNs entering a high firing regime without invoking any special mechanisms. The manipulation of cell membrane excitability by current injection can reproduce the oscillatory waveforms with stimulus at a lower concentration whose presentation alone does not evoke the "oscillations".

Meanwhile, this phenomenon is not a result of synchronized ensemble ORN spiking on the antenna. Abolishing the spiking activities in a specific sensillum abolished the oscillations but the slow LFP component remained intact, suggesting the "oscillations" are indigenous to the sensillum rather than a global effect. Further our results indicate that valence switches are not necessarily accompanied by the presence of oscillatory signals. Instead, the valence switch can simply be predicted by the summed responses of two major sensillum types. Once the summed activity crosses a certain threshold, the valence switch can happen.

4.2 Spatial and temporal Features of the olfactory neuronal ensembles

Despite a large body of literature looking into the anatomy and neural activities in the early stages of the fly olfactory system, a more comprehensive depiction of the functional organization and how the neural activities evolve dynamically in theses neural ensembles has been lacking, largely due to the limitations from the neural recording techniques.

In Chapter 3, I sought to address these issues by in vivo Calcium imaging, taking advantage of a novel lightsheet imaging system(Greer and Holy, 2019) that allowed exhaustive monitoring of the neural ensembles. I monitored 3 neuronal populations: ORNs (axonal terminals in the AL), the downstream iPNs (axonal terminals in the LH) and ePNs, among which ePNs had one input region and two output regions monitored near simultaneously.

4.2.1 The functional organization

To explore the organization principles of the functional units in the anatomical space, I examined the relationship between each ROI pair's functional distance and spatial distance. In general, the pairwise functional distance is to some extent linearly correlated with the spatial distance, indicating the change in the ROI tuning is more or less gradual in the anatomical space, with one exception being the ePN axonal terminals in the calyx, which exhibited a peripheral-versus-core organization.

To further examine the fine-grained functional-anatomical relationships, I devised a novel MDS-based visualization technique so that an ROI's functional feature, here the odor tuning profiles, can be directly mapped to its anatomical coordinates. Between ePNs and ORNs in the AL, the lateral regions' tunings are more conserved, whereas the medial regions are more variable in

tunings. The two higher order regions, the CL and LH, that the ePNs project to, mostly preserve the tuning types found in the AL. How would ePNs' and iPNs' projections interact in the LH, where the axonal terminals of the two populations converge, in response to various stimuli? My results suggest that, in the dorsal-lateral area, ePNs and iPNs have similar response strengths to all stimuli used in this study. Instead, the response strengths are more likely to differ in the remaining regions, depending on the stimulus. Interestingly, regions showing more inter-population variability also tend to be more variable among individuals for the same neuronal population.

Next, I asked how activities in the dendritic compartments (input) of the same neuronal population (ePN) can functionally influence the axonal terminals' (output) activities. As suggested by the overall shortening of response duration from the AL to CL/LH, some form of transformation may take place amid the signal propagation. This functional relationship was quantitatively modeled by the regression analyses, incorporating the fine temporal dynamics. Indeed, the results suggest the signals in the CL/LH are not direct replicates of those in the AL. The majority of AL ROIs have both positive (Its excitation imposes excitatory effect downstream) and negative (Its excitation imposes inhibitory effect downstream, while its inhibition has excitatory effect downstream) influences on the CL and LH ROIs, with a small fraction dominantly projecting either positive or negative influences. Most of the time, an AL ROI's positive and negative influences form spatially separate clusters in the CL and LH.

4.2.2 The temporal features and information encoding

As mentioned, the responses are dynamic rather than being static. How would these dynamics impact the encoding of stimuli? It's found that, for all populations/regions recorded, the initial response patterns (during the first 500ms of stimulation) evoked by various stimuli are highly

similar, and become more distinct, e.g. stimulus-specific, over the rest time course of the stimulus. Therefore, the fly olfactory circuits can respond to the appearance of a stimulus promptly, but the fly, knowing it's encountering an odor, may not be able to differentiate the stimulus at the very beginning. Taking a little extra time, the fly may gain a better sense of which exactly the stimulus is. Furthermore, this decorrelation process among response patterns accelerates as the signals traveling towards higher order centers.

Although the divergence from a common initial pattern is ubiquitous, how the pattern similarity between specific stimulus pairs evolves is individual dependent. Interestingly, the stimulus pairs exhibiting high inter-individual variability in ORNs become more and more consistent following along the path from ePN-AL, to ePN-CL and finally ePN-LH, indicating the odor pair relationship is getting stabilized along the ePN pathway, which may be potentially helpful to the preservation of some innate behaviors across individuals in the population (for instance, to differentiate an attractive odor from an aversive odor), regardless of the variation in the odor encoding at earlier stages. However, this reduction in inter-individual variability is not as apparent in the iPN axonal terminals.

In flies, Little attention has been paid to the ensemble dynamics after the stimulus termination. Results in this dissertation showed in lieu of simply diminishing activities as usually expected, new responses can emerge in a structural manner. Generally speaking, when responses in ROIs activated during stimulation are reducing, responses in another set of ROIs may arise. This results in response patterns that are nearly orthogonal, sometimes anti-correlated, to the patterns during stimulation. Furthermore, the OFF-responses seem to carry more unique information regarding the stimulus, as the OFF-patterns are more divergent in the coding space compared to the ON-patterns.

147

4.3 Methodological advancements

Lightsheet microscopy was previously applied for functional imaging on mice olfactory tissue (Xu et al., 2016) and the transparent zebrafish larvae(Ahrens et al., 2013; Chen et al., 2018; Greer and Holy, 2019; Xu et al., 2016). In this dissertation, I developed a full imaging procedure that realizes in vivo functional light-sheet imaging on Drosophila brains, including the brain dissection procedures, as well as the full automation of the recording process through a series of custom written scripts allowing low-level control of the components. This work offers solutions to two common hurdles in imaging data processing, that have been hindering the reliable extraction and interpretation of the relevant signals: 1. motion of the neural tissue, and 2. the ever-changing signal baseline, an inevitable side effect of calcium imaging. Another problem that may be unique to volumetric imaging data is the redundant sampling of the same functional unit across multiple planes, which I tackled with a hierarchical clustering based method that requires minimal prior knowledge about the neural anatomy (see methods in Chapter 4).

4.4 Future directions

To take the functional mapping one step further, it's possible to register the recorded regions into a common reference brain, as a post hoc staining process on the fly brain can be performed after the functional recordings. Then, algorithms such as ICA (Jefferis et al., 2007) can be applied to the registered functional data across individuals to provide a more quantitative investigation into the conservative/variable features, at the level of sub-regions. However, it's probably infeasible to perform one-to-one ROI matching in the MB and LH. The bouton-wise interaction between

ePNs and iPNs in the LH is better to be studied by imaging the two populations simultaneously from the same animal.

This study aims to capture the complete temporal dynamics with relatively long stimuli. But it would be interesting to ask how dynamic patterning happens in response to a brief stimulus. Consider the natural environment a fly lives in, the stimuli may present constantly, as well as in the form of "discrete" successive plumes, in which case the olfactory system does not have enough time to converge onto a stimulus-specific response pattern during the stimulus presentation. Does the dynamic patterning continue after stimulus termination? How the continual dynamic patterning may differ from the case of persistent stimulation? These questions may be answered by tests with brief stimuli, especially ones with a duration of less than 500ms.

What is the neural basis for pattern decorrelation? Surprisingly, my results suggest the decorrelation may start from the peripheral level, ORNs, where no local network regulates the inter-neuron activities. However, considering the ORN responses were recorded at the axonal terminals, which may be subject to feedback regulations from LNs, whether the decorrelation is an actual property of the ORNs or rather a result of feedback regulation needs further examination. Large scale imaging on the ORNs in the antenna is ideal but highly challenging. The antenna will be both a site to receive airborne molecules and to be probably immersed in saline for imaging, as most Calcium imaging techniques rely on water immersion objectives. A roundabout is to perform the same type of recording with the connections between LNs and ORNs blocked pharmacologically.

All in all, this dissertation presents new possibilities for the study of systems neuroscience in flies. Large scale neural recording is essential for cracking the complex neural systems. However, the progress in large scale recording also calls for a rethink on the research paradigms.

Facing a complex system, the concept of "causality" can become vague. For example, the classic paradigm to prove a set of neurons are responsible for a certain behavior is to perturb those neurons by knocking them out/blocking their communication to others, and observe whether the same behavior persists (such as aversion vs attraction). Now let's consider a simple case using artificial neural networks, as these models are decent analogies to the neural systems. Suppose we have a deep neural network with a small number of nodes at each layer, which is trained to classify images of dogs and cats. Dropping several nodes from a layer, analogous to knocking out some neurons, is possible to misclassify most of the dog images as cat images when given a relatively small test sample (just like the sample size from experiments is usually limited). Can we conclude these nodes are "cat-preferred" or "dog-antagonistic"? Or we should take an alternative view- the nodes are a subset of the feature extractors without a preference for the final output?

Along with the rapid growth in data dimension, "the curse of dimensionality" may also pose a real threat to the correct interpretation of experimental results. The representativeness of the samples may become dubious, as the amount of data required for achieving statistical significance can scale exponentially with the dimension. What's more, a working theory proposed to explain the data may be prone to the problem of "overfitting".

To address these issues, new methodological/theoretical tools are desired. Finally, the continual emergence of new research tools, both instrumental and theoretical, will allow for a major paradigm shift to bring the research to another level.